RESIDUAL LIFE PREDICTION AND DEGRADATION-BASED CONTROL OF MULTI-COMPONENT SYSTEMS

A Thesis
Presented to
The Academic Faculty

by

Li Hao

In Partial Fulfillment
of the Requirements for the Degree
Doctor of Philosophy in the
School of Industrial and Systems Engineering

Georgia Institute of Technology
May 2015

RESIDUAL LIFE PREDICTION AND DEGRADATION-BASED CONTROL OF MULTI-COMPONENT SYSTEMS

Approved by:

Professor Nagi Gebraeel, Advisor
School of Industrial and Systems Engineering
Georgia Institute of Technology

Professor Jianjun Shi, Co-Advisor
School of Industrial and Systems Engineering
Georgia Institute of Technology

Professor Chun Zhang
School of Industrial and Systems Engineering
Georgia Institute of Technology

Professor Kamran Paynabar
School of Industrial and Systems Engineering
Georgia Institute of Technology

Professor Jian Liu
Department of Systems and Industrial Engineering and Engineering management
The University of Arizona

Date Approved: 5 March 2015

To my parents, my husband,

and myself,

we together made this journey a lot memorable.

ACKNOWLEDGEMENTS

I would like to express the deepest appreciation to my advisors, Professor Nagi Gebraeel and Professor Jianjun Shi, for their support, patience, and encouragement throughout my Ph.D. studies.

Professor Gebraeel has taught me innumerable lessons and insights regarding to academic research, from creating research ideas and developing methodologies, to expressing contributions in the form of technical writing. I am grateful to him for holding me to a high research standard and enforcing strict validations for each research result. I would also like to express my gratitude to him for carefully reading and commenting on countless revisions of my research papers.

Professor Shi, has been always there to listen and give advices. Prof Shi has been supportive and has given me the freedom to pursue various projects. I am deeply grateful to him for his advices that helped me sort out the research ideas and the technical details of my work. He also encouraged me to develop and pursue my own career path. I would also like to express my deep thanks for his valuable help during my internship and full-time job hunting.

I would like to thank my committee members, Professor Chun Zhang, Professor Kamran Paynabar, and Professor Jian Liu for their dedications and constructive suggestions on my dissertation.

I also own my deep thanks to my good friend and colleague Dr. Rensheng Zhou, who offered me plenty of help during the first four years of my Ph.D. life.

I thank Dr. Linkan Bian and Dr. Kaibo Liu for their remarkable efforts in collaborating with me on research papers.

TABLE OF CONTENTS

LIST OF TABLES

LIST OF FIGURES

SUMMARY

The condition monitoring of multi-component systems utilizes multiple sensors to capture the functional condition of the systems, and allows the sensor information to be used to reason about the health information of the systems or components. This thesis focuses on modeling the relationship between multi-sensor information and component-level degradation, so as to prediction both system-level and component-level lifetimes. In addition, this thesis also investigates the dynamic control of component-level degradation so as to control the failure times of individual components based on real-time degradation monitoring.

The research topic that Chapter 3 focuses on is identifying component degradation signals from mixed sensor signals in order to predict component-level residual lives. Specifically, we are interested in modeling the degradation of systems that consist of two or more identical components operating under similar conditions. The key challenge here is that a defect in any of the components will excite the same defective frequency, which prevents an effective separation of the degradation signals of defective and non-defective components. To the best of our knowledge, no existing methodologies have investigated this research topic. In Chapter 3, we propose a two-stage vibration-based prognostic methodology for modeling the degradation processes of components with identical defective frequencies. The first stage incorporates the independent component analysis (ICA) to identify component vibration signals and reverse their original amplitude. The second stage consists of an adaptive prognostics method to predict component residual lives. In the simulated case study, we investigate the performance of the signal separation stage and that of the final residual-life prediction under different conditions. The simulation results show

reasonable robustness of the methodology.

In Chapter 4, we focus on characterizing the interactive relationship between product quality degradation and tool wear in multistage manufacturing processes (MMPs), in which machine tools are considered as components and the product quality measurements are considered as condition monitoring information. Due to the sequential structure of MMPs, the degradation status of a tool affects the product quality current stage, which, on the other hand, may affect the degradation of tools at subsequent stages. To the best of our knowledge, although existing literature has modeled the impact of product quality on the tooling catastrophic failure, no published work has targeted on the impact of product quality on the actual process of tool wear. To address this research topic, we propose an high-dimensional stochastic differential equation model to capture the interaction relationship between the process of tool wear and product quality. We then leverage real-time quality measurements to on-line predict the residual life of the MMP as a system. In the simulation study, we conclude that our methodology consistently performs better than a benchmark methodology that does not consider the impact of product quality on the process of tool wear or utilize real-time quality measurements.

Chapter 5 explores a new research direction, which is the dynamic control of component-level degradation in the parallel multi-component system, in which each component operates simultaneously to achieve an engineering objective. This parallel configuration is usually designed with some level of redundancy, which means when a small portion of components fails to operate, the remaining components can still achieve the engineering objective by increasing their workloads up to the designed capacities. Consequently, if the component degradation can be controlled, we can achieve better utilization of the redundancy to ensure consistent system performance. To do this, Chapter 5 assumes that the degradation rate of a component is directly related to its workload and develops a strategy of dynamic workload adjustment in

order to on-line control the degradation processes of individual components, and thus to control their failure times. The criterion of selecting the optimal workloads is to prevent the overlap of component failures. We conduct a simulated case study to evaluate the performance of our proposed methodology under different conditions.

CHAPTER I

INTRODUCTION

1.1 Research Background

Condition monitoring is the process of monitoring the health condition of a functioning system using real-time sensing technology. Based on the observed health information of the system, the fault or failure of the system may be predictable, which will reduce economy loss due to unexpected failure and emergencies. In addition, with system failure time being predictable, maintenance and control strategy can be determined with respect to the prediction. Due to the development of sensing technology, sensors become cheaper, more easily to be installed, this allows condition monitoring to be developed rapidly and applied to various of complicated industrial systems such as wind farms [3, 46, 75], machining systems [22, 70, 84], and civil engineering systems [39, 64, 71], etc.

Particularly, the condition monitoring of complex engineering systems that consist of multiple components, here after referred to as "multi-component systems", requires multiple sensors in order to capture overall information from different individual components. For example, in vibration monitoring of an aircraft engine system, multiple accelerometers are required to monitor the vibration from different components such as the fan, the motor, and the gearbox [25, 26]. Other examples of condition monitoring of multi-component systems can be found in monitoring gearboxes [11, 49, 83] and monitoring the product quality of manufacturing systems [91, 103, 110]. Consequently, it is very important to incorporate the condition monitoring information from different sensors to reason about the health condition of a system so as to predict the future performance (prognostics), such as system-level failure or component-level

failure.

An effective way to utilize condition monitoring is to construct a quantitative signal that can represent the health condition of the system in the past and provide information on how the system is likely to propagate in the future. Such a quantitative signal is referred to as a degradation signal in many literatures [42, 80]. Usually, the amplitude of a degradation signal may indicate the severity of a defect, and the increasing trend can capture the propagation of the defect. Therefore, to construct a mathematical model that can characterize this increasing form will help to predict the future performance of a system. Such a model is referred to as a degradation model in the literature [36, 43, 42, 76, 82, 106, 108]. Particularly, the degradation rates of identical systems may exihbit some variability. Gebraeel *et al.* [41, 42] proposed to model this phenomenon using a prior distribution of degradation rate and proposed a Bayesian approach to update the posterior distribution of the degradation rate associated with individual component .

In the case of a single-component system, (i.e., the degrading system consists of only one component), the degradation signal of the system is the same as that of the component. However, in a multi-component system, the degradation of the system (system-level degradation) is not necessarily equivalent to the degradation of individual components (component-level degradation). In fact, the system-level degradation is usually a consequence of the component-level degradation. For example, in vibration monitoring of a gearbox, the increasing trend of overall vibration, which can represent the system-level degradation, is usually due to the degradation of some specific bearings or gears [84].

Modeling the component-level degradation accurately may achieve confident prediction of system-level failure time (or lifetime). In addition, in some cases, even if a multi-component system may not encounter complete failure, some of its critical components may already be failed. For example, in a gearbox system, the vibration

level of a bearing is very small compared to the overall vibration, so the failure of the bearing may not be detected from system-level degradation monitoring. However, a failed bearing may cause severe damage in the future [84]. In this case, predicting component-level failure is also necessary. The objective of Chapter 3 in this thesis is to construct and model component-level degradation signals from condition monitoring information of a multi-component system, so as to predict component-level failures.

Compared to predicting component-level failure, predicting system-level failure from condition monitoring information seems to be a more straightforward approach. We may consider the entire system as a single "component" and use condition monitoring information to construct the degradation signal for prediction. However, this approach may not yield the prediction as accurate as considering the hidden effect of component degradation. Particularly, if the underline degradations of individual components exhibit complicated inter-relationship, simply ignoring this relationship will not accurately capture the degradation condition of the entire system. Chapter 4 of this thesis considers a scenario in which component degradation are interactive, i.e. the degradation status of one component may affect the degradation rate of another component. The objective of Chapter 4 is to prediction system-level failure by modeling this interactive hidden effect.

Another potential research direction is to control the component-level degradation in order to control their failure times. This is particularly necessary when a multi-component system does not allow several components to fail closely. For example, in a manufacturing system, it is common to have several identical workstations operating in parallel to meet a high demand. The specific workload on an individual workstation may affect its degradation rate and ultimately its failure time. If several workstations fail at the same time, the demand may no longer be satisfied. In order to prevent this unproductive situation, it is necessary to develop a control strategy to dynamically

adjust the workload on different components to control their failure times. Chapter 5 of this thesis considers the dynamic control problem in the application of parallel multi-component systems. The object of this research is to dynamically adjust the workloads of individual components to prevent the overlap of component failures.

In the following section, we will introduce each of the three aforementioned research topics in sequence.

1.2 Specific Research Topics

1.2.1 Vibration-Based Prognostics of Multi-Component Systems with Identical Degrading Components

The condition monitoring of engineering systems involves collecting sensor signals, such as temperature, vibration, crack propagation, etc., to enable fault detection (diagnostics) and facilitate remaining lifetime predictions (prognostics). One of the most popular condition monitoring techniques is vibration monitoring, which is well-suited for many applications, such as machine tools [59], power transformers [21], engines [13], electronic motors [79], wind turbines [25], and even structural systems [38]. Depending on the frequency range and other system characteristics, vibration can be measured in displacement, velocity, or acceleration. Typically, a sensor measures a mixture of vibration signals generated by the components of the system. This mixture can be transformed using signal processing techniques, such as the discrete Fourier transformation (DFT), into a spectrum of individual frequencies that are related to individual components. Some of these frequencies are generated only when specific faults or component defects occur. Examples of defects include imbalance, misalignment, bearing defects, gear defects, etc. The frequency associated with a specific defect is referred to as the "defective frequency" in this thesis.

It is not uncommon to observe a correlation between the amplitude of the defective frequency and the severity of the defect that is generating that frequency. In fact, there are several examples in the literature where amplitudes of defective frequencies

have been used to develop degradation signals for predicting failure times [12, 42, 53]. In Chapter 3, we are interested in modeling the degradation of systems that consist of two or more identical components operating under similar conditions, for example, two identical bearings mounted on the same shaft. The key challenge here is that a defect in any of the components will excite the same defective frequency. Without having dedicated sensors uniquely located near each component, it is not possible to distinguish between the defective and non-defective components simply from the spectrum analysis of sensor vibration signals. In this case, sensor vibration signals are considered as "inseparable" signals under traditional signal processing techniques. In reality, physical or structural constraints often create strong limitations for installing sensors close to each component of interest, thus presenting significant challenges in modeling degradation processes.

Chapter 3 proposes a two-stage vibration-based prognostic methodology for modeling the degradation processes of components with identical defective frequencies. The first stage uses independent component analysis (ICA) to separate component vibration signals from sensor vibration signals. ICA is a blind signal separation (BSS) technique that is used to separate mixtures of signals without necessarily relying on information about component signals themselves or the process by which the signals are mixed [23, 24, 57]. In our model, we assume that the signal measured by each sensor is a mixture of the vibration signals generated by individual components. We develop a novel approach that relies on signal transformation and ICA to separate the "inseparable mixtures" of component signals, i.e., vibrations signals with the same frequency. Once the signals are separated, they are used to construct the degradation signal for each component.

1.2.2 Interaction Between Tool Wear and Product Quality Degradation in Multistage Manufacturing Processes

Multistage manufacturing processes (MMPs) are widely known for their high throughput rates and relative flexibility. MMPs produce parts/products through a sequence of manufacturing stages that are equipped with tools for performing specific fabrication tasks. The performance and efficiency of an MMP are usually monitored via the quality of manufactured products. Typically, quality characteristics may be measured on the final products and/or at intermediate stages of the MMP. Deviations from the nominal values of these measurements (hereafter referred to as "quality degradation") are used to assess the efficiency of the MMP, which is deemed operational as long as the quality measurements of the manufactured products are within the engineering specification limits (i.e., parts are classified as conforming). Once these measurements exceed such pre-specified thresholds, parts are classified as nonconforming and the MMP is shutdown. Common causes of nonconforming products include errors in locating, tool wear, fixture errors, and other random factors [29, 34, 35, 51, 61, 116].

Tool wear has traditionally been seen as one of the most important factors that affect product quality degradation, and has been studied extensively in the literature. For example, The authors in [61, 73] investigated how the wear of locating pins affects the product quality in sheet metal forming and assembly processes. Another example can be found in metal cutting (i.e., machining) processes, in which tool wear was shown to be a main source of quality variation [51, 52, 116]. However, limited research efforts have been dedicated to investigate the effect of product quality on tool wear.

In MMPs, products are processed on sequential stages. Thus, in addition to the effect of tool wear on the product quality degradation, the quality degradation of outgoing products from a preceding stage also impacts the rate of tool wear in subsequent stages. In other words, there is a two-way interaction between tool wear and quality degradation. Take the cylinder head machining process [52] as an example.

This process consists of two stages: a drilling stage and a tapping stage. In the first stage, the tool wear of the drill bit impacts the quality of the hole, such as diameter, depth, straightness, and orientation, etc., whereas, in the second stage, the quality characteristics of the drilled hole impacts the wear rate of the tapping tool. Another example is the doorknob stamping process [60], in which the worn blanking die (tool) in the second stage generates burr (product quality degradation), which can affect not only final product quality but also the tool wear in the subsequent stages, as the burr on the part will accelerate the draw die worn out in the later forming operations.

Although the aforementioned interaction exists widely in MMPs, existing research has been most geared towards monitoring either tool wear or product quality, separately. Very few researchers have addressed the interaction between those two factors. One example is the QR-chain model proposed in [29], which studied how product quality degradation from preceding stages affects the probability of tool breakage in subsequent stages. In this model, the rate of tool wear is assumed to be independent from product quality degradation. The same model was implemented in the automotive body assembly process [31] to investigate how the wear-out of locating pins affects the assembly quality of outgoing products and how quality degradation of incoming products increased the probability of locating pin breakage.

In Chapter 4, we generalize the notion of the existing QR-chain model to incorporate the impact of quality degradation on the rate of tool wear instead of tool breakage. According to the literature in tool wear [100], the rate of tool wear tends to be higher as the "depth of cut" increases and vice versa, and the depth of cut is correlated to the product quality from preceding stages. For example, in a two-stage drilling and tapping process, if the diameter of the hole drilled in the first stage is too small, the tapping tool will cut more material to maintain the final product quality, which accelerates its tool wear. Our goal is to utilize a stochastic model to predict the RLD of the MMP by tracking product quality degradation. Within this context,

the failure of the MMP is assumed to be instigated by the occurrence of any non-conforming product. Consequently, non-conforming products will trigger the system shut-down and will not be able to enter subsequent stages. To do this, we develop a two-way interaction model that captures the interaction between tool wear and product quality degradation. The novelty of our work is that it allows us to predict the performance of the MMP, and thus provide ample time to plan for condition-based maintenance while preventing unexpected shutdown of the entire system. In addition, our work will also benefit the inventory management of tools. By monitoring the product quality characteristics and simultaneously accounting for tool wear, we can perform accurate prognostics on the MMP systems.

1.2.3 Degradation-Based Control Through Workload Adjustment in Parallel Multi-Component Systems

Among multi-component systems, one particular configuration is the one with a parallel structure, in which multiple components need to operate independently in parallel to simultaneously meet the system requirement. For example, the serial-parallel multistage manufacturing process consists of several stages, each of which contains several identical workstations arranged in parallel to simultaneously perform a specific operation to satisfy high production demand [40].

In a parallel multi-component system, when a component failure occurs, the remaining functional components have to be assigned with a heavier-than-usual workload to maintain system requirements. For example, in manufacturing systems, the maximum production rate (i.e., capacity) of a machine is usually designed to be higher than its normally assigned workloads, i.e., the system exhibits some level of natural redundancy to compensate for unexpected events. The Federal Reserve reported that the average redundancy in the US manufacturing industries is estimated to be around 20% [8]. While such redundancy structure by design attempts to provide a robust production scheme, it is not uncommon in practice that a large number of components

may possibly exhibit a similar degradation path, especially when similar workloads are assigned to those components. If the case happens, it will highly likely lead to an overlap of component failures and eventually result in loss of productivity.

To address this issue, the objective of Chapter 5 is to provide a dynamic workload adjustment strategy to prevent the overlap of component failures in parallel multi-component systems. Specifically, we assume that the degradation rate, which is a direct cause of the failure time, of a component is directly influenced by its workload. In other words, a component operating under a higher (lower) workload is assumed to degrade faster (slower). Based on this assumption, our key idea is to actively control the components degradation rate as well as the failure time via adjusting the components workload in real time. If the failure time of individual components can be accurately predicted and well controlled, then it is possible for us to prevent the overlap of component failures, which is greatly beneficial to the productivity, logistics, and maintenance planning.

In Chapter 5, we model the component degradation with a linear stochastic differential equation (SDE). To capture the variation in the degradation process due to material inhomogeneity and manufacturing uncertainty, we further assume that the degradation rate of an individual component is a random variable that follows a known prior distribution but the actual value is unknown. Next, at each decision epoch, we utilize real-time condition monitoring data to obtain an updated posterior distribution. Based on the updated distribution, we can then calculate the RLD of each component given a specific workload. With the predicted residual life in hand, an optimization framework is further proposed to determine the workload for individual components that prevents the overlap of component failures.

1.3 Thesis Organization

This thesis is organized as follows: Chapter 2 reviews existing literature pertaining to several research areas: the degradation modeling and prognostics of single-component systems, the condition monitoring of multi-component systems, signal separation techniques, research related to tool wear and product quality in MMPs, and the degradation modeling and control of MMPs. Chapter 3 introduces the proposed two-stage prognostics framework that can identify component degradation signals from identical components in vibration monitoring and predict component-level failure using an adaptive prognostics model. Chapter 4 describes the proposed interaction model that captures the interactive effect between product quality degradation and tool wear in MMPs in order to predict system-level failure based on the proposed model. Chapter 5 introduces the dynamic workload adjustment using real-time degradation monitoring information. Chapter 6 summarizes the thesis and introduces future research directions.

CHAPTER II

LITERATURE REVIEW

2.1 Degradation Modeling and Prognostics of Single - Component Systems

The literature on degradation modeling of single-component systems are relatively rich, and have relied on numerous statistical as well as stochastic models for characterizing degradation. Examples of such work include non-linear random-coefficient models developed by [76] to model degradation and estimate time-to-failure distributions. Other papers have modeled degradation using the Wiener process. For example, the authors in [36] proposed a time-scale transformation of the Wiener process to model the accumulated decay under of a component under variable stress levels. A similar approach was also presented in [108] where the authors considered two types of time-transformation, an exponential transformation and a power transformation suitable for different engineering applications. In [82], the authors utilized the Wiener process for accelerated degradation modeling and proposed a Bayesian approach to update the drift parameter as subsequent tests were completed. The model was then used to estimate a lifetime distribution of the component's population. Moreover, the authors in [106] incorporated random effects into the Wiener process to represent unit-to-unit variability among the degradation processes of different individuals.

Most of the above efforts focused primarily on estimating the lifetime distribution for a population of components. However, In [42], the authors developed two stochastic degradation models where real-time data from components operating in the field were used to update the model and estimate RLDs for partially degraded components. Nonetheless, it is important to note that most of the degradation modeling literature

have focused uniquely on modeling the degradation of single components. To the best of our knowledge, there is no existing literature that addresses the degradation modeling of multi-component systems, especially those with "inseparable" mixtures of component degradation signals.

2.2 Condition Monitoring of Multi-Component Systems

Literature on the condition monitoring of multi-component systems has addressed various industrial applications, such as the area of wind farms [3, 46, 75], machining systems [22, 70, 84], civil engineering systems [39, 64, 71], gearbox systems [11, 49, 83], and product quality of manufacturing systems [91, 103, 110]. Particularly, vibration monitoring is a very efficient way to capture the health condition of systems with rotational or reciprocal components. Examples of application areas of vibration monitoring include power transformers [17, 21, 54], engines [13, 104], electronic motors [45, 79, 89, 111], steam turbines [15], wind turbines [25, 26], gearboxes [11, 49, 83], Machining tools [59, 69, 88], and even structural systems [10, 38].

Traditionally, vibration monitoring literature has relied on two key assumptions: (1) sensors can be located on, or very close to, the component that is being monitored [41, 42, 53], and (2) the components of a system are different and thus generate different defective frequencies that can easily be identified through spectral analysis [42, 44, 45, 84]. These assumptions do not necessarily hold for many multi-component engineering systems. In reality, a system may consist of multiple identical components, and sensor placement can be constrained by the geometry and/or functionality. In such systems, a sensor signal may consist of a mixture of multiple vibration signals with the same defective frequencies. As a result, these signals cannot be separated using conventional signal processing techniques. Furthermore, the focus of most of the efforts has primarily been on fault detection and diagnosis. However, they do not consider the potential degradation of a defect, nor do they consider degradation-based

lifetime prediction.

2.3 Signal Separation Techniques

In Chapter 3, we focus on developing a prognostic framework that utilizes vibration monitoring of multi-component systems to predict component-level degradation. Our modeling approach involves a signal separation stage that is based on ICA, which is one of a blind signal separation (BSS) techniques. ICA assumes that the signals measured by a sensor is a linear combination of statistically independent signals unique to individual signal sources, which in our context are assumed to be the components of the system. ICA separates the signals by maximizing their independence. Different ICA algorithms include FastICA [58], AMUSE [102], SOBI [16] and JADE [24]. Other BSS algorithms include the blind deconvolution (BD), which models the relationship between sensor signals and component signals as a convolution [99, 101]. ICA and other BSS techniques have also been widely used for diagnostics and fault identification. For example, ICA has been applied on the detection of sensor drifts [63], the identification of variation patterns in a multistage manufacturing process [5], the investigation of the sources of noise in a diesel engine [72], and the detection of gear faults [87]. In addition, BD has been applied in the diagnosis of vibration systems [45, 113].

One of the major limitations of BSS techniques, including ICA and BD, is that these methods do not retain any information pertaining to the absolute amplitude of the signal [56]. That is, the relative relationship between the amplitudes of any two successive signals is preserved, but the actual value is not as will be shown later. As a result, ICA has not been widely used in prognostics or predictive degradation modeling since almost all prognostic models require the exact signal amplitude in order to predict lifetime and remaining lifetime. In Section 3.2.2, we will discuss how to overcome this limitation by proposing an amplitude recovery procedure.

2.4 Reliability and Prognostics of Multi-Component Systems

For multi-component systems, much research has focused on studying the relationship between system and component reliability. For example, one closely related topic is the k-out-of-n system, which means that a system within components is functional if and only if at least k components operate properly. The reliability of the system highly depends on the component reliability as well as the system structure. A detailed survey of reliability studies of the k-out-of-n systems can be found in [28]. Initial research efforts in this area focused on binary state systems, in which each component is assumed to have only two states: functional or failed [55, 90]. Recent research efforts have extended the assumption to be multiple states [50, 118].

In addition to the reliability studies, degradation modeling and prognostics of multi-component systems has also attracted much attention recently. Related examples include [19], which discussed the degradation modeling of multiple components when the degradation processes are inter-dependent. The authors in [47] focused on separating component degradation signals from sensor data that consist of mixed information from several identical components in a complex system. However, all these related publications focus only on identifying or modeling the degradation of the components.

2.5 Research Related to Tool Wear and Product Quality in MMPs

Research in two important aspects of any manufacturing systems, tool wear and product quality, have traditionally been treated separately. For example, there is a plethora of literature that focuses on the condition monitoring of tool wear [33, 86, 96]. Some have dealt with machine vision-based methods [65, 66], wear and debris analysis [95], and various types of sensor signals related to force measurements, vibration,

acoustic, etc. Techniques such as artificial neural networks and regression analysis proved to be widely popular in tool condition monitoring as noted in [95]. Other methods include wavelet analysis of force signals, acoustic emissions, vibrations, and spindle current with the goal of identifying tool wear, chipping, breakage, and chatter [117].

On the other hand, statistical process control (SPC) methods have been widely used to monitor product quality and capture the root causes of quality degradation, tool wear, and other process variables. Traditional SPC approaches include control charts [48, 78], regression adjustment [85, 93], and the cause-selection chart [92, 94]. SPC in MMPs is particularly complex because of the nature of the manufacturing sequence and the number of process variables involved. However, state-space models have proved to be effective in this area. The authors in [6, 61] proposed a state-space model to study the effects of process errors including tool wear on product quality in an automotive assembly process. The authors in [52] used a similar approach for a cylinder head machining process. Additional work by [35, 51] was also geared towards using state-space models to detect the potential sources of variation in product quality. See [103] for a comprehensive review of SPC methods involving MMPs.

Very little research has investigated the interaction between tool wear and quality degradation in MMPs. The most relevant studies can be found in [29, 31], where the authors proposed a QR-chain model. The QR-chain model assumes that tool wear linearly impacts quality degradation, and quality degradation affects the probability of tool breakage. The QR-chain model does not consider the effect of quality degradation on the instantaneous rate of tool wear, which is assumed to be constant at all time in each stage. The scope of the QR-chain model is limited to the survival analysis of the MMP.

2.6 Degradation Modeling and Control of MMPs

Discrete-time Markov chains (DTMC) [27, 98] and continuous-time Markov chains (CTMC) [2, 32] have been used to model degradation in MMPs. A continuous-state diffusion model was applied by [29] to model tooling degradation in MMPs. In contrast to much of the existing literature, our focus here is on controlling the degradation rates of MMP workstations by dynamically adjusting the production rates without violating demand requirements. Very few studies in the literature have addressed this specific problem. A relevant work was given in [97, 98], where the authors modeled workstation degradation using a DTMC and the transition probabilities from one degradation state to another is governed by the type of products that are dispatched to each individual workstation. Another relevant example is the work in [114], where the authors considered a scenario that an operation can be transferred between workstations to adjust their usage and hence control their corresponding hazard rates.

CHAPTER III

RESIDUAL LIFE PREDICTION OF MULTI-COMPONENT SYSTEMS WITH IDENTICAL COMPONENTS

In this chapter, we propose a simultaneous signal separation and prognostics framework for multi-component systems with inseparable component signals from identical components. In the signal separation stage, we apply an independent component analysis (ICA) algorithm to isolate component signals from mixed sensor signals, and propose an online amplitude recovery procedure to recover amplitude information that is lost after applying ICA. In the prognostics stage, we incorporate an adaptive prognostics method to model component degradation signals as continuous stochastic processes so as to predict the residual lifetimes of individual components. In the simulated case study, we investigate the performance of the signal separation stage and that of the final residual-life prediction under different conditions.

The remainder of this chapter is organized as follows: Section 3.1 discusses the model and defines the mixing relationship between components and sensor signals. Section 3.2 describes the signal separation procedure and the challenges of applying ICA. We also discuss an amplitude recovery procedure to approximately recover signal amplitude. Section 3.3 reviews the adaptive prognostics model, and discusses how it fits within our framework. Section 3.4 focuses on a numerical study that investigates the effectiveness of signal separation and the accuracy of residual-life prediction.

3.1 System Description and Modeling Approach

This chapter is based on the vibration monitoring of multi-component systems. Typically in vibration monitoring, defective frequencies are only generated as a result of the initiation or existence of mechanical faults and defects. Similar to the assumptions made in [42], we assume that amplitude of a defective frequency is correlated with the severity of the underlying degradation process. The term "degradation signal" is used to define the behavior of the amplitude of the defective frequency over a component's lifetime.

In this framework, we focus on the degradation phase that begins at the very first onset of a defect and ends at the time of failure. We consider a system that, among other constituent components, contains at least $n \geq 2$ identical components operating under the same conditions. An example is a wind turbine that has two or more identical bearings rotating at the same speed or two or more pairs of gears with the same mesh frequency. Consequently, a defect in any of these identical components will generate the same defective frequency, which we denote as f^*. This implies that the signal measured by each sensor will consist of an *inseparable mixture* of component-specific vibration signals. Thus, conventional methods used for spectral analysis cannot be used to distinguish between the degradation levels of the components in question. Furthermore, we assume that vibration is measured periodically using $m \geq n$ sensors, typically accelerometers. We consider applications where sensors cannot be placed in close proximity to the degrading components due to physical and/or functional constraints. Instead, sensors can only be placed on an external structure, for example, the outside of a gearbox. As a result, each sensor captures only a proportion of the vibration signals generated by each component. This proportion will depend on sensor location, material properties, damping, etc.

Our goal is to develop a prognostic methodology for modeling degradation and predicting the remaining lifetimes of partially degraded components with an identical

defective frequency. To achieve this, we develop a two-stage methodology that involves a signal separation stage followed by degradation modeling and remaining life prediction. In the first stage, ICA is used to separate sensor signals into individual component-specific signals. The resulting component signals are then used to predict the remaining lifetimes of their corresponding components using the degradation-based prognostic modeling approach developed in [42].

3.1.1 Problem Formulation

We start by defining $x_i(t_k)$ as the time domain vibration signal measured by sensor i at some observation time t_k (hereafter referred to as the "sensor vibration signal"), for $i = 1, 2, \ldots, m$ and $k = 1, 2, \ldots, M$, where t_M represents the last observation time. We assume that $x_i(t_k)$ is a linear combination of the vibration signals generated by each component j (hereafter referred to as the "component vibration signal"), which we denote as $s_j(t_k)$. Note that in this context, the linearity assumption is an approximation of the real mechanism by which sensors capture the vibration signals generated by the components. In reality, this mechanism is relatively complex and indeed more complicated than a simple linear model. However, there is a rich literature that has utilized the linearity assumption for similar purposes, especially for systems that are small in size and have a high rigidity. Examples include [49, 72, 87, 112, 114]. One example was presented in [87] which considered vibration monitoring of gearboxes, and argued that the linear assumption can hold if the accelerometers are mounted on rigid gearboxes. In this chapter, we consider a similar setting, and we focus on applications that involve vibration monitoring of mechanical systems with similar properties, i.e., applications where the linearity assumption can be valid. Thus, a sensor vibration signal $x_i(t_k)$ can be expressed as follows:

$$x_i(t_k) = a_{i,1}s_1(t_k) + a_{i,2}s_2(t_k) + ... + a_{i,n}s_n(t_k) + e_i(t_k), \text{ for } k = 1, 2, \ldots, M, \quad (1)$$

where $0 \leq a_{i,j} \leq 1$ $(j = 1, \ldots, n)$ is a real-valued element that represents the proportion of the vibration generated by component j that is captured by sensor i. The constraint on $a_{i,j}$ implies that each sensor can capture no more than 100% of the vibration generated by an individual component. The term $e_i(t_k)$ represents the sensor noise, which is assumed to be Gaussian.

For a system with m sensors and n identical components, the relationship between sensor vibration signals and component vibration signals can be expressed in matrix form as follows:

$$\mathbf{x}(t_k) = \mathbf{A}\mathbf{s}(t_k) + \mathbf{e}(t_k), \text{for } k = 1, 2, \ldots, M, \tag{2}$$

where $\mathbf{x}(t_k) = [x_1(t_k); x_2(t_k); \ldots; x_m(t_k)]$, $\mathbf{s}(t_k) = [s_1(t_k); s_2(t_k); \ldots; s_n(t_k)]$, and $\mathbf{e}(t_k)$ $= [e_1(t_k); e_2(t_k) \ \ldots; e_m(t_k)]$ represent the vectors of sensor vibration signals, component vibration signals, and sensor noise, respectively. The matrix $\mathbf{A} = \{a_{i,j}\}, (i = 1, \ldots, m, j = 1, \ldots, n)$, defines the mixing process. The assumption that $m \geq n$ guarantees that $\mathbf{A}$ is full column rank. This is necessary and sufficient for capturing the vibration signals generated by all n identical components. Note that the special case, $m = n$, can be used to describe the scenario where a dedicated sensor is used to monitor each component.

3.1.2 Pre-processing Using DFT

Equation 2 shows the relationship of the time domain vibration signals. In order to model the degradation of the n identical components considered in this setting, we need to find their amplitudes of the defective frequency f^*. The amplitude of the defective frequency can be used as a proxy for the underlying physical degradation, and can therefore be used to estimate the residual lifetime of the corresponding component [42]. For this purpose, the DFT is used to extract the frequency content of the time domain signals.

The DFT converts a signal into a set of complex sinusoids that are ordered by their

frequencies. Thus, the DFT of component signal $s_j(t_k)$ at defective frequency f^* can be expressed in the complex form $s_{j,R}^{f^*}(t_k)+js_{j,I}^{f^*}(t_k)$, where $s_{j,R}^{f^*}(t_k)$ and $s_{j,I}^{f^*}(t_k)$ are the real and imaginary parts of the DFT of $s_j(t_k)$ at frequency f^*, respectively. Similarly, we denote the DFT of the vectors $\mathbf{s}(t_k)$, $\mathbf{x}(t_k)$, and $\mathbf{e}(t_k)$ in Eq. 2 at f^* by complex vectors $\mathbf{s}_R^{f^*}(t_k)+j\mathbf{s}_I^{f^*}(t_k)$, $\mathbf{x}_R^{f^*}(t_k)+j\mathbf{x}_I^{f^*}(t_k)$, and $\mathbf{e}_R^{f^*}(t_k)+j\mathbf{e}_I^{f^*}(t_k)$, respectively. Since DFT is a linear transformation, the linear relationship in Eq. 2 remains valid. The model for the transformed frequency domain signals is therefore given as:

$$[\mathbf{x}_R^{f^*}(t_k) + j\mathbf{x}_I^{f^*}(t_k)] = \mathbf{A}[\mathbf{s}_R^{f^*}(t_k) + j\mathbf{s}_I^{f^*}(t_k)] + [\mathbf{e}_R^{f^*}(t_k) + j\mathbf{e}_I^{f^*}(t_k)], \tag{3}$$

for $k = 1, 2, \ldots, M$. The amplitude of component vibration signal $s_j(t_k)$ at the defective frequency f^* is given by $\sqrt{\left[s_{j,R}^{f^*}(t_k)\right]^2 + \left[s_{j,I}^{f^*}(t_k)\right]^2}$. We denote this amplitude as $s_j^{f^*}(t_k)$. As mentioned earlier, this amplitude represents the severity of degradation at time t_k. Therefore, the sequence $\{s_j^{f^*}(t_1), \ldots, s_j^{f^*}(t_M)\}$ can be used to construct the degradation signal unique to the component ("component degradation signal" for short).

Since $\mathbf{A}$ is real-valued matrix, Eq. 3 can be separated into two partitions:

$$\begin{aligned} \mathbf{x}_R^{f^*}(t_k) &= \mathbf{A}\mathbf{s}_R^{f^*}(t_k) + \mathbf{e}_R^{f^*}(t_k) \text{ for } k = 1, 2.... \\ \mathbf{x}_I^{f^*}(t_k) &= \mathbf{A}\mathbf{s}_I^{f^*}(t_k) + \mathbf{e}_I^{f^*}(t_k) \text{ for } k = 1, 2.... \end{aligned} \tag{4}$$

Both the real part $\mathbf{x}_R^{f^*}(t_k)$ and the imaginary part $\mathbf{x}_I^{f^*}(t_k)$ can be derived by applying the DFT on the observed sensor vibration signal $\mathbf{x}(t_k)$. Thus, we can estimate the mixing matrix $\mathbf{A}$ using either the observations of real parts $\mathbf{x}_R^{f^*}(t_1), \ldots, \mathbf{x}_R^{f^*}(t_M)$ or the observations of imaginary parts $\mathbf{x}_I^{f^*}(t_1), \ldots, \mathbf{x}_I^{f^*}(t_M)$. After the matrix $\mathbf{A}$ is estimated, component vibration signals can be calculated using linear regression. In this work, we focus only on using the real parts. We refer to $\mathbf{x}_R^{f^*}(t_k)$, $\mathbf{s}_R^{f^*}(t_k)$, and $\mathbf{e}_R^{f^*}(t_k)$ as the vectors of "real sensor signal", "real component signal", and "real sensor noise", respectively.

Particularly, we assume that the phase angle of any component vibration signal, given by $\arctan \frac{s_{j,R}^{f^*}(t_k)}{s_{j,I}^{f^*}(t_k)}$, remains relatively constant for any point in time t_k. The reason is that the phase angle of a defective vibration signal is determined by the location of the defect on the component as well as the steadiness of its rotating speed. We assume that 1) once the defect occurs, the location of the defect on one component cannot be altered by external environment such as the degradation of other components; 2) the rotation speed of the system is controlled to be steady. Thus, our assumption of constant phase angle holds. Consequently, $s_{j,R}^{f^*}(t_k) \propto s_{j,I}^{f^*}(t_k)$, and as a result $s_{j,R}^{f^*}(t_k) \propto s_j^{f^*}(t_k)$ for any time t_k. This represents that the real component signal preserves the shape of its corresponding component degradation signal and can be considered as an indicator of the severity of component degradation.

3.2 Signal Separation Using ICA

As we discussed earlier, the first step of our methodology involves signal separation. Specifically, we apply ICA on the real sensor signals in Eq. 4 to estimate the matrix $\mathbf{A}$. ICA focuses on separating statistically independent signals from these linear mixtures without requiring specific knowledge of the mixing process. To guarantee the unique decomposition of the signal mixtures into statistically independent signals, ICA assumes that at most one of the statistically independent signals follows a Gaussian distribution and that the noise variables all follow Gaussian distributions. For detailed explanation, the reader may refer to [57].

However, there are some key challenges associated with applying ICA to our problem setting. The first challenge is that ICA assumes that the linear mixture consists of *statistically independent* signals unique to individual components. However, the vector of real component signals $\mathbf{s}_R^{f^*}(t_k)$ in Eq. 4 may not necessarily satisfy this requirement. In fact, its elements will always exhibit some level of correlation. To see this, consider the fact that the amplitude of a degradation signal tends to increase as

the severity of physical degradation increases. In other words, the sequence of real component signals $[s_{j,R}^{f^*}(t_1), \ldots, s_{j,R}^{f^*}(t_M)]$ of component j will exhibit an increasing trend. If multiple (identical) components begin to degrade, it is clear that their corresponding degradation signals will possess a significant level of correlation due to a common increasing trend.

To eliminate this correlation, we remove the common increasing trend by focusing on modeling the increments of the signals instead of the actual signals themselves. We let $\Delta\mathbf{s}^{f^*}(t_k) = \mathbf{s}_R^{f^*}(t_{k+1}) - \mathbf{s}_R^{f^*}(t_k)$ represent the increments of the real component signals at time t_k ("component increments" for short), and define the sequence $[\Delta\mathbf{s}^{f^*}(t_1), \ldots, \Delta\mathbf{s}^{f^*}(t_M)]$ as i.i.d. samples of a random vector $\Delta\mathbf{S}^{f^*}$. Then, we assume that all elements of $\Delta\mathbf{S}^{f^*}$ are mutually independent. This assumption means that the variations in the degradation signal among the individual components are independent from one another. Similarly, we define $\Delta\mathbf{x}^{f^*}(t_k)$ and $\Delta\mathbf{e}^{f^*}(t_k)$ as the sensor increments and error increments, respectively, with corresponding random vectors $\Delta\mathbf{X}^{f^*}$, and $\Delta\mathbf{E}^{f^*}$. The model in Eq. 4 can now be re-expressed in terms of random vectors as follows:

$$\Delta\mathbf{X}^{f^*} = \mathbf{A}\Delta\mathbf{S}^{f^*} + \Delta\mathbf{E}^{f^*} \tag{5}$$

The second challenge with applying ICA to our problem setting is that it does not preserve amplitude information. To explain this, consider the following expansion of Eq. 5:

$$\begin{aligned}\Delta\mathbf{X}^{f^*} &= [\mathbf{a}_1, \mathbf{a}_2 ..., \mathbf{a}_n][[\Delta S_1^{f^*}; \Delta S_2^{f^*}; ...; \Delta S_n^{f^*}] + \Delta\mathbf{E}^{f^*} \\ &= \sum_{j=1}^{n} \frac{1}{b_j}\mathbf{a}_j[b_j \Delta S_j^{f^*}] + \Delta\mathbf{E}^{f^*}\end{aligned}$$

where $\mathbf{a}_j$ is the j^{th} column of $\mathbf{A}$, $\Delta S_j^{f^*}$ is the j^{th} component increment, and b_j is an arbitrary scalar. The linear combination as well as the assumption of independent component increments hold for any value of b_j. Therefore, ICA cannot be used to determine the true amplitude of $\Delta S_j^{f^*}$ or the true norm of the column $\mathbf{a}_j$ $(j = 1, 2, ...n)$.

To address this challenge we develop an online amplitude recovery procedure for approximately recovering the amplitude content of the estimated degradation signals (as will be shown later in Section 3.2.2).

3.2.1 The Implementation of ICA

ICA is applied to a historical training data set consisting of sensor increments with the goal of estimating the mixing matrix $\mathbf{A}$. To guarantee a unique solution, ICA typically assumes unit-variance of the source signals, which in our modeling framework are represented by the component increments $\Delta\mathbf{S}^{f^*}$. Consequently, we let $\Sigma_{\mathbf{S}}$ denote the covariance matrix of $\Delta\mathbf{S}^{f^*}$, and define $\Delta\tilde{\mathbf{S}}^{f^*} = \Sigma_{\mathbf{S}}^{-\frac{1}{2}}\Delta\mathbf{S}^{f^*}$, where $\Delta\tilde{\mathbf{S}}^{f^*}$ represents a random vector of signals increments with unit-variance and independent elements. Using this representation, we can now express Eq. 5 as follows:

$$\begin{aligned}\Delta\mathbf{X}^{f^*} &= \mathbf{A}\Sigma_{\mathbf{S}}^{\frac{1}{2}}\Delta\tilde{\mathbf{S}}^{f^*} + \Delta\mathbf{E}^{f^*} \\ &= \tilde{\mathbf{A}}\Delta\tilde{\mathbf{S}}^{f^*} + \Delta\mathbf{E}^{f^*},\end{aligned} \tag{6}$$

where $\tilde{\mathbf{A}} = \mathbf{A}\Sigma_{\mathbf{S}}^{\frac{1}{2}}$.

Our objective now is to use ICA to estimate the matrix $\tilde{\mathbf{A}}$. We begin by performing an eigen-decomposition of the covariance matrix of $\Delta\mathbf{X}^{f^*}$, which we denote by $\Sigma_{\mathbf{X}}$. Since $\Delta\tilde{\mathbf{S}}^{f^*}$ has unit variance, then $\Sigma_{\mathbf{X}}$ can be expressed as $\Sigma_{\mathbf{X}} = \tilde{\mathbf{A}}\tilde{\mathbf{A}}^T + \Sigma_{\mathbf{E}}$, where $\Sigma_{\mathbf{E}}$ represents the covariance matrix of $\Delta\mathbf{E}^{f^*}$. If we assume that all elements in $\Delta\mathbf{E}^{f^*}$ are mutually independent and have equal variance σ_E^2, then $\Sigma_{\mathbf{X}}$ can be expressed as $\Sigma_{\mathbf{X}} = \tilde{\mathbf{A}}\tilde{\mathbf{A}}^T + \sigma_E^2\mathbf{I}$. Consequently, the eigenvector matrix of $\Sigma_{\mathbf{X}}$, denoted as $\mathbf{P}$, is equal to that of $\tilde{\mathbf{A}}\tilde{\mathbf{A}}^T$, and the eigenvalues of $\Sigma_{\mathbf{X}}$, denoted as $\lambda_i, i = 1, 2, ..., m$, are the eigenvalues of $\tilde{\mathbf{A}}\tilde{\mathbf{A}}^T$ plus σ_E^2. For notation convenience, we denote the diagonal matrix that has $\lambda_i, i = 1, 2, ..., m$ on the diagonal as $\mathbf{\Lambda_X}$ and the diagonal matrix that has the eigenvalues of $\tilde{\mathbf{A}}\tilde{\mathbf{A}}^T$ on the diagonal as $\mathbf{\Lambda_A}$. Thus, $\mathbf{\Lambda_A} = \mathbf{\Lambda_X} - \sigma_E^2\mathbf{I}$. Consequently, according to the definition of eigen-decomposition, $\tilde{\mathbf{A}}\tilde{\mathbf{A}}^T = \mathbf{P}[\mathbf{\Lambda_X} - \sigma_E^2\mathbf{I}]\mathbf{P}^T$, which implies that $\tilde{\mathbf{A}} = \mathbf{P}\mathbf{\Lambda_A}^{-\frac{1}{2}}\mathbf{Q}$, where $\mathbf{Q}$ is a unknown orthogonal matrix.

The value of σ_E^2 is usually unknown and can be estimated from data. To do this, we rely on the fact that $\tilde{\mathbf{A}}$ is an m-by-n matrix with full column rank, which means that the first $(m-n)$ smallest eigenvalues of $\tilde{\mathbf{A}}\tilde{\mathbf{A}}^T$ are equal to zero. Thus, by ranking the eigenvalues of $\Sigma_{\mathbf{X}}$, we have $\lambda_1 \geq \lambda_2 \geq ... \geq \lambda_n > \sigma_E^2 = \lambda_{n+1} = \lambda_{n+2} = ... = \lambda_m$. Therefore, σ_E^2 can be estimated by taking the average of $\lambda_{n+1}, \lambda_{n+2}, ..., \lambda_m$.

The next step involves optimization where the objective is to estimate the orthogonal matrix $\mathbf{Q}$. For every feasible value of $\mathbf{Q}$, there will be a corresponding estimated component increments calculated based on Eq. 6. Since the true component increments are statistically independent, the optimal $\mathbf{Q}$ will correspond to the estimated component increments that exhibit maximum independence. Usually independence is measured using fourth-order statistics, such as the fourth-order cumulants [24] and the Kurtosis [58]. In this work, we utilize an optimization algorithm based on the theory of the fourth-order cumulants known as "JADE" (proposed in [24]).

For any random vector $\mathbf{w}$, its fourth-order cumulants of the p^{th}, q^{th}, u^{th}, and v^{th} elements is defined as

$$\begin{aligned} C_{p,q,u,v}(\mathbf{w}) = & E[w_p w_q w_u w_v] - E[w_p w_q]E[w_u w_v] \\ & - E[w_p w_u]E[w_q w_v] - E[w_p w_v]E[w_q w_u] \end{aligned}$$

According to the properties of fourth-order cumulants stated in [81], if $\mathbf{w}$ is a random vector with statistically independent elements, all of its cross-cumulants $(p, q, u, v \neq p, p, p, p)$ are equal to 0. Thus, maximizing independence between estimated component increments is equivalent to minimizing all cross-cumulants between the estimated component increments. Using the JADE algorithm, $\mathbf{Q}$ is estimated by minimizing the sum of squares of a subset of all cross-cumulants of estimated component increments. We denote the estimated value of $\mathbf{Q}$ as $\hat{\mathbf{Q}}$. Subsequently, the estimator of $\tilde{\mathbf{A}}$, denoted as $\hat{\mathbf{A}}$, can be estimated using $\mathbf{P}{\mathbf{\Lambda}_{\mathbf{A}}}^{-\frac{1}{2}}\hat{\mathbf{Q}}$.

Due to the loss of amplitude after ICA stated earlier, the estimated matrix $\hat{\mathbf{A}}$

does not contain any amplitude information. Thus, if we want to estimate $\mathbf{s}_R^{f^*}(t_k)$ using $\hat{\mathbf{A}}$ based on Eq. 4, the least-square estimation result, denoted by $\tilde{\mathbf{s}}^{f^*}(t_k) = [\hat{\mathbf{A}}^T\hat{\mathbf{A}}]^{-1}\hat{\mathbf{A}}^T\mathbf{x}_R^{f^*}(t_k)$ for $, k = 1, 2, \ldots, M$, will not preserve the amplitude information, either. Instead, it will only preserve the shape of $\mathbf{s}_R^{f^*}(t_k)$. As mentioned earlier, $\mathbf{s}_R^{f^*}(t_k)$ is an indicator of the component degradation, thus, $\tilde{\mathbf{s}}^{f^*}(t_k)$ preserves the shapes of component degradation signals but does not reflect the actual degradation levels of individual components. In other words, for any component j, the amplitude of $\tilde{s}_j^{f^*}(t_k)$ is proportional to the amplitude of component degradation signal j with an unknown ratio. Consequently, we refer to $\tilde{\mathbf{s}}^{f^*}(t_k)$ as the vector of "un-scaled" degradation signals. However, in the application of prognostics, estimating the actual amplitude of a component degradation signal is crucial to predict its remaining useful lifetimes. Consequently, in what follows, we propose a data-driven "amplitude recovery procedure" capable of approximately recovering the amplitude information of component degradation signals.

3.2.2 On-line Amplitude Recovery Procedure

The amplitude recovery procedure is used for online estimation of the true amplitude level of component degradation signals in systems operating in the field. Our procedure is developed on the premise that individual components in the system experience what we define as a "2-phase" degradation pattern; i.e., a non-defective phase of operation followed by a phase of gradual degradation until failure. Note that this degradation pattern is typical in many mechanical applications. One example was presented in [42], where the authors considered the degradation of bearings and identified a similar "2-phase" pattern shown in Fig. 1. Recall that the amplitude of the defective frequency f^* is typically close to zero as long as no defect exists. Thus, during the non-defective phase of an individual component, the amplitude of

its degradation signal computed at f^* is typically close to zero. Once a defect occurs, it marks the beginning of the subsequent degradation phase, and is typically accompanied by a sudden spike in amplitude. This spike is considered as the "initial degradation level" of a component. Since we focus on the degradation of identical components, we assume that the initial degradation levels of identical opponents are equal to the same value, denoted as Z. The above "2-phase" phenomenon is the basis on which we develop the on-line amplitude recovery procedure.

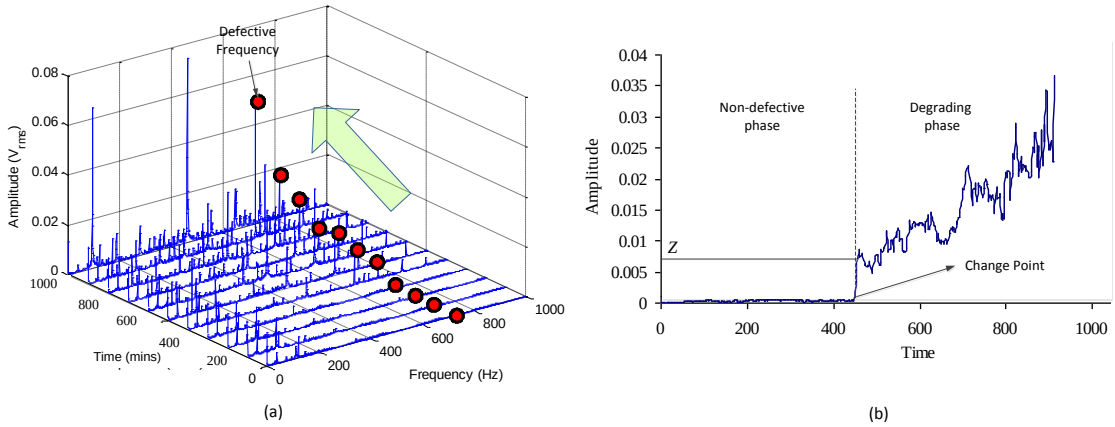

Figure 1: Signal characteristics

To better understand how the on-line amplitude recovery works, first assume that matrix $\hat{\mathbf{A}}$ has been evaluated by applying ICA to a historical database of training signals with characteristics discussed earlier in the chapter. Now consider a system consisting of at least 2 or more identical components, and assume that real-time vibration signals are being measured by multiple sensors. Using $\hat{\mathbf{A}}$, we can separate the degradation signals of the identical components in real-time. Next, we assume that at any time instance only one component transitions from the non-defective phase into the degradation phase. Then, we let $t_{(1),d}$ denote the transition time of the first degraded component, where subscript d corresponds the onset of the degradation phase. From a practical standpoint, $t_{(1),d}$ can be identified by applying an online change point detection algorithm such as CUSUM [14] to the component degradation

signals. Therefore, before $t_{(1),d}$, all components are in the non-defective phase, and all sensors exhibit closed-to-zero amplitude at f^*. At $t_{(1),d}$, only one component exhibit a spike at frequency f^*, which causes all sensors to exhibit a spike at f^* at this time epoch with various amplitudes. We denote the highest amplitude among all sensors at epoch $t_{(1),d}$ as $\max(\mathbf{x}^{f^*}(t_{(1),d}))$. By the assumptions made in our framework, $\max(\mathbf{x}^{f^*}(t_{(1),d}))$ will likely correspond to the sensor that is closest to the component that first degrades, and thus, will be most sensitive to the initial degradation level Z. Consequently, we use $\max(\mathbf{x}^{f^*}(t_{(1),d}))$ as an estimator of the initial degradation level Z.

For every component j, we expect to capture its transition time, denoted as $t_{j,d}$, using an online change-point detection algorithm such as CUSUM [14]. At $t_{j,d}$, the corresponding amplitude of the unscaled degradation signal of component j is denoted as $\tilde{s}_j^{f^*}(t_{j,d})$. Recall that the true degradation signal of component j at $t_{j,d}$ should be equal to Z, which can be estimated by $\max(\mathbf{x}^{f^*}(t_{(1),d}))$. Thus, the ratio of its true degradation signal to its un-scaled degradation signal (i.e. the "re-scaling ratio"), R_j, is defined as:

$$R_j = \frac{\max(\mathbf{x}^{f^*}(t_{(1),d}))}{\tilde{s}_j^{f^*}(t_{j,d})} \quad for\ j = 1, 2, ..., n. \tag{7}$$

Consequently, the true amplitude of the component's degradation signal can be recovered according to

$$\hat{s}_j^{f^*}(t_k) = R_j \times \tilde{s}_j^{f^*}(t_k) \tag{8}$$

where $\tilde{s}_j^{f^*}(t_k)$ is the amplitude of the unscaled component signal evaluated using ICA at time t_k and $\hat{s}_j^{f^*}(t_k)$ is the corresponding "re-scaled" degradation signal.

Remark: $\max(\mathbf{x}^{f^*}(t_{(1),d}))$ is maximized when dedicated sensors are placed directly on the components being monitored. That is, the highest amplitude among all sensors at the first on-set of a defect will be "almost equivalent" to that of the initial degradation level. Under this condition, the amplitudes of component degradation

signals will be completely recovered. However, since this work is focused on applications with physical and functional restrictions on sensor placement, the proposed amplitude recovery procedure provides only an approximate method for recovering the amplitude information.

Figure 2 summarizes the first stage of the proposed methodology described in Sections 3.1 and 3.2. The first graph in Fig. 2 illustrates the time-domain periodic waveform acquired by two sensors $x_1(t_k)$ and $x_2(t_k)$, as an example. Each waveform is assumed to contain a specific defective frequency f^*. The real-parts of the DFTs of $x_1(t_k)$ and $x_2(t_k)$ are shown in the second graph, in which the values of the two sensors at f^* are selected as $x_{1,R}^{f^*}(t_k)$ and $x_{2,R}^{f^*}(t_k)$. The third graph shows the two real sensor signals constructed by successive sampling. The fourth graph illustrates the signal detrending by computing sensor increments $\Delta X_1^{f^*}$ and $\Delta X_2^{f^*}$. Next, ICA is applied to $\Delta X_1^{f^*}$ and $\Delta X_2^{f^*}$ to estimate the mixing matrix $\tilde{\mathbf{A}}$, which is then utilized to estimate the un-scaled degradation signals, denoted as $\tilde{s}_1^{f^*}(t_k)$ and $\tilde{s}_2^{f^*}(t_k)$ $k = 1, 2, \ldots, M$, illustrated in the fifth graph. The sixth graph illustrates the amplitude recovery procedure and plots the estimated amplitude of the component signals $\hat{s}_1^{f^*}(t_k)$ and $\hat{s}_2^{f^*}(t_k)$, $k = 1, 2, \ldots, M$.

3.3 Degradation Modeling and Prognostics

The second stage of our prognostic framework incorporates an adaptive prognostics model to characterize component degradation signals. This prognostics model is developed on the premise that the functional form of a component degradation signal can be modeled as a continuous-time continuous-state stochastic process, which is similar to the one presented in [42]. After the model is developed, the RLDs of individual components can be updated in real-time using partially-observed component degradation signals. The residual lifetime of each component is defined as the time required for the trajectory of the component degradation signal to reach a pre-specified

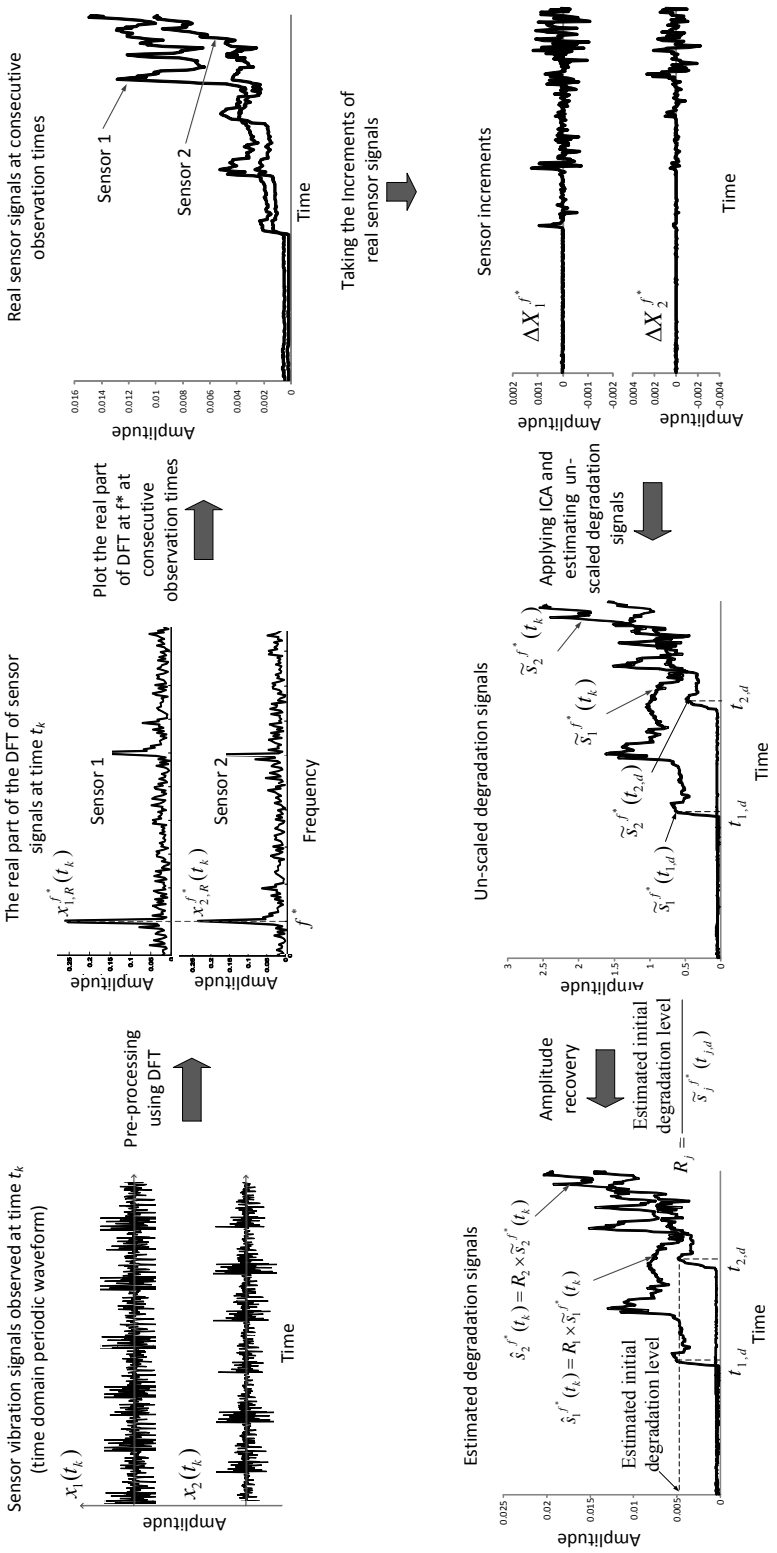

Figure 2: The procedure of the first stage in our proposed framework

failure threshold.

The prognostics model for a specific component j can be expressed as follows:

$$s_j^{f^*}(t) = \eta(t; \mathbf{\Theta}_j, \mathbf{\Phi}) + \epsilon(t), \tag{9}$$

where $s_j^{f^*}(t)$ represents the degradation signal of component j, $\eta(\cdot)$ represents the parametric functional forms used to model the path of the degradation signal (e.g., linear, exponential, polynomial), $\mathbf{\Phi}$ is a vector of known coefficients that are assumed to be the same for all identical components, $\epsilon(t)$ represents the signal noise and is assumed to be a Brownian motion, and $\mathbf{\Theta}_j$ is a vector of stochastic coefficients that takes a unique value for each specific component j. In another words, the values of the stochastic coefficients may differ for individual identical components, which represents the "unit-to-unit variability" that exists between identical components due to manufacturing differences, material inhomogeneity, etc.. To capture the unit-to-unit variability, we assume that the actual value of $\mathbf{\Theta}_j$ is unknown for component j but is expected to follow a known prior distribution, whose pdf is denoted by $\pi(\mathbf{\Theta}_j)$.

Remark: The assumption of Brownian motion error has been widely used to characterize the stochastic error in the literature of degradation modeling [36, 42, 106]. This assumption is only for the purpose of degradation modeling and not related to the success of the signal separation stage, which relies on the assumption that all component increments are statistically independent and non-Gaussian. This assumption can still be satisfied if the noise term $\epsilon(t)$ follows another type of stochastic process.

We denote the residual lifetime of component j as T_j. Before the component starts to degrade, its residual lifetime is equivalent to its lifetime. The cdf of its lifetime (i.e., the probability that T_j is less than some time t), which is equivalent to the probability that the trajectory of the degradation signal reaches the pre-defined

threshold (denoted by γ) before t, is given by the following expression:

$$\begin{aligned} Pr(T_j \leq t) &= Pr(s_j^{f^*}(t) \geq \gamma) \\ &= \int_{\mathbf{\Theta_j}} Pr(s_j^{f^*}(t) \geq \gamma \mid \mathbf{\Theta}_j)\pi(\mathbf{\Theta}_j)d\mathbf{\Theta}_j \end{aligned} \tag{10}$$

As the real-time observations of its component degradation signal become available, the posterior distribution of $\mathbf{\Theta}_j$ can be updated given the observations using a Bayesian approach. For example, if a sequence of degradation signals $s_j^{f^*}(t_1)$,$s_j^{f^*}(t_2)$, $\ldots$, $s_j^{f^*}(t_k)$ is observed at the following times $t_1, t_2, \ldots, t_k$, then the posterior distribution of $\mathbf{\Theta}_j$ evaluated at observation time t_k can be expressed as follows:

$$p(\mathbf{\Theta}_j|s_j^{f^*}(t_1), s_j^{f^*}(t_2), \ldots, s_j^{f^*}(t_k)) \propto l(s_j^{f^*}(t_1), s_j^{f^*}(t_2), \ldots, s_j^{f^*}(t_k)|\mathbf{\Theta}_j)\pi(\mathbf{\Theta}_j), \tag{11}$$

where $p(\mathbf{\Theta}_j|s_j^{f^*}(t_1), s_j^{f^*}(t_2), \ldots, s_j^{f^*}(t_k))$ is the posterior distribution of the stochastic coefficients updated at the t_k, $l(s_j^{f^*}(t_1), s_j^{f^*}(t_2), \ldots, s_j^{f^*}(t_k)|\mathbf{\Theta}_j)$ is the likelihood function, and $\pi(\mathbf{\Theta}_j)$ is the prior distribution of $\mathbf{\Theta}_j$.

After the posterior distribution is evaluated, the cdf of the RLD of the component satisfies a similar expression to Eq. 10 as follows:

$$\begin{aligned} &Pr(T_j \leq t|s_j^{f^*}(t_1), \ldots, s_j^{f^*}(t_k)) \\ &\quad = Pr(s_j^{f^*}(t+t_k) \geq \gamma \mid s_j^{f^*}(t_1), \ldots, s_j^{f^*}(t_k)) \\ &\quad = \int_{\Theta_j} Pr(s_j^{f^*}(t+t_k) \geq \gamma \mid \mathbf{\Theta}_j)p(\mathbf{\Theta}_j|s_j^{f^*}(t_1), \ldots, s_j^{f^*}(t_k))d\mathbf{\Theta}_j \end{aligned} \tag{12}$$

the Bayes framework improves the prediction of RLD by reducing the uncertainty corresponding to the posterior distribution of $\mathbf{\Theta}_j$.

Figure 3 provides an overall illustration of the RLD updating framework using a real-time component degradation signal. When no observations are available at time t_0 (as shown in the first graph), the life distribution is computed based on the prior information of the stochastic parameter $\mathbf{\Theta}_j$. When the component degradation signal is observed up to t_1 (as shown in the second graph), the posterior distribution

of $\boldsymbol{\Theta}_j$ is updated using the Bayesian approach. Using the degradation model with the updated parameter, we can develop the posterior RLD for the partially degraded component. Furthermore, when the component degradation signal is observed up to t_2 (as shown in the third graph), the posterior distribution of $\boldsymbol{\Theta}_j$ is further updated, which can be used to revise the posterior RLD for the component.

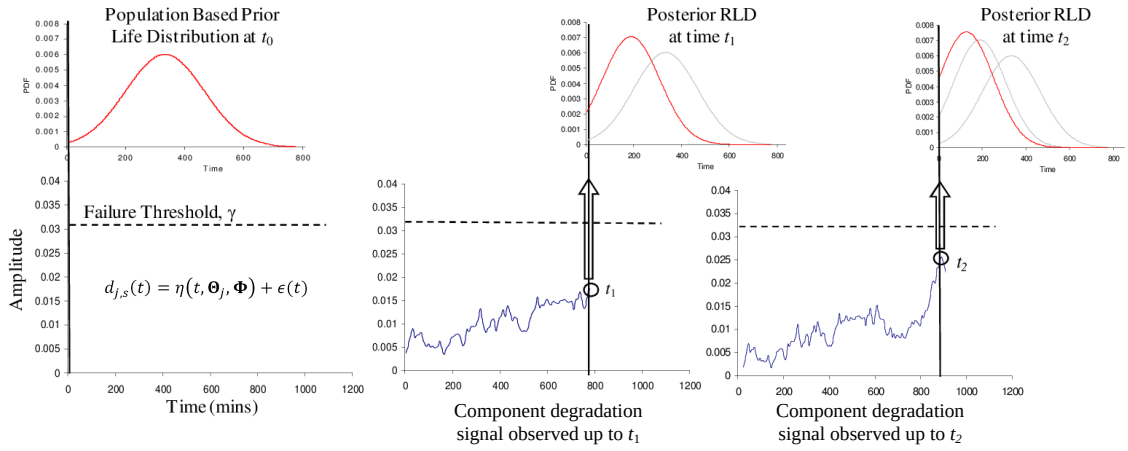

Figure 3: The RLD updating process for the component level adaptive prognostic methodology

For demonstration purpose, we utilize the base case model presented in [42], which considered an exponential functional form with a multiplicative Brownian motion error, to study the performance of our methodology. This base-case model is incorporated in our simulation study. According to this model, the degradation signal of the j^{th} $(j = 1, 2, \ldots, n)$ component is characterized by the following expression:

$$s_j^{f^*}(t) = Z \exp(\beta_j t + \epsilon(t)) \tag{13}$$

where Z is the constant initial degradation level that we have discussed in Section 3.2.2, β_j represents the degradation rate of component j, and $\epsilon(t)$ represents the error fluctuations and is assumed to be a centered Brownian motion with variance $\sigma^2 t$. In this base-case model, the stochastic parameter is β_j, whose prior distribution is assumed to be normal with mean μ_1 and variance σ_1^2. Note that μ_1, σ_1^2, and σ^2 are

assumed to take the same values for identical components.

Given that we have observed the following sequence of degradation signals $s_j^{f^*}(t_1)$, $s_j^{f^*}(t_2)$, ..., $s_j^{f^*}(t_k)$, the posterior distribution of β_j follows a normal distribution with mean $\mu_{j,k}$ and variance $\sigma_{j,k}^2$, where

$$\mu_{j,k} = \frac{\sigma_1^2 \ln(s_j^{f^*}(t_k)) + \mu_1 \sigma^2}{\sigma_1^2 t_k + \sigma^2},$$
$$\sigma_{j,k}^2 = \frac{\sigma^2 \sigma_1^2}{\sigma_1^2 t_k + \sigma^2}.$$

Consequently, the RLD of a component j evaluated at time t_k is given as:

$$Pr(T_j \leq t \mid s_j^{f^*}(t_1), \ldots, s_j^{f^*}(t_k)) = Pr(\ln(s_j^{f^*}(t_k + t)) \geq \gamma \mid s_j^{f^*}(t_1), \ldots, s_j^{f^*}(t_k)) \quad (14)$$
$$= \Phi(\frac{\tilde{\mu}_j(t_k + t) - D}{\tilde{\sigma}_j(t_k + t)}),$$

where $\Phi(\cdot)$ is the cdf of a standard normal random variable, $\tilde{\mu}_j(t_k + t) = \ln(s_j^{f^*}(t_k)) + \mu_{j,k} t$ and $\tilde{\sigma}_j^2(t_k + t) = \sigma_{j,k}^2 t^2 + \sigma^2 t$. The median of the RLD is used as a prediction of the residual lifetime.

3.4 A Numerical Example Using Simulated Degradation Signals

In this section, we use simulated degradation signals to evaluate the performance of our proposed methodology. First, we will describe the simulation set-up and the procedure. Then, we will conduct sensitivity analysis on variables that may affect the performance of the signal separation stage, which include the level of noise in component degradation signals ("degradation noise" for short) and the correlation between component increments. Finally, we will investigate the sensitivity of the residual life prediction to the correlation between component increments, the degradation noise, and the re-scaling ratio discussed in Section 3.2.2.

3.4.1 Simulation Set-up and Procedure

In our numerical example, we consider a system with two identical components whose degradation processes can be monitored using three vibration sensors. We design this

specific set-up according to the assumption that the number of sensors, denoted as m, is greater than or equal to the number of components, denoted as n, which is a general assumption that guarantees full column rank of the mixing matrix $\mathbf{A}$. Fig. 4 shows the hypothetical system used for our simulation study. The three sensors are labeled as "Sensor 1", "Sensor 2", and "Sensor 3", whereas the components are labeled as "Component A", and "Component B". In reality, this system simulates a gearbox with two identical bearings (A and B). Sensors 1, 2, and 3 represent 3 accelerometers mounted on the outside of the gearbox.

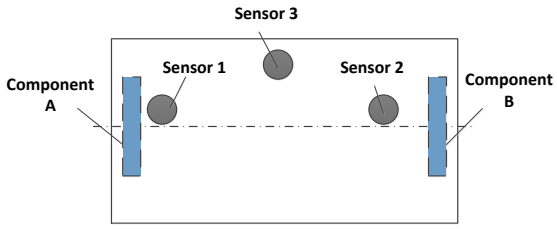

Figure 4: Simulation set-up

We assume the vibration signals measured by each sensor is a linear combination of the vibration resulting from potential defects on Component A and/or B. For illustrative purposes, we define the mixing matrix $\mathbf{A}$ as $[0.9, 0.6; 0.6, 0.8; 0.7, 0.7;]$. The specific value of each element of $\mathbf{A}$, denoted by $a_{i,j}$ (for $i = 1, 2, 3$ and $j = 1, 2$), represents the proportion of the vibration signal of component j captured by sensor i, which depends on the relative distance between the sensor and the component. Specifically, the value of each element is positively correlated with the inverse of the corresponding distance, and it cannot exceed 1 unless the sensor is dedicated to the component.

In what follows, we outline the steps used to simulate the signals in this numerical study:

1. For each component j, we simulate the time corresponding to the change-point of its degradation signal, $t_{j,d}$, using the uniform distribution $U[10, 50]$. In other

words, the period $[0, t_{j,d}]$ corresponds to the length of the non-defective phase of component degradation signal j.

2. For each component j, $j = 1, 2$, we simulate the time-domain vibration signal for each time t_k, $k = 1, \ldots, M$, which we denote by $s_j(t_k)$. t_1 and t_M represent the time epochs when the system initially starts to operate and when the system stops, respectively. t_M is expected to be long enough to have two components run to failure. Specifically, $M = 300$ in this study. For $t_k < t_{j,d}$, we let the amplitude of $s_j(t_k)$ at the defective frequency f^* be a small value close to zero. In this study, the amplitude is randomly chosen from the following distribution $U[4\times10^{-4}, 6\times10^{-4}]$. For $t_k \geq t_{j,d}$, we let the amplitude of $s_j(t_k)$ at the defective frequency f^* increase randomly in t_k according to the stochastic model expressed in Eq. 13. The simulated component vibration signals for Components A and B can be represented as $s_1(t_k)$ and $s_2(t_k)$.

3. We compute the corresponding sensor vibration signals, $x_1(t_k)$, $x_2(t_k)$, and $x_3(t_k)$ based on $s_1(t_k)$ and $s_2(t_k)$ using Eq. 2. We use the mixing matrix $\mathbf{A}$ defined earlier in this section. Examples of component vibration signals $s_1(t_k)$ and $s_2(t_k)$ and sensor vibration signals $x_1(t_k)$, $x_2(t_k)$, and $x_3(t_k)$ are shown in Fig. 5. As mentioned earlier in Section 3, component degradation signals are obtained by taking the exact amplitude of the component vibration signals at frequency f^*. The two component degradation signals are detonated as $s_1^{f^*}(t_k)$ and $s_2^{f^*}(t_k)$, for $k = 1, \ldots, M$.

4. The sensor vibration signals $x_1(t_k)$, $x_2(t_k)$, and $x_3(t_k)$ are then used to compute the estimated degradation signals $\hat{s}_1^{f^*}(t_k)$ and $\hat{s}_2^{f^*}(t_k)$. To do this, we follow the procedure outlined in Fig. 2. The estimated degradation signals are used to predict the RLD of each component using the base-case model discussed in Section 5. The median of the RLD is utilized as a prediction of the residual

lifetime of each component.

5. To be able to benchmark the performance of our model, we compare the residual life predictions computed using the estimated degradation signals $\hat{s}_1^{f^*}(t_k)$ and $\hat{s}_2^{f^*}(t_k)$ with those computed using the true component degradation signals $s_1^{f^*}(t_k)$ and $s_2^{f^*}(t_k)$. The residual life predictions of the true degradation signals are also computed using the base-case model discussed in Section 5. The accuracy of the prediction is evaluated using the following equation:

$$\text{error} = \frac{|\text{Predicted Lifetime - Actual Lifetime}|}{\text{Actual Lifetime}},$$

where the "Actual Lifetime" is the time point at which the component degradation signal crosses a pre-specified failure threshold, and the "Predicted Lifetime" is equal to the observation level plus the predicted residual lifetime.

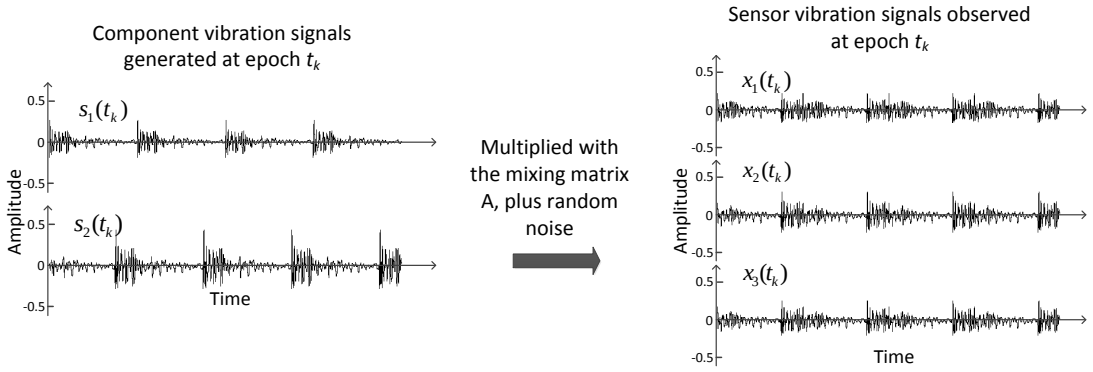

Figure 5: Sample time-domain component vibration signals (on the left) and the corresponding sensor vibration signals (on the right)

Figure 6 presents an example of a pair of component degradation signals (represented by solid curves) and their corresponding estimated signals (represented by dashed curves). The horizontal line drawn at 0.025 in Fig. 6 represents the failure threshold. From Fig. 6, we observe that the shape of a component degradation signal can be estimated accurately, but the amplitude of the signal is not completely recovered. This bias is mainly due to the amplitude recovery procedure.Particularly,

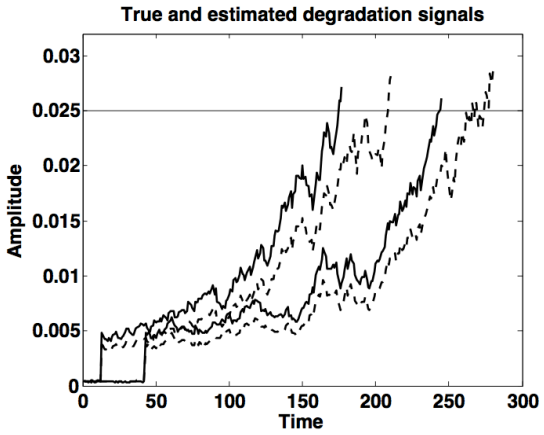

Figure 6: An example of true degradation signals and the corresponding estimated degradation signals

due to the bias/error induced by the amplitude recovery procedure, at the time epoch when the true degradation signal crosses the failure threshold (i.e. the true failure time), the estimated degradation signal has not yet crossed the failure threshold. Consequently, the estimated signal takes a slightly longer time to reach the failure threshold.

3.4.2 Sensitivity Analysis of the Signal Separation Stage

The performance of the signal separation stage relies on the effectiveness of ICA. One of the necessary assumption for using ICA is the independence between the component increments. In this section, we study the performance of ICA when this assumption is not satisfied. This is accomplished by adjusting the correlation coefficient between the Brownian motion errors of the two component degradation signals. In addition, we also study the impact of the degradation noise on the effectiveness of the ICA algorithm. The noise level is controlled by the variance of the Brownian motion error in a component degradation signal.

The performance of the signal separation is evaluated by the difference between the true and the estimated mixing matrices, in which the value of the true matrix has been specified earlier in this section. Since the ICA algorithm can not preserve the norm

of each column in the matrix (as discussed in Section 4), we focus on comparing the normalized matrices to remove any unnecessary biases. We let $\mathbf{A}^N$ and $\hat{\mathbf{A}}^N$ denote the normalized matrices of the true $\mathbf{A}$ and the estimated matrix $\hat{\mathbf{A}}$. Each column of the normalized matrix is computed by normalizing the corresponding column of the original matrix. The value of $\mathbf{A}^N$ is $\mathbf{A}^N = [0.6985, 0.4915; 0.4657, 0.6554; 0.5433, 0.5735]$. We compare $\hat{\mathbf{A}}^N$ with $\mathbf{A}^N$ using the Frobenius norm of $\delta\mathbf{A}^N = \hat{\mathbf{A}}^N - \mathbf{A}^N$, which is considered as a measurement of the estimation error of the mixing matrix.

Signal separation is performed at 10 levels of correlation, (correlation coefficient equal to $0, 0.1, \ldots, 0.9$), and 10 levels of degradation noise (the variance of the Brownian motion error equal to $0.0005, 0.001, \ldots, 0.005$). Fig. 7 illustrates three sample degradation signals corresponding to three levels of the Brownian motion variance: 0.0005, 0.0015, and 0.0025. It is clear that the degradation signal with a higher Brownian motion variance is more noisy.

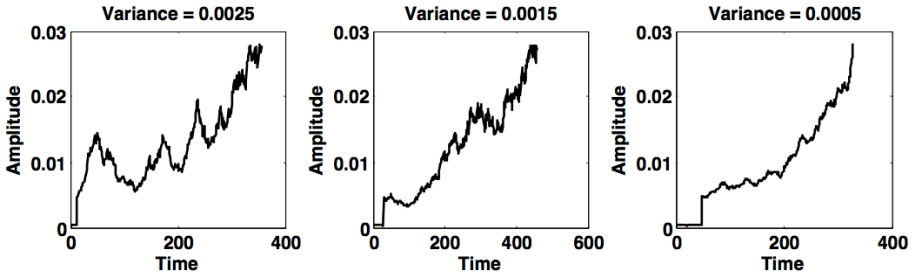

Figure 7: Sample signals corresponding to three variance levels

In total, there are $10 \times 10 = 100$ testing scenarios. For each scenario, we conduct 200 rounds of simulations. The signals from each round is utilized to compute $\hat{\mathbf{A}}$ as well as the corresponding $\| \delta\mathbf{A}^N \|_F$. Then, we choose the median of these 200 values for $\| \delta\mathbf{A}^N \|_F$'s as a point estimator of the estimation error. Fig. 8 shows the estimation errors for the 100 scenarios.

It is clear that the estimation error increases as the level of correlation increases. This is expected since increasing the correlation results in greater deviations from the assumption of independence. On the other hand, the level of Brownian motion

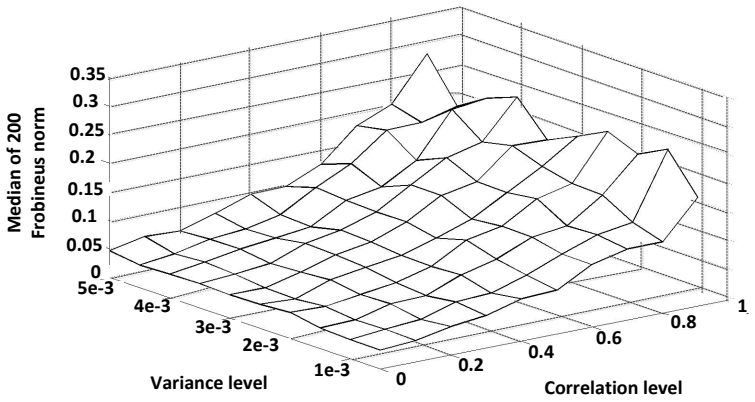

Figure 8: The median of 200 Frobenius norms under 100 conditions

variance does not exhibit a significant impact on the estimation error. We believe the reason for this is that the level of degradation noise mainly affects the amplitude of the component increments. Since ICA does not preserve amplitude information, changing the noise level has little effect on the performance of ICA.

3.4.3 Sensitivity Analysis of the Residual Life Prediction

In this section, we will investigate the effects of three variables on accuracy of the residual life prediction. The first variable is the degradation noise. Although this variable does not significantly affect the signal separation stage as we have investigated, it may affect the stage of prognostics, since a higher noise in the degradation signals may reduce the effectiveness of residual life prediction. The second variable is the correlation between component increments. From Section 3.4.2, we have concluded that this correlation affects signal separation. Thus, it will also affect the residual life prediction. The third variable is the re-scaling ratio. How well we estimate the re-scaling ratio has a direct impact on the efficiency of the amplitude recovery, and thus will impact the residual life prediction.

3.4.3.1 The impact of degradation noise

In this study, we investigate the effect of degradation noise on residual life prediction. Similar to Section 3.4.2, the noise level is controlled by tuning the variance parameter of the Brownian motion. We investigate the effects of three levels of variance: 0.0025, 0.0015, 0.0005. Three sample degradation signals corresponding to the three variance levels are already shown earlier in Fig. 7.

For each level of variance, 100 simulation runs are performed, out of which 20 are used as training signals to estimated the mixing matrix. The average of the 20 estimated matrices is utilized as the final estimator of the mixing matrix $\hat{\mathbf{A}}$. The rest 80 runs are used for validation. For each round in the validation set, the estimation $\hat{\mathbf{A}}$ is applied to compute the estimated degradation signals of both components in this round. Next, we assume each estimated degradation signal is partially observable up to several lifetime percentiles (evaluated post facto): 10%, 20% until 90% of the component's actual lifetime. For each component, given its partially-observed degradation signal, we predict its residual lifetime and calculate the corresponding prediction error. The prediction errors at different lifetime percentiles for the 80 rounds of simulation in the validation set are summarized in Fig. 9, where Parts (a), (b), and (c) correspond to the three variance levels. The right column of Fig. 9 illustrates the prediction errors associated with the estimated degradation signals, while the left column presents the prediction errors using the true degradation signals as the benchmark.

We conduct a one-side t-test, a one-side F-test, and a one-side Wilcoxon rank sum test to compare the mean, the variance, and the median of the prediction errors of the estimated versus the true degradation signals. The null hypothesis for each of the three tests is that the corresponding statistics (the mean, the variance, or the median) of the prediction errors of true and estimated degradation signals are equal. The alternative hypothesis is that the corresponding statistics of the prediction errors

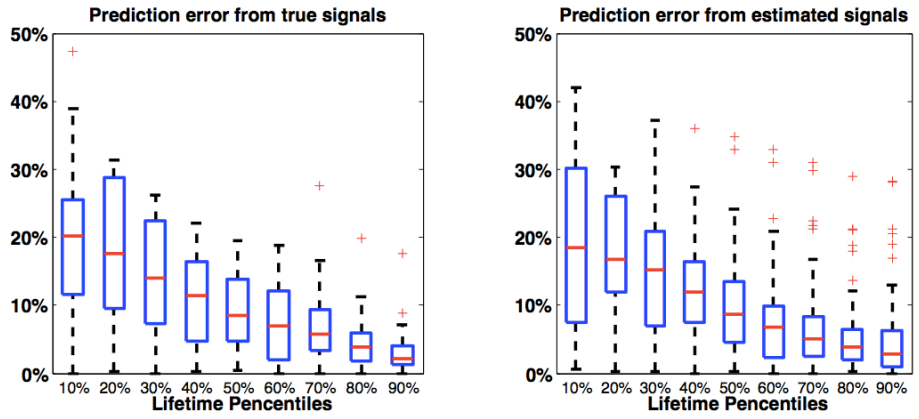

(a) Variance=0.0025

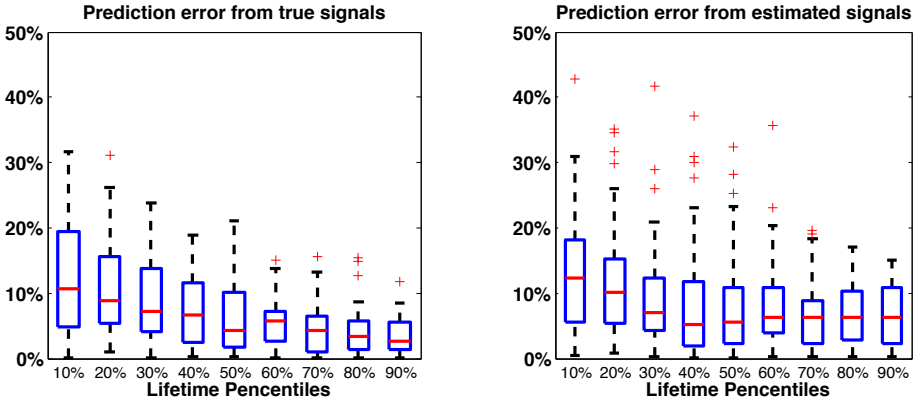

(b) Variance=0.0015

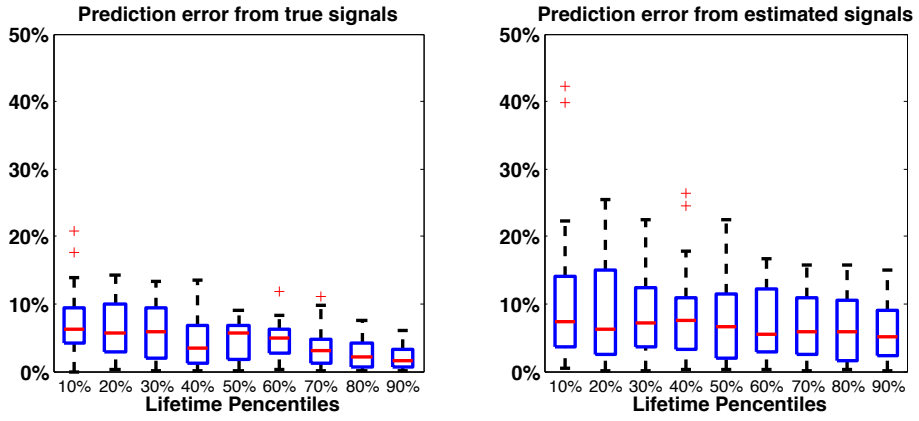

(c) Variance=0.0005

Figure 9: Comparing prediction errors from true and estimated component signals at three variance levels

of estimated degradation signals is higher than that of the prediction errors of true degradation signals. The significance of a test is represented by the p-value.

The corresponding p-values are listed below in Tables 1, 2, and 3, with p-values smaller than 0.05 highlighted in boldface. According to the tables, each hypothesis test is conducted under various conditions including different variance levels of the Brownian motion error and different levels of the lifetime percentile. The p-values smaller than 0.05 indicate that we will reject the null hypothesis at 5% significant level under the corresponding test conditions. In other words, under the corresponding conditions, we can conclude that the corresponding statistics of the prediction errors of estimated degradation signals is significantly higher than that of the prediction errors of true degradation signals.

Table 1: The p-values of the t-test corresponding to the three variance groups

Percentile	10%	20%	30%	40%	50%	60%	70%	80%	90%
Var=0.0025	0.587	0.689	0.707	**0.0405**	0.213	0.222	0.219	**0.023**	$\mathbf{2.26e^{-3}}$
Var=0.0015	0.192	0.103	0.106	0.095	**0.042**	**0.0041**	**0.006**	**0.0013**	$\mathbf{2.8e^{-5}}$
Var=0.0005	**0.045**	**0.013**	**0.0049**	**0.0030**	**0.0042**	**0.0028**	$\mathbf{5.8e^{-4}}$	$\mathbf{3.4e^{-5}}$	$\mathbf{1.1e^{-6}}$

Table 2: The p-values of the f-test corresponding to the three variance groups

Percentile	10%	20%	30%	40%	50%	60%	70%	80%	90%
Var=0.0025	0.207	0.628	0.207	0.469	**0.014**	**0.018**	$\mathbf{9e^{-4}}$	$\mathbf{1.9e^{-7}}$	$\mathbf{1.8e^{-12}}$
Var=0.0015	**0.0041**	$\mathbf{3e^{-4}}$	$\mathbf{1e^{-4}}$	$\mathbf{9e^{-4}}$	$\mathbf{2e^{-4}}$	$\mathbf{9e^{-4}}$	$\mathbf{8e^{-4}}$	**0.0010**	$\mathbf{1e^{-4}}$
Var=0.0005	$\mathbf{1e^{-4}}$	$\mathbf{2e^{-4}}$	**0.0024**	**0.0032**	$\mathbf{8e^{-4}}$	$\mathbf{2e^{-4}}$	$\mathbf{9e^{-4}}$	$\mathbf{4e^{-4}}$	$\mathbf{1.1e^{-6}}$

Table 3: The p-values of the Wilcoxon rank sum test corresponding to the three variance groups

Percentile	10%	20%	30%	40%	50%	60%	70%	80%	90%
Var=0.0025	0.604	0.538	0.551	0.092	0.423	0.377	0.895	0.089	$\mathbf{2e^{-4}}$
Var=0.0015	0.169	0.152	0.189	0.506	0.098	**0.010**	**0.0036**	$\mathbf{5e^{-4}}$	$\mathbf{1e^{-4}}$
Var=0.0005	0.547	0.270	0.216	**0.0003**	**0.017**	**0.047**	**0.0026**	$\mathbf{3e^{-4}}$	$\mathbf{1.3e^{-5}}$

From Fig. 9 and Tables 1, 2, and 3, we can summarize the following observations:

1. The prediction errors of both true and estimated degradation signals decrease

as the variance of the Brownian motion decreases. This is expected because reducing the noise level usually improves predictability.

2. For each type of hypothesis test, the number of lifetime percentiles associated with p-values smaller than 0.05 increases as the noise level decreases. This observation may be due to the fact that when using true component signals, reducing the noise level directly results in significant improvements in prediction accuracy. However, this is not necessarily the case for the estimated component signals, as there is an additional error that is introduced by the signal separation step. Reducing degradation noise does not improve the performance of signal separation as discussed in Section 3.4.2.

3.4.3.2 The effect of correlation between component increments

As demonstrated in Section 3.4.2, the correlation between component signals significantly affects the signal separation step. Here, we evaluate the accuracy of residual life prediction under different correlation levels. Similar to Section 3.4.2, we control the correlation by adjusting the correlation coefficient between the Brownian motion errors of the two component degradation signals. We test three levels of correlation coefficient: 0, 0.5, and 1. Signals are simulated and prediction errors are evaluated in a similar manner to what is presented in Section 3.4.3. The prediction errors are shown in Fig. 10, in which the left and right columns correspond to the prediction errors of true and estimated degradation signals, respectively. From Fig. 10, it is clear that when the correlation coefficient is zero, there is no significant difference between the prediction errors from estimated signals versus those evaluated using the true signals. However, as the correlation coefficient is increased to 0.5 and 1, the accuracy of the residual-life prediction decreases significantly. The reason is that increasing the correlation coefficient will contaminate the accuracy of the signal separation, which will eventually affect the accuracy of the residual life prediction.

3.4.3.3 The effectiveness of the online amplitude recovery procedure

Here, we focus on the impact of the amplitude recovery procedure on the accuracy of residual life prediction. An important factor that affect the performance of the amplitude recovery procedure is the re-scaling ratio. In Section 3.2.2, we have discussed that the value of the re-scaling ratio depends on how well we estimate the initial degradation level Z. In this section, we test the effect of 4 different estimates of Z on the accuracy of the residual life prediction. The first estimates is equal to the true value of Z, which will recover 100% of the amplitude. To choose the second value, we note that $\mathbf{A} = [0.9, 0.6; 0.6, 0.8; 0.7, 0.7;]$, which indicates that $x_1(t_k) = 0.9s_1(t_k) + 0.6s_2(t_k) + e_1(t_k)$, $x_2(t_k) = 0.6s_1(t_k) + 0.8s_2(t_k) + e_2(t_k)$, $x_3(t_k) = 0.7s_1(t_k) + 0.7s_2(t_k) + e_3(t_k), k = 1, 2, ...$ At time $t_{(1),d}$, if component A degrades first, we will have $\max(\mathbf{x}^{f^*}(t_{(1),d})) \approx 0.9Z$. On the other hand, if component B degrades first, we will have $\max(\mathbf{x}^{f^*}(t_{(1),d})) \approx 0.8Z$. In general, components A and B will have an equal probability to degrade. Thus, on average, the estimate is equal to $0.85Z$. The third and fourth estimates of Z are chosen to be $0.55Z$ and $0.25Z$, which corresponds to even worse estimates the re-scaling ratio.

Signals are simulated and prediction errors are evaluated in a similar manner to what is presented in Section 3.4.3. However, different from the previous simulation, we will not follow the re-scaling procedure described in Section 3.2.2 to estimate $\max(\mathbf{x}^{f^*}(t_{(1),d}))$. Instead, we will manually specify the value $\max(\mathbf{x}^{f^*}(t_{(1),d}))$ to be equal to one of the 4 values (Z, $0.85Z$, $0.55Z$, and $0.25Z$) and calculate the residual life predictions for each component at different lifetime percentiles. Fig. 11 illustrates the prediction errors under the four estimates of the initial degradation level. In this figure, the word "ratio" in the title of each graph represents the ratio of the estimate to the true Z. It can be seen that the prediction errors when ratio=1 and ratio=0.85 do not exhibit significant difference. This insignificance can be explained by Fig. 6, in which the estimated degradation signals (dashed curves) are biased

from the corresponding true degradation signals (solid curves). Although this bias is observable, the failure times of the estimated degradation signals are not significantly different from those of true degradation signals. Thus, we will not expect a significant difference between the lifetime prediction errors. However, the prediction errors increases significantly as the ratio decreases to 0.55 and further to 0.25. This is expected, since a significant decrease in the ratio will eventually results in unreliable prediction. In reality, the ratio is related to the distance between a sensor and a component. Therefore, we recommend that in order to improve the performance of the residual-life prediction for each individual component, at least one sensor should be located as close as possible to one of the components that are being monitored, especially if they are identical or generate the same signal frequency.

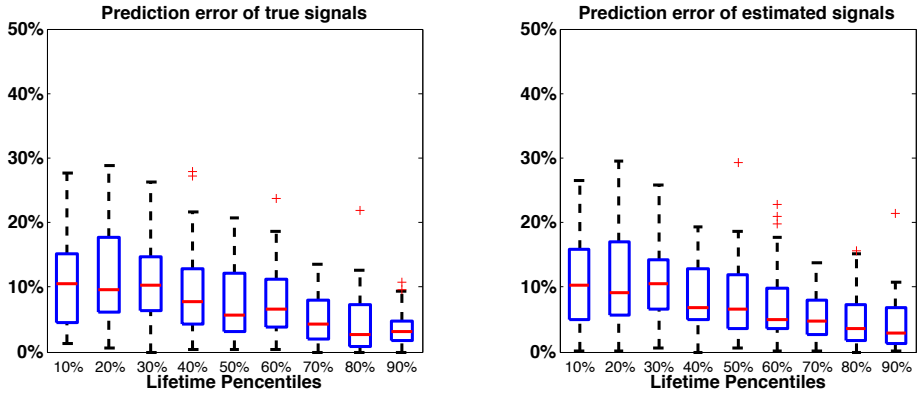

(a) correlation coefficient = 0

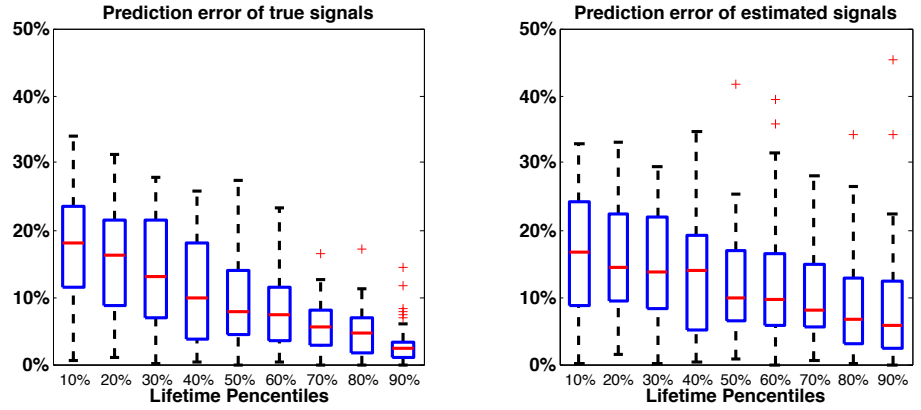

(b) correlation coefficient = 0.5

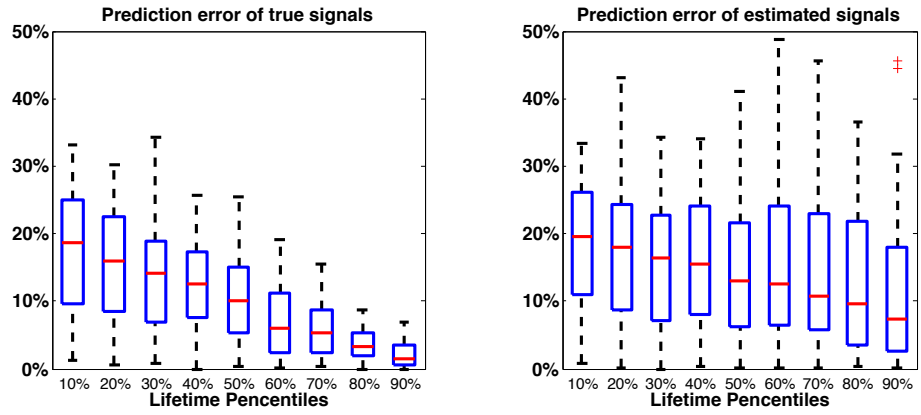

(c) correlation coefficient = 1

Figure 10: The accuracy of the residual-life prediction under three correlation levels

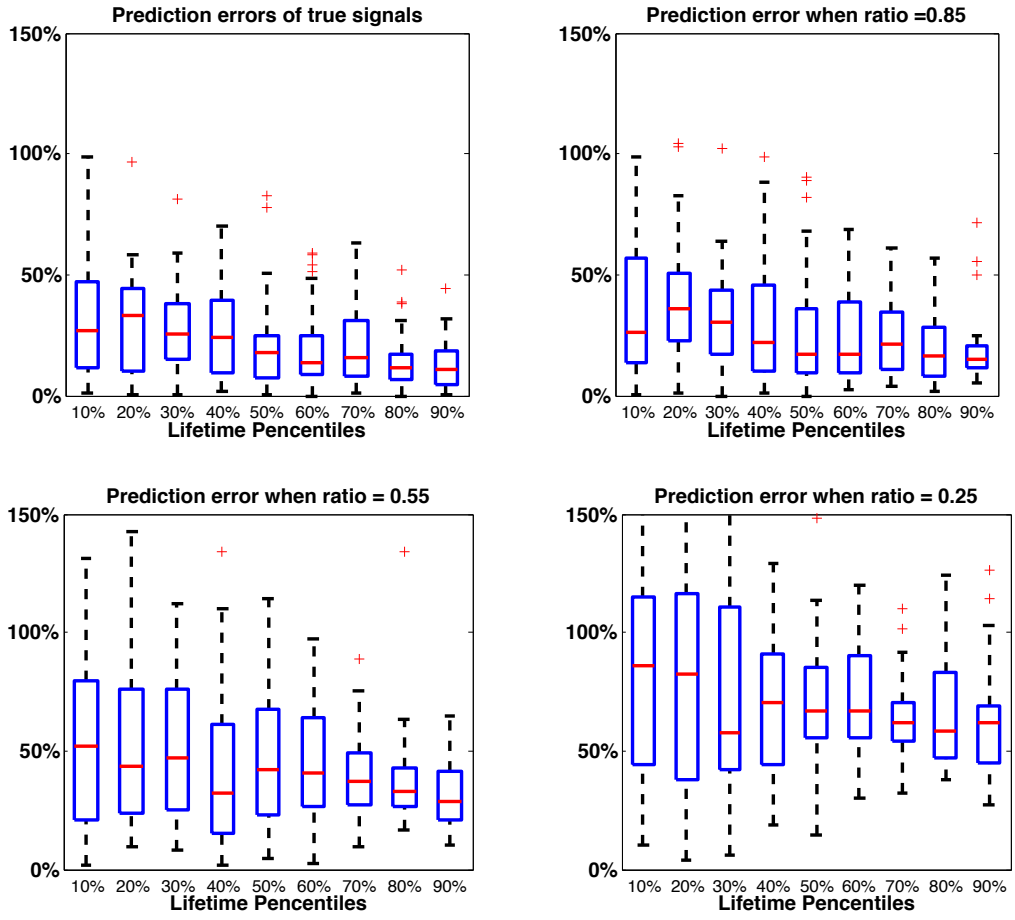

Figure 11: The accuracy of the residual-life prediction under different estimates of the initial degradation level

CHAPTER IV

RESIDUAL LIFE PREDICTION OF MULTISTAGE MANUFACTURING PROCESSES WITH INTERACTION BETWEEN TOOL WEAR AND PRODUCT QUALITY DEGRADATION

In this chapter, we characterize the interactive relationship between tool wear and product quality degradation in MMPs for the purpose of accurately predict the RLD of MMPs. We propose an interaction model that utilizes a linear model to represent the impact of tool wear on quality degradation and a stochastic differential equation model to capture the impact of quality degradation on the instantaneous rate of tool wear. We then propose a Bayesian framework that incorporates real-time quality measurements to on-line update the RLD of MMPs. We also conduct numerical studies to test the performance of our methodology and compare with an existing methodology.

This chapter is organized as follows: Section 4.1 presents the stochastic methodology used to model the interaction between tool wear and quality degradation. Section 4.2 discusses how to estimate the model parameters based on historical data, as well as how to predict and update the RLD of the MMPs. Section 4.3, we present a series of simulation-based numerical studies. The goal is to study the performance of our methodology and evaluate its sensitivity with respect to model parameters. Section 4.4 discusses the implementation of our proposed methodology in real-world industries.

4.1 Prognostics Model Considering Tool Wear and Quality Degradation Interaction

In this section, we first propose two individual models for characterizing the effect of tool wear on quality degradation and that of quality degradation on tool wear in MMPs, respectively. We assume that the instantaneous rate of tool wear is linearly dependent on quality degradation, which is modeled as a Brownian motion process with a linear drift that is a function of the level of quality degradation. Subsequently, the two models are synergized into a hybrid modeling framework to capture the interaction between tool wear and quality degradation. The hybrid modeling framework is eventually used to predict the distribution of the remaining time before an MMP produces a non-conforming product, i.e., the RLD of the MMP.

We consider an MMP with M stages, each of which is equipped with a single tool, and N quality measurement points. We let $S_m(t)$ represent the level of tool wear at stage m at time t for $m = 1, 2, \ldots, M$. Also, let $Y_n(t)$ represent the level of quality degradation (i.e., the deviation of the product quality measurement from its nominal value) at measurement point n for $n = 1, 2, \ldots, N$. Thus, $\mathbf{S}(t) = (S_1(t), S_2(t), ..., S_M(t))'$ and $\mathbf{Y}(t) = (Y_1(t), Y_2(t), ..., Y_N(t))'$ characterize tool wear and quality degradation at M stages and N quality measurement points, respectively. For example, in the sheet metal assembly process [61], $\mathbf{Y}(t)$ corresponds to the deviation of measurement points in the body coordinates and $\mathbf{S}(t)$ corresponds to the wear of locating pins. Another example is the stamping process [29], in which $\mathbf{Y}(t)$ represents the size of the burr on the edge of the part, and $\mathbf{S}(t)$ represents the tool wear of dies.

4.1.1 Modeling the Product Quality Degradation

We begin by formally characterizing the effect of tool wear on product quality degradation. We assume that the main assignable cause of part quality degradation is tool

wear. All other types of operational errors, such as fixture errors, location errors, and other sources can be lumped and considered as "process noise". The effect of tool wear and process noise on quality degradation is defined by the following linear model:

$$Y_n(t) = \mathbf{a}_n'\mathbf{S}(t) + \mathbf{b}_n'\mathbf{Z}(t), \tag{15}$$

for $n = 1, 2, \ldots, N$, where $\mathbf{Z}(t) = (Z_1(t), Z_2(t), ..., Z_P(t))'$ represents the process noise in MMPs. $\mathbf{a}_n = (a_{1,n}, a_{2,n}, \ldots, a_{M,n})'$ and $\mathbf{b}_n = (b_{1,n}, b_{2,n}, \ldots, b_{P,n})'$ are the coefficients that characterize how $\mathbf{S}(t)$ and $\mathbf{Z}(t)$ impact $Y_n(t)$, respectively. Typically, the values of $\mathbf{a}_n$ and $\mathbf{b}_n$ as well as the functional forms of $\mathbf{S}(t)$ and $\mathbf{Z}(t)$ can be determined based on specific applications, such as the auto-body assembly process [31]. We assume the following specific forms of $\mathbf{S}(t)$ and $\mathbf{Z}(t)$:

1. $\mathbf{Z}(t)$ follows a P-dimensional Brownian motion process with zero mean and covariance matrix $\mathbf{\Sigma_Z}t$.

2. $\mathbf{S}(t)$ evolves according to a vector of continuous stochastic processes, the specific form of which is presented in Section 4.1.2.

Hence, the matrix form of Eq. 15 can be rewritten as follows:

$$\mathbf{Y}(t) = \mathbf{A}'\mathbf{S}(t) + \mathbf{B}'\mathbf{Z}(t), \tag{16}$$

where $\mathbf{A}=(\mathbf{a}_1, \mathbf{a}_2, \ldots, \mathbf{a}_N)$ and $\mathbf{B}=(\mathbf{b}_1, \mathbf{b}_2, \ldots, \mathbf{b}_N)$.

The linear assumption presented in Eq. 15 and Eq. 16 has been systematically justified and widely used in the literature to character the tool wear on product quality in manufacturing processes [29, 31, 61, 109]. When the physical process knowledge is available, the linear functional form can be used as a reasonably good approximation to characterize the underlying process in many manufacturing systems. Some examples include the sheet metal assembly process [61] and the cylinder head machining process [52]. When the physical process knowledge is not available, the

authors in [109] suggests using this linear model since this linear model represents main effects, which usually have more significant impacts than higher order effects.

4.1.2 Modeling Tool Wear

Next, we develop a model that characterizes the effect of quality degradation on tool wear. Specifically, tool wear at stage m is modeled by the following SDE:

$$dS_m(t) = R_m^I(t)dt + dW_m(t), \tag{17}$$

for $m = 1, 2, \ldots, M$, where $R_m^I(t)$ represents the instantaneous rate of tool wear that is governed by the level of quality degradation, and $W_m(t)$ is a Brownian motion process with the diffusion parameter $\sigma_{W,m}$ and is used to capture the randomness of the tool wear process. Thus, $W_m(t)$ is a stochastic process with independent increments that follow a normal distribution with zero mean and variance $\sigma_{W,m}^2 t$. $W_m(t)$ is assumed to be statistically independent from $\mathbf{Z}(t)$.

We focus on a base-case stochastic model where the instantaneous wear rate $R_m^I(t)$ takes the linear form expressed below:

$$R_m^I(t) = R_m + \mathbf{c}_m' \mathbf{Y}(t), \tag{18}$$

for $m = 1, 2, \ldots, M$, where R_m represents the natural rate of tool wear at stage m, and the second part captures the rate of tool wear affected by quality degradation with $\mathbf{c}_m = (c_{1,m}, c_{2,m}, \ldots, c_{N,m})'$ being an N-dimensional column vector of coefficients describing how quality degradation, $\mathbf{Y}(t)$, impacts the instantaneous rate of tool wear. The linear assumption presented in Eq. 18 is a special case of the phenomenon that the tool wear at a subsequent stage is positively correlated to its "depth of cut" [100], which is directly affected by the product quality from the preceding stages. For example, in a two-stage drilling and tapping process, if the diameter of the hole drilled in the first stage is smaller than its specification, the tapping tool will need to cut more material to maintain the final product quality, which will accelerate its tool wear.

Without further information, a linear model, as a case in point, is a reasonable choice to demonstrate our proposed methodology for characterizing the impact of quality degradation on the instantaneous rate of tool wear, which has not been investigated in the existing literature. Depending on the specific real-world applications, different functional forms can be incorporated as the extensions of our proposed model.

Using the expression of the instantaneous rate of tool wear expressed in Eq. 18, we can rewrite the SDE model expressed in Eq. 17 as:

$$dS_m(t) = [R_m + \mathbf{c}'_m \mathbf{Y}(t)]\, dt + dW_m(t), \tag{19}$$

for $m = 1, 2, \ldots,\ M$. The matrix-vector form can be expressed as follows:

$$d\mathbf{S}(t) = [\mathbf{R} + \mathbf{C}'\mathbf{Y}(t)]\, dt + d\mathbf{W}(t), \tag{20}$$

where $d\mathbf{S}(t)$=$(dS_1(t), dS_2(t), \ldots, dS_M(t))'$, $\mathbf{R}$=$(R_1, R_2, \ldots, R_M)'$, $\mathbf{C}$=$(\mathbf{c}_1, \mathbf{c}_2, \ldots, \mathbf{c}_N)$, and $d\mathbf{W}(t) = (dW_1(t), dW_2(t), \ldots, dW_M(t))'$. $\mathbf{W}(t)$ represents an M-dimensional Brownian motion process, whose covariance matrix is represented by $\mathbf{\Sigma_W}t$, where $\mathbf{\Sigma_W} = diag(\sigma^2_{W,1}, \sigma^2_{W,2}, \ldots, \sigma^2_{W,M})$. Since every element of $\mathbf{W}(t)$ is assumed to be statistically independent of $\mathbf{Z}(t)$, $\mathbf{W}(t)$ is also statistically independent of $\mathbf{Z}(t)$.

4.1.3 Interaction Between Tool Wear and Quality Degradation

Leveraging the two models expressed in Eq. 16 and Eq. 20, we develop a hybrid model that captures the interaction between tool wear and quality degradation in MMPs. By substituting Eq. 16 in Eq. 20, quality degradation can be expressed in terms of tool wear as follows:

$$d\mathbf{Y}(t) = [\mathbf{A}'\mathbf{R} + \mathbf{A}'\mathbf{C}'\mathbf{Y}(t)]\, dt + \mathbf{A}' d\mathbf{W}(t) + \mathbf{B}' d\mathbf{Z}(t). \tag{21}$$

Recall that $\mathbf{W}(t)$ and $\mathbf{Z}(t)$ represent two independent Brownian motion processes. Thus, $\mathbf{A}'\mathbf{W}(t)$+$\mathbf{B}'\mathbf{Z}(t)$ is an N-dimensional Brownian motion process that we denote as $\mathbf{W}^*(t)$, which has covariance matrix $\mathbf{\Sigma}^* t$ with $\mathbf{\Sigma}^* = \mathbf{A}'\mathbf{\Sigma_W}\mathbf{A} + \mathbf{B}'\mathbf{\Sigma_Z}\mathbf{B}$. For

notational convenience, we let $\mathbf{\Delta}=\mathbf{A}'\mathbf{C}'$. Thus, Eq. 21 can be rewritten as follows:

$$d\mathbf{Y}(t) = [\mathbf{A}'\mathbf{R} + \mathbf{\Delta}\mathbf{Y}(t)]\, dt + d\mathbf{W}^*(t). \tag{22}$$

By choosing various forms of $\mathbf{A}$ and $\mathbf{C}$, Eq. 22 can be used to describe different MMP configurations. For example, if an MMP has a series configuration and quality measurements are taken after each stage, quality degradation (tool wear) of a specific stage will only be affected by tool wear (quality degradation) of the current and the preceding stages. Consequently, $\mathbf{A}$ and $\mathbf{C}$ will be upper-triangular matrices. Similarly, if an MMP has a parallel configuration, the interaction between tool wear and quality degradation will be limited to what occurs within each stage. Thus, $\mathbf{A}$ and $\mathbf{C}$ will each be a diagonal matrix.

4.2 Parameter Estimation and RLD Updating

We discuss in this section how to estimate the model parameters involved in the interaction model, and how to estimate and update RLD of the MMP system using the real-time quality measurements.

4.2.1 Estimating and Updating the Model Parameters

Our model is used to describe the interaction between tool wear and quality degradation across a population of similar MMPs. The model consists of deterministic parameters used to characterize features that are relatively constant/fixed across the population of MMPs, and stochastic parameters that capture variability among individual MMPs.

In our model, we assume that $\mathbf{A}$, $\mathbf{B}$, and $\mathbf{\Delta}$ are fixed parameters, since they are typically dependent on the configuration of the MMP and can be determined using the locations of tools and the layout of measurement points. Examples in which such assumptions were used can be found in the 2-dimensional assembly process studied in [61], the 3-dimensional auto-body assembly process investigated in [73],

and the cylinder-head machining process analyzed in [52]. In all of these studies, the randomness and variability resulting from $\mathbf{A}$, $\mathbf{B}$, and $\mathbf{\Delta}$ were considered insignificant.

$\mathbf{\Sigma}^*$ is also assumed to be constant. $\mathbf{\Sigma}^*$ is determined by $\mathbf{\Sigma_W}$ and $\mathbf{\Sigma_Z}$, where $\mathbf{\Sigma_Z}$ is the variance of the process noise and $\mathbf{\Sigma_W}$ is the variance of the Brownian motion error of tool wear. Typically, $\mathbf{\Sigma_Z}$ can be determined using the physical configuration of the systems and is often assumed to be constant in most of the existing literature. For example, in the auto-body assembly process investigated by [29], the authors defined process noise as the random orientation of the contacting point between the locating pin and the locating hole on a raw product. They proved that process noise followed a known distribution that was derived through knowledge of the physical system. Other examples include machining processes studied in [51, 116], where the variance of the process noise was determined by engineering knowledge. With regards to the other noise component, $\mathbf{\Sigma_W}$, it corresponds to noise in the tool wear process. As will be discussed later, the natural rate of tool wear is assumed to be random. In reality, the noise $\mathbf{\Sigma_W}$ is usually an insignificant source of variation when compared to the variation in the rate of tool wear [7, 72, 77]. Therefore, it is reasonable to assume that $\mathbf{\Sigma}^*$ is deterministic.

Different from the deterministic parameters discussed above, the natural rate of tool wear is assumed to be stochastic and follow a prior distribution. In other words, each time a specific tool is replaced, its natural rate of tool wear is assumed to be a random draw from its prior distribution. Specifically, we assume that the vector of natural rates of tool wear $\mathbf{R}$ follows a prior distribution, which we denote by $\pi(\mathbf{R})$. The functional form of $\pi(\cdot)$ can be obtained through subjective information or estimated using historical data. For illustrative purposes, we assume that $\pi(\mathbf{R})$ is a multivariate normal distribution with mean vector $\boldsymbol{\mu}_\mathbf{R}$ and covariance matrix $\mathbf{\Sigma_R}$, where $\boldsymbol{\mu}_\mathbf{R} = (\mu_{\mathbf{R},1}, \ldots, \mu_{\mathbf{R},M})'$and $\mathbf{\Sigma_R} = diag(\sigma^2_{\mathbf{R},1}, \ldots, \ \ \sigma^2_{\mathbf{R},M})$.

Next, we use *in-situ* quality measurements of the MMP to update the prior distribution of $\mathbf{R}$. To do this, assume that quality measurements are taken at discrete observation epochs t_0, t_1, t_2,..., t_k, where t_0 represents the epoch when the MMP starts to operate and t_k is the most recent observation epoch. Furthermore, we assume that quality measurements are observed at a constant sampling interval, i.e., $t_1 - t_0 = t_2 - t_1 = \ldots = t_k - t_{k-1} = \delta_t$. At t_0, we assume that the initial quality degradation of the MMP is $\mathbf{0}$, which indicates that no quality degradation occurs. Let $\{\mathbf{y}(t_0), \ldots, \mathbf{y}(t_k)\}$ represent the observed values of quality measurements, where $\mathbf{y}(t_0) = \mathbf{0}$. The posterior distribution of $\mathbf{R}$ can be expressed as follows:

$$p(\mathbf{R}|\mathbf{y}(t_0), \ldots, \mathbf{y}(t_k), \mathbf{A}, \mathbf{B}, \boldsymbol{\Delta}, \boldsymbol{\Sigma}^*) \propto f(\mathbf{y}(t_0), \ldots, \mathbf{y}(t_k)|\mathbf{R}, \mathbf{A}, \mathbf{B}, \boldsymbol{\Delta}, \boldsymbol{\Sigma}^*)\pi(\mathbf{R}),$$

where $f(\mathbf{y}(t_0), \ldots, \mathbf{y}(t_k)|\mathbf{R}, \mathbf{A}, \mathbf{B}, \boldsymbol{\Delta}, \boldsymbol{\Sigma}^*)\pi(\mathbf{R})$ is the likelihood function of quality observations given parameters ($\mathbf{R}$, $\mathbf{A}$, $\mathbf{B}$, $\boldsymbol{\Delta}$, $\boldsymbol{\Sigma}^*$). According to our assumption, $\mathbf{y}(t_0)$ is a constant vector with value $\mathbf{0}$. Thus, we have:

$$p(\mathbf{R}|\mathbf{y}(t_0), \ldots, \mathbf{y}(t_k), \mathbf{A}, \mathbf{B}, \boldsymbol{\Delta}, \boldsymbol{\Sigma}^*) \propto f(\mathbf{y}(t_1), \ldots, \mathbf{y}(t_k)|\mathbf{R}, \mathbf{A}, \mathbf{B}, \boldsymbol{\Delta}, \boldsymbol{\Sigma}^*)\pi(\mathbf{R}), \quad (23)$$

According to Eq. 22, $\mathbf{y}(t_i)$, for $i = 1, \ldots, k$, follows a Brownian motion with a linear drift. Thus, using the Markovian property $f(\mathbf{y}(t_1), \ldots, \mathbf{y}(t_k)|\mathbf{R}, \mathbf{A}, \mathbf{B}, \boldsymbol{\Delta}, \boldsymbol{\Sigma}^*)$ can be decomposed as follows:

$$f(\mathbf{y}(t_1), \ldots, \mathbf{y}(t_k)|\mathbf{R}, \mathbf{A}, \mathbf{B}, \boldsymbol{\Delta}, \boldsymbol{\Sigma}^*) = \prod_{i=1}^{k} f_i(\mathbf{y}(t_i)|\mathbf{y}(t_{i-1}), \mathbf{R}, \mathbf{A}, \mathbf{B}, \boldsymbol{\Delta}, \boldsymbol{\Sigma}^*) \quad (24)$$

where $f_i(\mathbf{y}(t_i)|\mathbf{y}(t_{i-1}), \mathbf{R}, \mathbf{A}, \mathbf{B}, \boldsymbol{\Delta}, \boldsymbol{\Sigma}^*)$ represents the p.d.f. of $\mathbf{y}(t_i)$ given $\mathbf{y}(t_{i-1})$, $\mathbf{R}$, $\mathbf{A}$, $\mathbf{B}, \boldsymbol{\Delta}, \boldsymbol{\Sigma}^*$. When $\boldsymbol{\Delta}$ is a full rank matrix, $\mathbf{y}(t_i)|\left(\mathbf{y}(t_{i-1}), \mathbf{R}, \mathbf{A}, \mathbf{B}, \boldsymbol{\Delta}, \boldsymbol{\Sigma}^*\right)$ follows a multivariate normal distribution with mean vector $\boldsymbol{\mu}_{\mathbf{Y}}(t_i)$ and covariance matrix $\boldsymbol{\Sigma}_{\mathbf{Y}}(t_i)$ [8]. The explicit formulation of $\boldsymbol{\mu}_{\mathbf{Y}}(t_i)$ is:

$$\boldsymbol{\mu}_{\mathbf{Y}}(t_i) = e^{\delta_t \Delta}\mathbf{y}(t_{i-1}) + \mathbf{UR},$$

where $\mathbf{U} = \left[e^{\delta_t \boldsymbol{\Delta}} - \mathbf{I}\right] \boldsymbol{\Delta}^{-1}\mathbf{A}'$. $\boldsymbol{\Sigma}_{\mathbf{Y}}(t_i)$ can be evaluated by solving an ordinary differential equation (ODE) system. In particular, $\boldsymbol{\Sigma}_{\mathbf{Y}}(t_i) = \mathbf{X}(t)|_{t=\delta_t}$, where $\mathbf{X}(t)$ is the

solution of the following ODE system:

$$\frac{d\mathbf{X}(t)}{dt} = \mathbf{\Delta}\mathbf{X}(t) + \mathbf{X}(t)\mathbf{\Delta}' + \mathbf{\Sigma}^* \tag{25}$$

$$\mathbf{X}(0) = \mathbf{0}$$

Note that $\mathbf{\Sigma_Y}(t_i)$ does not depend on t_i, we have $\mathbf{\Sigma_Y}(t_1) = \ldots = \mathbf{\Sigma_Y}(t_k) = \mathbf{X}(t)|_{t=\delta_t}$.

Based on the aforementioned distribution of $\mathbf{y}(t_i)|\left(\mathbf{y}(t_{i-1}), \mathbf{R}, \mathbf{A}, \mathbf{B}, \mathbf{\Delta}, \mathbf{\Sigma}^*\right)$, we show in Proposition 4.1 below, that the posterior distribution of $\mathbf{R}$ also follows a multivariate normal distribution.

Proposition 4.1: *Given real-time quality measurements* $\{\mathbf{y}\left(t_0\right), \ldots, \mathbf{y}(t_k)\}$ *and model parameters* $\mathbf{A}, \mathbf{B}, \mathbf{\Delta}, \mathbf{\Sigma}^*$*, the posterior distribution of* $\mathbf{R}$ *follows a multivariate normal distribution with mean* $\boldsymbol{\mu}_{\mathbf{R},k}$ *and covariance matrix* $\mathbf{\Sigma}_{\mathbf{R},k}$*, where*

$$\boldsymbol{\mu}_{\mathbf{R},k} = \mathbf{\Sigma}_{\mathbf{R},k}\left[\sum_{i=1}^{k}\left[\mathbf{y}(t_i) - e^{\delta_t\Delta}\mathbf{y}(t_{i-1})\right]'\Sigma_{\mathbf{Y}}^{-1}(t_i)\mathbf{U} + \boldsymbol{\mu}_{\mathbf{R}}'\mathbf{\Sigma}_{\mathbf{R}}^{-1}\right]',$$

$$\mathbf{\Sigma}_{\mathbf{R},k} = (k\mathbf{U}'\mathbf{\Sigma}_{\mathbf{Y}}^{-1}(t_1)\mathbf{U} + \mathbf{\Sigma}_{\mathbf{R}}^{-1})^{-1}.$$

Proof of Proposition 4.1:

Proposition 4.1 updates the posterior distribution of $\mathbf{R}$ by synergistically leveraging historical knowledge (its prior distribution) as well as current observations (real-time quality measurements). This step can be done using the Bayesian theory in Eq. 23. In the following proof, we will show that posterior distribution of $\mathbf{R}$ actually follows a multivariate normal distribution. The detailed proof is as follows:

According to Eq. 24, $f(\mathbf{y}(t_1), \ldots, \mathbf{y}(t_k)|\mathbf{R}, \mathbf{A}, \mathbf{B}, \mathbf{\Delta}, \mathbf{\Sigma}^*)$ can be decomposed as follows:

$$f(\mathbf{y}(t_1), \ldots, \mathbf{y}(t_k)|\mathbf{R}, \mathbf{A}, \mathbf{B}, \mathbf{\Delta}, \mathbf{\Sigma}^*) = \prod_{i=1}^{k} f_i(\mathbf{y}(t_i)|\mathbf{y}(t_{i-1}), \mathbf{R}, \mathbf{A}, \mathbf{B}, \mathbf{\Delta}, \mathbf{\Sigma}^*),$$

where $f_i(\mathbf{y}(t_i)|\mathbf{y}(t_{i-1}), \mathbf{R}, \mathbf{A}, \mathbf{B}, \mathbf{\Delta}, \mathbf{\Sigma}^*)$ represents the p.d.f. of a multivariate normal distribution with mean $\boldsymbol{\mu}_{\mathbf{Y}}(t_i) = e^{\delta_t\Delta}\mathbf{y}(t_{i-1}) + \mathbf{UR}$ and covariance matrix $\mathbf{\Sigma}_{\mathbf{Y}}(t_i)$, which can be solved using the ODE system expressed in Eq. 25. Hence, according

to Eq. 23, the expression of $p(\mathbf{R}|\mathbf{y}(t_0),\ldots,\mathbf{y}(t_k),\mathbf{A},\mathbf{B},\boldsymbol{\Delta},\boldsymbol{\Sigma}^*)$ can be expanded as follows:

$$\begin{aligned}
&p(\mathbf{R}|\mathbf{y}(t_0),\ldots,\mathbf{y}(t_k),\mathbf{A},\mathbf{B},\boldsymbol{\Delta},\boldsymbol{\Sigma}^*)\\
&\quad\propto \exp\left\{-\frac{1}{2}\left[\sum_{i=1}^{k}\left(\mathbf{y}(t_i)-\boldsymbol{\mu}_{\mathbf{Y}}(t_{i-1})\right)'\Sigma_{\mathbf{Y}}^{-1}(t_i)\left(\mathbf{y}(t_i)-\boldsymbol{\mu}_{\mathbf{Y}}(t_{i-1})\right)\right]\right\}\\
&\qquad\times\exp\left\{-\frac{1}{2}\left[(\mathbf{R}-\mu_{\mathbf{R}}{}')\boldsymbol{\Sigma}_{\mathbf{R}}^{-1}(\mathbf{R}-\mu_{\mathbf{R}}{}')\right]\right\}.
\end{aligned}$$

We substitute the expression of $\boldsymbol{\mu}_{\mathbf{Y}}(t_i)$ using $e^{\delta_t\Delta}\mathbf{y}(t_{i-1})+\mathbf{UR}$ and $\boldsymbol{\Sigma}_{\mathbf{Y}}(t_i)$ using $\boldsymbol{\Sigma}_{\mathbf{Y}}(t_1)$, for $i=1,2,\ldots,k$. Thus, we have:

$$\begin{aligned}
&p(\mathbf{R}|\mathbf{y}(t_0),\ldots,\mathbf{y}(t_k),\mathbf{A},\mathbf{B},\boldsymbol{\Delta},\boldsymbol{\Sigma}^*)\\
&\quad\propto\exp\left\{-\frac{1}{2}\mathbf{R}'(k\mathbf{U}'\boldsymbol{\Sigma}_{\mathbf{Y}}^{-1}(t_1)\mathbf{U}+\boldsymbol{\Sigma}_{\mathbf{R}}^{-1})\mathbf{R}\right\}\\
&\qquad\times\exp\left\{-\left[\sum_{i=1}^{k}\left(\mathbf{y}(t_i)-e^{\delta_t\Delta}\mathbf{y}(t_{i-1})\right)'\Sigma_{\mathbf{Y}}^{-1}(t_i)\mathbf{U}+\boldsymbol{\mu}_{\mathbf{R}}'\boldsymbol{\Sigma}_{\mathbf{R}}^{-1}\right]\mathbf{R}\right\}\\
&\quad\propto\exp\left\{-\frac{1}{2}(\mathbf{R}-\boldsymbol{\mu}_{\mathbf{R},k})'\boldsymbol{\Sigma}_{\mathbf{R},k}^{-1}(\mathbf{R}-\boldsymbol{\mu}_{\mathbf{R},k})\right\},
\end{aligned}$$

where $\boldsymbol{\mu}_{\mathbf{R},k}=\boldsymbol{\Sigma}_{\mathbf{R},k}\{\sum_{i=1}^{k}\left[\mathbf{y}(t_i)-e^{\delta_t\Delta}\mathbf{y}(t_{i-1})\right]'\Sigma_{\mathbf{Y}}^{-1}(t_i)\mathbf{U}+\boldsymbol{\mu}_{\mathbf{R}}'\boldsymbol{\Sigma}_{\mathbf{R}}^{-1}\}'$ and $\boldsymbol{\Sigma}_{\mathbf{R},k}=(k\mathbf{U}'\boldsymbol{\Sigma}_{\mathbf{Y}}^{-1}(t_1)\mathbf{U}+\boldsymbol{\Sigma}_{\mathbf{R}}^{-1})^{-1}$.

According to Proposition 4.1, the expression of $p(\mathbf{R}|\mathbf{y}(t_0),\ldots,\mathbf{y}(t_k),\mathbf{A},\mathbf{B},\boldsymbol{\Delta},\boldsymbol{\Sigma}^*)$ can be represented by the p.d.f. of a multivariate normal distribution with mean vector $\boldsymbol{\mu}_{\mathbf{R},k}$ and covariance matrix $\boldsymbol{\Sigma}_{\mathbf{R},k}$. Once we obtain the posterior distribution of $\mathbf{R}$, we utilize this updated distribution as well as the real-time quality measurements $\mathbf{y}(t_0),\ldots,\mathbf{y}(t_k)$ to further update the RLD of the MMP functioning in the field. Details are provided in the following subsection.

4.2.2 Updating the RLD of the MMP

The residual life of an MMP functioning in the field is the first time when any quality measurement exceeds a pre-defined failure threshold. Let T_k represent the residual life of the MMP at time t_k and ℓ_m represent the quality failure threshold at the m^{th}

stage. The distribution of T_k can be expressed as follows:

$$P\left(T_k \leq t|\mathbf{y}(t_0),\ldots,\mathbf{y}(t_k)\right) = 1 - P\left(\mathbf{Y}(t_k+t) \leq \ell|\mathbf{y}(t_0),\ldots,\mathbf{y}(t_k)\right), \qquad (26)$$

where $\ell = (\ell_1,\ldots,\ \ell_M)'$. Similar definition of system failure has been widely used in the reliability literature, examples include [42, 76, 105, 107]. Based on Eq. 26, calculating the RLD is equivalent to estimating the distribution of $\mathbf{Y}(t_k+t)|\left(\mathbf{y}(t_0),\ldots,\mathbf{y}(t_k)\right)$.

We have proved in Proposition 4.1 that the posterior distribution of $\mathbf{R}$ given $\{\mathbf{y}(t_0),\ldots,\mathbf{y}(t_k)\}$ follows a multivariate normal distribution with mean vector $\boldsymbol{\mu}_{\mathbf{R},k}$ and covariance matrix $\boldsymbol{\Sigma}_{\mathbf{R},k}$. In addition, we have proved in Section 4.2.1 that for all $i = 1,\ldots,k$, $\mathbf{Y}(t_i)|(\mathbf{y}(t_i),\mathbf{R})$ follows a multivariate normal distribution with mean vector $\boldsymbol{\mu}_{\mathbf{Y}}(t_i)$ and covariance matrix $\boldsymbol{\Sigma}_{\mathbf{Y}}(t_i)$.

Similarly,$\mathbf{Y}(t_k+t)|\left(\mathbf{y}(t_0),\ldots,\mathbf{y}(t_k),\mathbf{R}\right)$ also follows a multivariate normal distribution with mean vector $\boldsymbol{\mu}_{\mathbf{Y}}(t) = e^{t\boldsymbol{\Delta}}\mathbf{y}(t_k) + \left[e^{t\boldsymbol{\Delta}} - \mathbf{I}\right]\boldsymbol{\Delta}^{-1}\mathbf{A}'\mathbf{R}$ and covariance matrix $\boldsymbol{\Sigma}_{\mathbf{Y}}(t) = \mathbf{X}(t)|_{t=t}$, where $\mathbf{X}(t)$ is the solution to the ODE system in Eq. 25. If we define $\mathbf{U}_t = \left[e^{t\boldsymbol{\Delta}} - \mathbf{I}\right]\boldsymbol{\Delta}^{-1}\mathbf{A}$, according to [20], the distribution of $\mathbf{Y}(t_k+t)|\left(\mathbf{y}(t_0),\ldots,\mathbf{y}(t_k)\right)$, without conditioning on $\mathbf{R}$, still follows a multivariate normal distribution with mean vector $e^{t\boldsymbol{\Delta}}\mathbf{y}(t_k) + \mathbf{U}_t\boldsymbol{\mu}_{\mathbf{R},k}$ and covariance matrix $\boldsymbol{\Sigma}_{\mathbf{Y}}(t) + \mathbf{U}_t\boldsymbol{\Sigma}_{\mathbf{R},k}\mathbf{U}_t'$. Consequently, the RLD of the MMP can be calculated based on the distribution of $\mathbf{Y}(t_k+t)|\left(\mathbf{y}(t_0),\ldots,\mathbf{y}(t_k)\right)$. Since $\mathbf{Y}(t_k+t)|\left(\mathbf{y}(t_0),\ldots,\mathbf{y}(t_k)\right)$ is normally distributed, the distribution of $T_k \leq t|\mathbf{y}(t_0),\ldots,\mathbf{y}(t_k)$ is skewed. Thus, we utilize the median of $T_k \leq t|\mathbf{y}(t_0),\ldots,\mathbf{y}(t_k)$ as the residual life prediction.

4.3 Numerical Studies

We conduct a series of numerical studies to evaluate the performance of our proposed methodology and utilize the QR-chain model by [29] as the benchmark to compare the performance. To the best of our knowledge, the QR-chain model is the only existing method that addresses a similar research area — modeling the interactive relationship between tool wear and quality degradation in MMPs with the goal of

reliability estimation. Our work is a generalization of the QR-chain model, since we address the impact of quality degradation on the actual process of tool wear rather than the impact on tool breakage, which is a fundamental shift from the previous paradigm. Also, our model incorporates real-time quality measurements rather than only historical data, and thus can be used to obtain real-time estimation of system residual life instead of static off-line reliability estimate. Therefore, we use the QR-chain model as a benchmark to investigate how much improvement can be obtained in predicting the system lifetime by utilizing our methodology.

To implement the QR-chain model in a fair manner, we assume an identical linear model for quality degradation $\mathbf{Y}(t)$ as our proposed quality model described in Eq. 16. Note that the QR-chain model only focuses on the impact of quality degradation on the probability of tool breakage rather than the rate of tool wear. Thus, when the impact of quality degradation on tool breakage is ignored, the model of tool wear in the QR-chain model can be expressed as follows:

$$d\mathbf{S}(t) = \mathbf{R}dt + d\mathbf{W}(t). \tag{27}$$

where the tool wear rate is equal to $\mathbf{R}$ but not related to $\mathbf{Y}(t)$.

Comparing the equation above to our proposed tool-wear model in Eq. 20, we note that the QR-chain model, when it does not consider failures due to tool breakage, is a special case of our proposed model by letting the matrix $\mathbf{C}$ equal to $\mathbf{0}$.

In what follows, we first describe the simulation set-up and the procedure we use to simulate the signals of tool wear and quality degradation. Next, we discuss the method for estimating the model parameters and testing the linear assumption in Eq. 19 and Eq. 20. Finally, we compare the performance of our methodology as well as its sensitivity to different parameter values to the QR-chain model. Model parameters studied in the sensitivity analysis include the amplitude of process noise, the magnitude of the impact of quality degradation on tool wear, and the number of stages.

4.3.1 Simulation Framework and Signal Generation

Our simulation set-up is inspired by the single-stage sheet metal stamping process presented in [30], the same authors as the QR-chain model, who used a similar quality model to study quality-based maintenance. The stamping process (as shown in Fig. 12 [30]) has two dies, an outer die and an inner die, which are subject to tool wear and thus will cause the dimensional deviation of formed products. The quantitative impact of tool wear on quality degradation is estimated using a series of experiments conducted by [62]. The detailed result with only first-order terms is as follows:

$$\begin{aligned}\text{output part quality} &= 0.1136 \times \text{tool wear of outer die} \\ &+ 0.0219 \times \text{tool wear of outer die} + 0.019 \times \text{incoming part quality} + \text{noise},\end{aligned} \tag{28}$$

In addition, the authors in [30] characterized the tool wear of both outer and inner dies using the same model in the QR-chain formulation shown in Eq. 27. They obtained the tool wear parameters through real stamping processes.

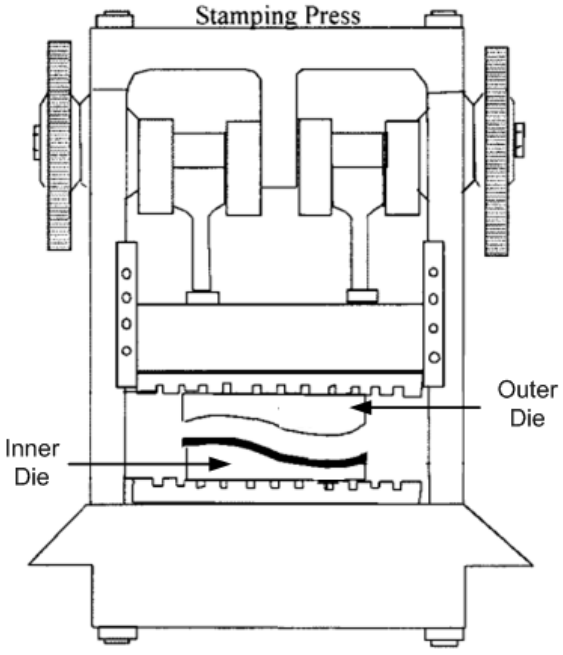

Figure 12: Stamping process

Table 4: Parameter values used for generating degradation signals

	Source	True Value	Estimated Value
$\mathbf{A}$	[28]	$\begin{pmatrix} 0.1136 & 0.0216 & 4.1e^{-5} \\ 0.0219 & 4.16e^{-4} & 7.91e^{-6} \\ 0 & 0.1136 & 0.0216 \\ 0 & 0.0219 & 4.16e^{-4} \\ 0 & 0 & 0.1136 \\ 0 & 0 & 0.0219 \end{pmatrix}$	Pre-specified
$\mathbf{B}$	[28]	$\begin{pmatrix} 0.019 & 3.16e^{-4} & 6.859e^{-4} \\ 1 & 0.019 & 3.16e^{-4} \\ 0 & 1 & 0.019 \\ 0 & 0 & 1 \end{pmatrix}$	Pre-specified
$\mathbf{C}$	Subjective knowledge	$\begin{pmatrix} 4 & 20 & 0 \\ 4 & 12 & 0 \\ 0 & 4 & 20 \\ 0 & 4 & 12 \\ 0 & 0 & 4 \\ 0 & 0 & 4 \end{pmatrix}' \times 10^{-3}$	$\begin{pmatrix} 4.2 & 19.7 & 0 \\ 4.01 & 12 & 0.04 \\ 0.04 & 3.78 & 19.8 \\ 0 & 3.93 & 12.1 \\ 0 & 0 & 3.67 \\ 0 & 0 & 3.86 \end{pmatrix}' \times 10^{-3}$
h	Subjective knowledge	1000	Pre-specified
$\mathbf{\Sigma}_Z$	[28] and subjective knowledge	$diag(230, 1, 1, 1) \times 10^{-4}$	Pre-specified
$\mathbf{\Sigma}_W$	[28]	$diag(7.14, 2, 7.14, 2, 7.14, 2) \times 10^{-9} h$	$diag(7.12, 1.99, 7.13, 2, 6.91, 1.95) \times 10^{-6}$
$\boldsymbol{\mu}_R$	[28]	$diag(6.94, 4.14, 6.94, 4.14, 6.94, 4.14) \times 10^{-6} h$	$diag(7.15, 4.03, 6.95, 3.98, 7.04, 4.1) \times 10^{-3}$
$\mathbf{\Sigma}_R$	Subjective knowledge	$diag(5.35, 1.9, 5.35, 1.9, 5.35, 1.9) \times 10^{-6}$	$diag(5.31, 1.76, 4.95, 1.87, 5.85, 1.74) \times 10^{-6}$
$\boldsymbol{\ell}$	Subjective knowledge	$(0.5, 0.5, 0.5)'$	Pre-specified
δ_t	Subjective knowledge	1	Pre-specified

In this section, we would like to formulate a numerical study framework that resembles real-world applications related to the QR-chain model. In this way, we can compare the performance of our proposed methodology with the QR-chain model on a fair base. Hence, we focus on an MMP system with three consecutive stamping stages, each of which satisfies the quantitative model in Eq. 28. We assume that product quality is monitored after each stage. The process noises consist of the incoming raw part error as well as the measurement noise at each stage. The corresponding simulation set-up is illustrated in Fig. 13. We determine simulation parameters according to Eq. 28 and tool wear parameters in [30]. Parameters that are not provided in Eq. 28 or [30] are determined by subjective knowledge. All simulation parameters are listed in Table 4. Note that the unit of tool-wear parameters in [30] is "per operation". Here we assume sampling is taken every 1000 operations and compute parameter values accordingly.

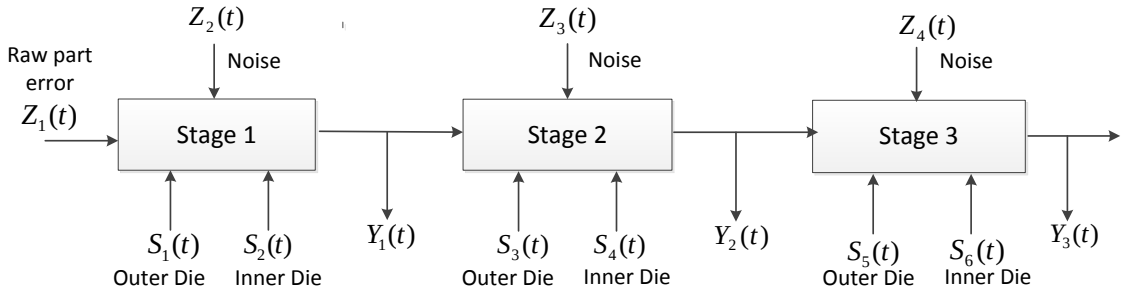

Figure 13: Simulation set-up

We simulate tool wear $\mathbf{S}(t)$ and quality degradation $\mathbf{Y}(t)$ according to the interactive model presented in Eq. 16 and Eq. 20 in Section 4.1. The details are described as follows:

Step 1: Generate a realization of the nature rate of tool wear $\mathbf{R}$ according to its prior distribution, *i.e.*, the multivariate normal distribution with mean vector $\boldsymbol{\mu}_{\mathbf{R}}$ and covariance matrix $\boldsymbol{\Sigma}_{\mathbf{R}}$. The values of $\boldsymbol{\mu}_{\mathbf{R}}$ and $\boldsymbol{\Sigma}_{\mathbf{R}}$ are specified in Table 4.

Step 2: Set $\mathbf{S}(t_0) = \mathbf{0}$ and $\mathbf{Y}(t_0) = \mathbf{0}$;

Step 3: At any epoch t_i, for $i \geq 1$, Simulate the values of $\mathbf{S}(t_i)$ and $\mathbf{Y}(t_i)$ iteratively:

(3.a.) Given $\mathbf{R}$ and $\mathbf{Y}(t_{i-1})$, generate $\mathbf{S}(t_i)$ according to Eq. 20;

(3.b.) Given $\mathbf{S}(t_i)$, generate $\mathbf{Y}(t_i)$ according to Eq. 16. Stop when $\mathbf{Y}(t_i)$ exceeds the failure threshold $\mathbf{l}$.

4.3.2 Parameter Estimation and Goodness-of-Fit Testing

The parameters involved in our proposed methodology are determined in two ways: (1) We assume that the values of $\mathbf{A}$, $\mathbf{B}$, and $\mathbf{\Sigma_z}$ are determined by the physical configuration of the MMP, and thus can be obtained based on expert knowledge. Similar examples of utilizing expert knowledge can be found in [31, 61, 73]. (2) On the other hand, the prior mean and variance of the nature rate of tool wear $\boldsymbol{\mu}_{\mathbf{R}}$ and $\mathbf{\Sigma_R}$, the error variance error $\mathbf{\Sigma_W}$, and the coefficient matrix $\mathbf{C}$ may not be obtained via expert knowledge. Thus, we estimate these parameters using historical quality degradation and tool wear measurements in a regression framework. The detailed procedure is explained below:

According to the model in Eq. 19, given the monitored quality degradation and tool wear measurements for stage m, the difference between two consecutive tool wear levels $S_m(t_{i-1})$ and $S_m(t_i)$ can be expressed as follows:

$$S_m(t_i) - S_m(t_{i-1}) = \int_{t_{i-1}}^{t_i} \left[R_m + \mathbf{c}_m' \mathbf{Y}(\omega)\right] d\omega + W_m(\delta_t),$$

for $m = 1, 2, \ldots, M$. The right-hand-side of the above expression involves the integration of stochastic process $\mathbf{Y}(\omega)$, which is challenging to estimate directly. Instead, we exploit an approximation, which assumes $\mathbf{Y}(\omega)$ as constant during (t_{i-1}, t_i) if the samping interval δ_t is small. That is, $\mathbf{Y}(\omega) \approx \mathbf{Y}(t_{i-1})$, for $\omega \in (t_{i-1}, t_i)$. Hence, $S_m(t_i) - S_m(t_{i-1})$ can be approximated as follows:

$$S_m(t_i) - S_m(t_{i-1}) \approx \left[R_m + \mathbf{c}_m' \mathbf{Y}(t_{i-1})\right] \delta_t + W_m(\delta_t).$$

By virtue of this discretization, $S_m(t_i) - S_m(t_{i-1})$ follows a normal distribution with the mean $[R_m + \mathbf{c}'_m \mathbf{Y}(t_{i-1})]\,\delta_t$ and the variance $\sigma^2_{w,m}\delta_t$, where $\sigma^2_{w,m}\delta_t$ is the variance of the noise term $W_m(\delta_t)$. Consequently, parameters R_m, $\mathbf{c}'_m$, and $\sigma^2_{w,m}$ can be estimated through regression.

Suppose the last observation epoch is t_k. Let $\{\mathbf{s}(t_0), \ldots, \mathbf{s}(t_k)\}$ and $\{\mathbf{y}(t_0), \ldots, \mathbf{y}(t_k)\}$ represent the observed tool wear and quality degradation, respectively. Thus, the regression based estimation results for each $m = 1, 2, \ldots, M$ are as follows: $\left[\hat{R}_m, \hat{\mathbf{c}}'_m\right] = (\mathbf{X}'\mathbf{X})^{-1}\mathbf{X}'\delta\mathbf{S}_m$ and $\hat{\sigma}^2_{w,m} = \frac{|\left[1-\mathbf{X}(\mathbf{X}'\mathbf{X})^{-1}\mathbf{X}'\right]\delta\mathbf{S}_m|^2}{k-m-1}$, where $\delta\mathbf{S}_m$= $(s_m(t_1) - s_m(t_0),\ \ldots,$ $s_m(t_k) - s_m(t_{k-1}))$ and $\mathbf{X} = (1, \mathbf{y}'(t_0); 1, \mathbf{y}'(t_1); \ldots; 1, \mathbf{y}'(t_k))$. The r^2 value of each regression represents how well the linear assumption in Eq. 19 holds in the data. A high r^2 value will indicate a sufficient linearity. If the linearity does not hold, a higher-order model may be necessary.

Usually, multiple runs of MMP operations are required to have a sufficient number of estimated values. Then, we can use multiple $\hat{R}_m$ to estimate the prior mean and variance of R_m, which are represented by $\mu_{R,m}$ and $\sigma^2_{R,m}$. We can also take the average of all $\widehat{\mathbf{c}}'_m$ and $\hat{\sigma}^2_{w,m}$ to get a more reliability estimates.

In this numerical study, we generate a training data set that consists of simulated tool wear $\mathbf{S}(t)$ and quality degradation $\mathbf{Y}(t)$ from 50 runs of simulation according to the specifications listed in Table 4. The average r^2 value from regression applied to the training set when $m = 1, 2,\ 3,\ 4,\ 5,\ 6$ is equal to 0.98, 0.99, 0.91, 0.95, 0.42, 0.61, respectively. The fifth and sixth r^2 values that correspond to the outer and inner dies on the 3^{rd} stage are lower than those of dies on the other two stages. This is because according to the simulation configuration, the slope of regression represented by $\mathbf{c}'_m$ is smaller when $m = 5,\ 6$ compared to when $m = 1, 2, 3, 4$, which reduces the sum-of-square regression. From the overall r^2 values we can see that the linear model in Eq. 19 can sufficiently represent the simulated data. We list the estimated values of $\hat{\mathbf{C}}$, $\hat{\mathbf{\Sigma}}_{\mathbf{W}}$, $\hat{\boldsymbol{\mu}}_{\mathbf{R}}$ and $\hat{\mathbf{\Sigma}}_{\mathbf{R}}$ based on the training data set in Table 4. It is demonstrated in

Table 4 that our estimated values are very close to their true values. These estimated parameter values are subsequently used to predict the system residual life in the following subsections.

4.3.3 Performance Comparison

4.3.3.1 When the impact of product quality on tool wear exists (i.e., **C** *is equal to the value in Table 4)*

First we compare the performance of our methodology with the QR-chain model when no real-time quality measurements are available. Under this condition, according to the derivation in Section 4.2, our work will rely on historical information to derive a lifetime distribution/reliability of the system. Similarly, the QR-chain model also computes off-line system reliability. To investigate the accuracy of reliability estimation using both methodologies, we simulate the actual system reliability by generating 1000 runs of simulation and record their actual lifetimes.

We present in Fig. 14 the estimated system reliability without incorporating real-time quality measurements based on our proposed model, the QR-chain model, and the actually simulated data. We observe that the reliability estimate based on our model is very close to the simulated reliability. However, the reliability estimate based on the QR-chain model demonstrates a bias caused by overestimate. We believe that this bias is mainly caused by the fact that the QR-chain model does not account for the effect of quality degradation on the instantaneous rate of tool wear, which tends to accelerate quality degradation and the system failure.

Next, we compare the performance of our methodology with the QR-chain model when real-time quality measurements are available. According to Section 4.2, our methodology can incorporates real-time quality measurements to online update the RLD of the system, which provides up-to-date information of the predicted lifetime. Since the QR-chain model does not incorporate real-time monitoring information to refine/update its model, the predicted lifetime is calculated solely based on the

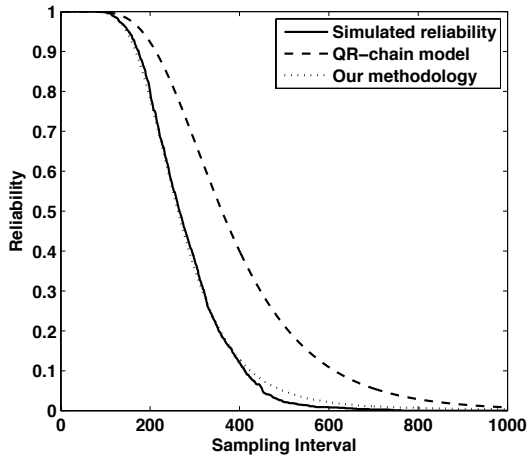

Figure 14: System reliability when $\mathbf{C}$ is equal to the value in Table 4

following logic: At any observation epoch, if an MMP has not failed yet, we compute the conditional lifetime distribution given the survival at current epoch using the reliability curve presented in Fig. 14. Then, we choose the median of the conditional lifetime distribution as the updated lifetime prediction.

The quantity of performance measurement is the lifetime prediction error defined below in Eq. 29:

$$\text{prediction error} = |1 - \frac{\text{Current observation epoch + Predicted residual life}}{\text{True lifetime}}| \quad (29)$$

Here, Current observation epoch + Predicted residual life is equal to the predicted lifetime, and the true lifetime is obtained via the simulated signals.

Particularly, for each run of simulation, we predict the residual life of the MMP at the 10^{th}, 20^{th}, ... , 90^{th} lifetime percentiles. In other words, we estimate its residual life when 10%, 20%, ..., 90% of the system lifetime is revealed. Then, we calculate the prediction error according to Eq. 29.

We generate a testing data set that consists of simulated data from 50 runs of simulation. The prediction errors of the testing data set using both our methodology and the QR-chain model are presented in Fig. 15. We observe that the prediction error from our methodology exhibits progressive reduction as we incorporate more

real-time observations, while the prediction error from the QR-chain model remains high at all lifetime percentiles. We believe that this is due to two reasons: First, the QR-chain model does not account for the effect of quality degradation on tool wear, which tends to accelerate quality degradation and the system failure, and thus leads to a consistent bias in the prediction. Second, the estimated reliability according to the QR-chain model is a static estimate based on the reliability data, whereas our approach incorporates the real-time quality measurements that capture the latest status of the system.

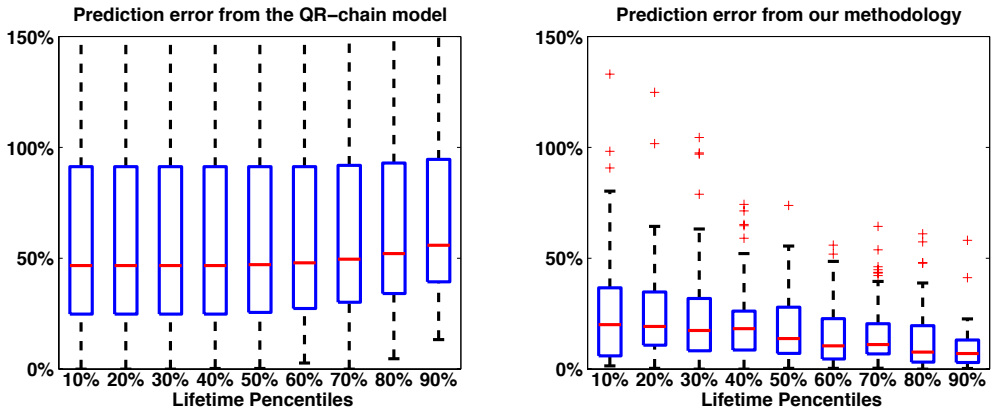

Figure 15: Comparison of prediction error associated with our methodology and the QR-chain model when **C** is equal to the value in Table 4

*4.3.3.2 When the impact of product quality on tool wear does not exist (i.e., **C**=0)*

In this subsection, we focus on the situation when the impact of product quality on the rate of tool wear does not exist, which is the situation that the QR-chain model is capable of modeling. Same as Section 4.3.3.1, the performance comparison consists of two parts:

First, we compare the performance of our methodology with the QR-chain model when no real-time quality measurements are available. Actual system reliability is computed by generating 1000 runs of simulation and recording their lifetimes. Fig. 16 illustrates the estimated system reliability based on our methodology, the QR-chain

model, and the simulated reliability. We observe that reliability estimates based on the two methodologies are both very close to the simulated reliability. This is because when the impact of product quality on the instantaneous rate of tool wear does not exist and no real-time quality measurements are available, both methodologies utilize the same model and the same historical data to capture system reliability.

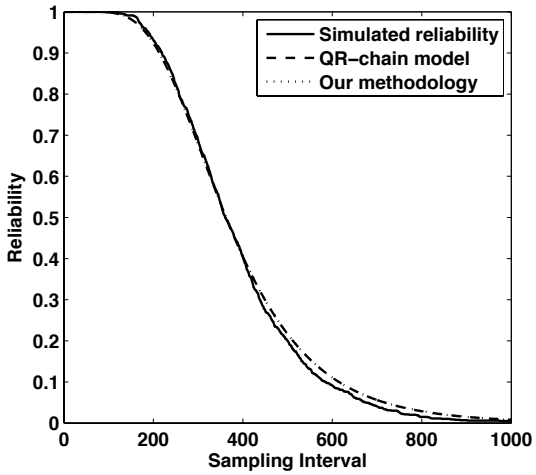

Figure 16: System reliability when $\mathbf{C} = \mathbf{0}$

Second, we compare the performance of our methodology with the QR-chain model when real-time quality measurements are available. Same as in Section 4.3.3.1, we generate data from 50 runs of simulation and show the lifetime prediction errors from both methodologies at the 10^{th}, 20^{th}, ... , 90^{th} lifetime percentiles in Fig. 17. We notice that the prediction error from the QR-chain model is significantly lower than what presented in Fig. 15. This is mainly due to the fact that when the impact of quality degradation on the instantaneous rate of tool wear (represented by $\mathbf{C}$) does not exist, the lifetime distribution estimated from the QR-chain model is not biased. We also observe that the prediction error from our methodology exhibits similar progressive reduction as shown in Fig. 15. On the contrary, prediction error from QR-chain model remains at a high level at all lifetime percentiles. This difference is mainly due to the fact that the prediction using the QR-chain model solely based on the

survival of MMP, whereas our approach incorporates real-time quality measurements that capture the latest degradation status of the system to reason about the future degradation of the system.

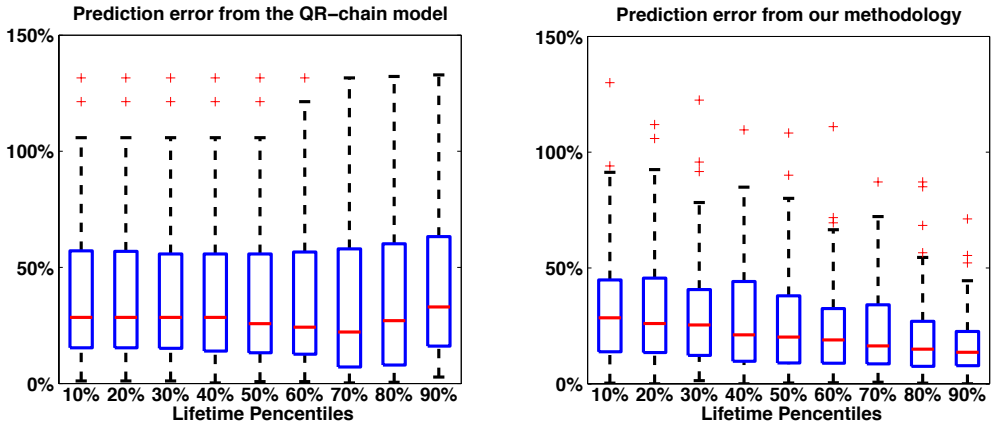

Figure 17: Comparison of prediction error associated with our methodology and the QR-chain model when $\mathbf{C} = \mathbf{0}$

4.3.4 Sensitivity Analysis

In this subsection, we investigate how the performance of our model changes at the values of key model parameters change. Specifically, we conduct three numerical experiments with the goal of studying how the accuracy of the lifetime prediction changes under (1) different amplitudes of process noise, (2) different magnitudes of impact from quality degradation on the instantaneous rate of tool wear and(3) different numbers of stages. To facilitate the simulation process, we begin with a baseline set-up with parameter values chosen according to Table 4. We then define two factors: n_1 and n_2, where n_1 is used to define different noise levels, and n_2 is used to scale the matrix $\mathbf{C}$. The detailed procedure of the sensitivity analysis is summarized below:

1. **Experiment I**: evaluate the effect of the amplitude of process noise by multiplying the value of $\mathbf{\Sigma_Z}$ in Table 4 with the scale parameter n_1, where $n_1 = 0.1,\ 0.5,\ 1,\ 2,\ 5$.

2. **Experiment II:** evaluate the effect of the magnitude of impact from quality degradation on the instantaneous rate of tool wear by multiplying the value of $\mathbf{C}$ in Table 4 with n_2, where $n_2 = 0,\ 0.5,\ 1,\ 2,\ 4$.

3. **Experiment III:** evaluate the effect of the number of stages by choosing $M = 3,\ 6,\ 9,\ 12,\ 15$. The values of the other parameters related to this experiment are listed in the Appendix.

For each of these three experiments, we generated 50 runs of simulation and present the average prediction errors from both methodologies at the 30^{th}, 60^{th}, and 90^{th} lifetime percentiles in Fig. 18, 19, and 20, respectively. We observe that:

1. The prediction error from both models increase with the amplitude of process noise (scaled by n_1). This is because a higher process noise will lower the prediction accuracy.

2. As the magnitude of the impact from quality degradation on tool wear (scaled by n_2) increases, the prediction error from the QR-chain model increases while the prediction error from our methodology decreases. This is because a higher amplitude of matrix $\mathbf{C}$ accelerates the system failure, and thus the QR-chain model yields a higher bias in predicting the lifetimes. On the other hand, $\mathbf{C}$ is compounded in both the instantaneous rate of tool wear and the process noise. Under current parameter setting, increasing the amplitude of $\mathbf{C}$ increases the ratio of the instantaneous rate of tool wear vs. the process noise, which improves the prediction accuracy of our methodology.

3. Prediction errors from both methodologies slightly decrease as the number of stages increase. This is because as the number of stages increases, the impact of tool wear and process noise from preceding stages on the quality degradation of subsequent stages increases (reflected in matrices $\mathbf{A}$ and $\mathbf{B}$), which tend to

accelerate the system failure. This is equivalent to increasing the ratio of the instantaneous rate of tool wear vs. the process noise. Thus, both methodologies show improved accuracy.

4. The prediction error from our methodology improves as the lifetime percentile increases. This is because our methodology leverages the real-time quality measurements to on-line update the RLD of the systems.

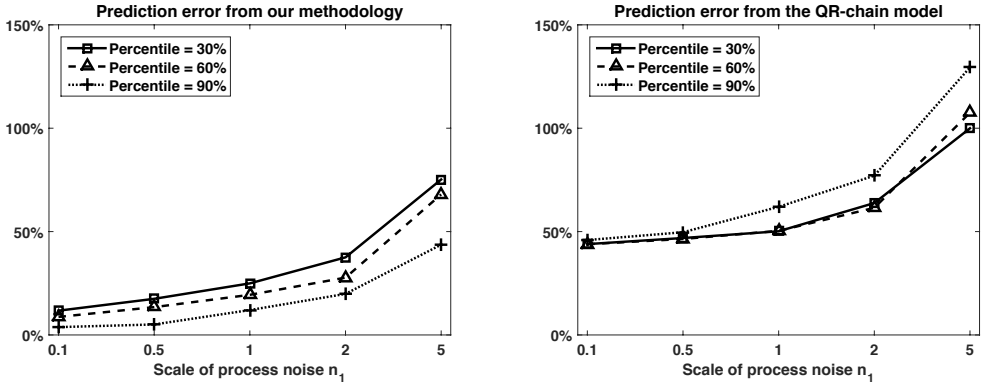

Figure 18: Average prediction errors at different scales of process noise

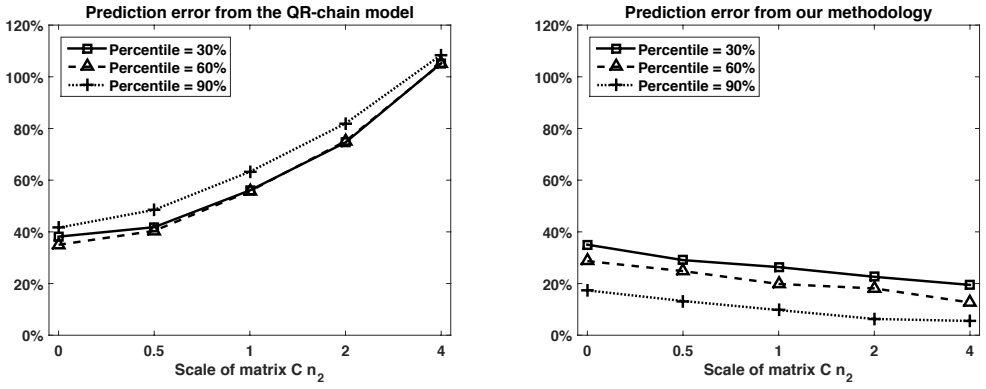

Figure 19: Average prediction errors at different scales of matrix $\mathbf{C}$

4.4 Details for Industrial Implementation

In this section, we describe the procedure of applying our methodology in real industrial applications, which will serve as a guideline for practitioners.

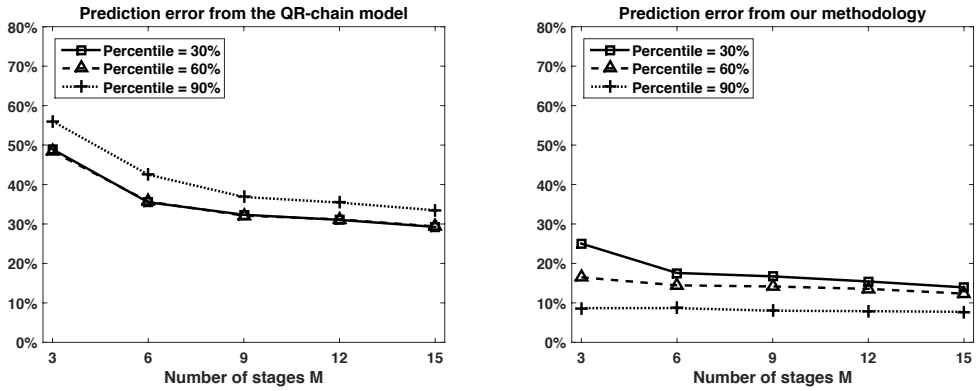

Figure 20: Average prediction errors at different number of stages

First, several model parameters in our methodology need to be determined using the configuration of the MMPs: The constant model parameters $\mathbf{A}$ and $\mathbf{B}$ that represent the impact of tool wear and process noise on quality degradation should be derived based on the configuration of the MMP, which includes the layout of the manufacturing stages, the locations of quality measurement points, the characteristic of process noise, etc. Take the auto-body assembly process presented [31] as an example. Matrix $\mathbf{A}$ can be calculated using the geometrical relationship between the locating pin (tool) and the quality measurement points on the raw parts. Matrix $\mathbf{B}$ can be calculated considering the randomness of allocating raw parts onto the locating pin. The variance of process noise $\mathbf{\Sigma}_Z$ represents the significance of the noise, which may include the sensitivity of the quality monitoring sensors, the precision of allocating raw parts onto each stage, etc.

Second, model parameters regarding to tool wear, including $\boldsymbol{\mu}_{\mathbf{R}}$, $\mathbf{\Sigma}_{\mathbf{R}}$, $\mathbf{\Sigma}_{\mathbf{W}}$, and $\mathbf{C}$ need to be estimated from historical data. Requirements of historical data are outlined below:

1. Several MMPs with an identical configuration need to be monitored from the beginning of operation until failure.

2. Both tool wear and product quality degradation in each MMP need to be observed periodically, i.e., using on-line quality and tool wear monitoring techniques.

3. Without loss of generality, the observation (sampling) interval can be set as a constant. The value of the interval may vary in different applications.

With the historical data available, parameters can be estimated by following the same linear regression procedure discussed in Section 4.3.2.

Finally, with the above model parameters estimated off line, we can incorporate real-time quality measurements to on-line update the RLD of an MMP functioning in the field. This requires real-time quality measurements only. No tool wear monitoring is needed. The observation interval can be set to be equal to that of the historical data. The procedure of updating the RLD has been discussed in Section 4.2. In summary, with quality degradation being observed up to any epoch t_k, we first update the posterior distribution of the natural rate of tool wear $\mathbf{R}$ according to Proposition 4.1. Based on the posterior distribution, the RLD of the MMP is updated according to Eq. 26. Finally, we utilize the median of the RLD as the residual life prediction.

CHAPTER V

CONTROLLING THE RESIDUAL LIFE DISTRIBUTION OF PARALLEL MULTI-COMPONENT SYSTEMS THROUGH WORKLOAD ADJUSTMENT

Complex systems often consist of multiple components that are required to work together in parallel to satisfy a specific engineering objective. As an example, in manufacturing processes, several identical machines may need to operate together in parallel to fabricate the same products simultaneously in order to meet the high production demand. This parallel configuration is usually designed with some level of redundancy to compensate for unexpected events. In this way, when only a small portion of components fails to operate due to either unexpected machine downtime or scheduled maintenance, the remaining components can still achieve the engineering objective by increasing their workloads up to the designed capacities. However, the workload of a component apparently impacts the components degradation rate as well as its failure time. Specifically, this paper considers the case that a higher workload assignment accelerates the components degradation and vice versa. Based on this assumption, we develop a methodology to actively control the degradation as well as the predicted failure time of each component by dynamically adjusting its workloads. Our goal is to prevent the overlap of component failures within a certain time period through taking advantage of the natural redundancy of the parallel structure, which may potentially lead to a better utilization of maintenance resources as well as a consistently ensured production throughput. A numerical study is used to evaluate the performance of the proposed methodology under different scenarios.

This chapter is organized as follows. Section 5.1 describes the problem formulation

and introduces the component degradation model. Next, Section 5.2 derives the RLD of components, based on which Section 5.3 develops our proposed workload adjustment strategy. Validation studies using a simulated case study are given in Section 5.4.

5.1 Component Degradation Modeling

5.1.1 Problem Formulation

We consider a parallel multi-component system that consists of M components operating in parallel to perform the same type of operations. We define the largest amount of operations each component is capable to perform *in a unit time* as the capacity of the component, which is denoted as U_m for component m. The actual amount of operations that each component performs in a unit time is defined as the workload, which is denoted as $u_m(t)$ for component m at time t. By default, we have $0 \leq u_m(t) \leq U_m$, for $m = 1, 2, \ldots, M$. If component m fails at time t, then $u_m(t) = 0$. We further denote by $TH(t)$ the throughput of the system at time t, which is defined as the summation of workloads from all components, i.e., $TH(t) = \sum_{m=1}^{M} u_m(t)$. Let $\tilde{M}(t)$ be the number of components that are functional/operational at time t. Thus, the capacity (i.e., the maximum throughput) of the system at time t is equal to $\sum_{m=1}^{\tilde{M}(t)} U_m$. Note that $TH(t) = \min[\sum_{m=1}^{\tilde{M}(t)} U_m, D]$, in which D represents the production demand, or the targeted throughput. In other words, when the capacity offered by the remaining functional components is smaller than the demand, it indicates a loss of productivity in the system. Therefore, it is important to separate the overlap of component failures to ensure a consistently satisfactory throughput. To highlight our main idea, here we assume that the demand is constant and components only perform one type of operation. It is worth of mentioning that the unit of workload, throughput, demand, and capacity may be either discrete or continuous, depending on the application areas. For example, in discrete manufacturing processes, the unit

can be the number of parts fabricated per hour, while in a continuous system (e.g., the power grid), the unit can be megawatt (MW).

Fig. 21 illustrates the structure of the parallel multi-component system investigated in this chapter.

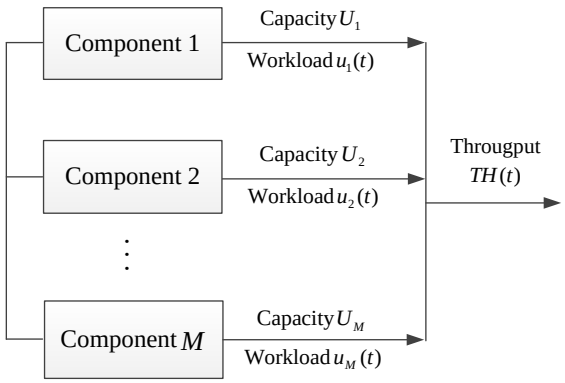

Figure 21: The structure of parallel multi-component systems

5.1.2 Degradation Modeling Framework

As we know, degradation is a natural and inevitable process due to performing operations. A component is considered to be failed when the degradation level of the component exceeds a pre-defined failure threshold. The failure threshold is often determined either by industrial standards [42] or based on the data-driven approach [74] (e.g., using the last observations before failure in all historically failed data to estimate the failure threshold). Once a component becomes failed, it has to be repaired/replaced to restore to the original healthy status before it can restart to operate properly.

Here, we would like clarify that the only type of component failure we consider in this chapter is the failure due to degradation, which is the only failure mode considered in most existing research in the degradation modeling area [18, 37, 42, 74, 76, 106, 115]. We admit that various other failure modes exist in reality, such as the catastrophic failure. However, we decide to leave the research about various failure modes into future work. In addition, it is common that the degradation of a component could

potentially affect the quality of the performed operations. Yet, this chapter does not consider component failure due to unsatisfactory quality of the performed operations but only due to its own degradation. In fact, modeling the relationship between component degradation and the quality of operations requires extensive study on system configurations and mathematically modeling [29] and will be investigated in future work.

We define $S_m(t)$ to be the amplitude of the degradation signal of component m at time t. We start by introducing a generic degradation model, in which $S_m(t)$ is modeled as a stochastic differential equation:

$$dS_m(t) = r_m(t)dt + dW_m(t), \tag{30}$$

Here $r_m(t)$ is the instantaneous degradation rate, and $W_m(t)$ is a Brownian motion with variance $\sigma_m^2(t)$, in which σ_m is defined as the diffusion parameter.

In the proposed work, we explicitly model the relationship between the instantaneous degradation rate $r_m(t)$ and the workload $u_m(t)$ for component m at time t. To model such relationship is indeed a challenging task, as it is highly dependent on the specific application and working condition. Research efforts have been made attempting to characterize this relationship between working condition and degradation rate through historical data as well as reasonable mathematical assumptions [36]. The novelty of our work is to study the workload adjustment strategy for better controlling the degradation process of components by leveraging this relationship function.

Here, to highlight our main idea, we focus on a special case that the instantaneous degradation rate $r_m(t)$ is proportional to the workload $u_m(t)$:

$$r_m(t) = \beta_m u_m(t), \tag{31}$$

where β_m is defined as the *degradation coefficient* of component m in this chapter. This linear assumption is consistent with our intuition as a component degrades faster

when it has higher workload assigned. Substitute Eq. 31 into Eq. 30, the degradation model in Eq. 30 can then be rewritten as:

$$dS_m(t) = \beta_m u_m(t)\, dt + dW_m(t). \tag{32}$$

In what follows, we provide a metal cutting example to illustrate the linearity assumption in Eq. 31. In this example, the component refers to the cutting tool that removes material from the work piece. The workload corresponds to the production rate, i.e., the number of parts being machined in a unit time. In a standard metal cutting process, there are typically two key parameters that determine the tool life: cutting speed V and cutting length L. The actual cutting time for machining one part is expressed as L/V. If we denote T_l as the tool life, then the total number of machined parts during the lifetime of a tool can be calculated as $T_l V/L$. The total production time is given by $T_p{=}\frac{T_l V}{u \times L}$ (recall u is the production rate). It is clear that T_p is inversely proportional to the degradation rate r. Assuming that the cutting length L remains constant, we have the following:

$$r \propto \frac{u}{T_l V}. \tag{33}$$

From [100], we also know that the tool life can be expressed as:

$$T_l \propto V^{-\frac{1}{\alpha}}, \tag{34}$$

where α depends on operational variables.

Furthermore, [68] modeled the relationship between cutting speed V and production rate u as:

$$\frac{Const}{u} = T_d + \frac{Const}{V},$$

where T_d is the idle time between two consecutive operations.

Building upon the model proposed by [68], we consider a scenario in which adjusting the production rate is achieved by adjusting the idle time T_d. Consequently,

by combining Eq. 33 and 34, we can see that: $r \propto u$. In future work, we will extend this linear model into a more general case when dealing with different applications and conditions.

Recall that β_m represents the "*degradation coefficient*" of component m. In this chapter, we assume the exact value of β_m is unknown and random. This assumption of unit-to-unit variability has been widely adopted in the literature [18, 37, 42, 74, 115] to capture the variation in the degradation processes due to material inhomogeneity and other manufacturing related uncertainty. Specifically, we model β_m as a random variable whose prior distribution is a normal distribution: $\beta_m \sim N(\kappa_m, \tau_m^2)$, where κ_m and τ_m^2 denote the mean and the variance, respectively. Here, the probability of $\beta_m \leq 0$ is often very small and thus is ignored in the chapter. In the next section, this prior distribution of β_m will be updated by using real-time measurements collected from condition monitoring via a Bayesian approach.

5.1.3 Degradation Model Updating

As mentioned earlier, the degradation model in Eq. 32 is updated by using *in-situ* monitoring data. The goal is to incorporate the most recent degradation status of the components to improve decision making regarding workload adjustments. Without loss of generality, we assume that condition monitoring and workload adjustment are performed at discrete observation epochs $t_0, t_1, \ldots, t_k$, where t_k is the most recent observation epoch, and the sampling intervals are constant, i.e., $t_1 - t_0 = t_2 - t_1 = \ldots t_k - t_{k-1} = \delta t$. Furthermore, let $S_m(t_k)$ be the amplitude of the degradation signal of component m at observation time t_k and $u_m(t_{k-1})$ be the corresponding workload assigned to that component during the interval (t_{k-1}, t_k). Using Eq. 32, we can see that $\delta S_m(t_k) = S_m(t_k) - S_m(t_{k-1})$ satisfies the following:

$$\delta S_m(t_k) = \beta_m u_m(t_{k-1})\, \delta t + W_m(t_k) - W_m(t_{k-1}).$$

Based on the property of Brownian motion, we have $W_m(t_k) - W_m(t_{k-1}) \sim N(0, \sigma_m^2 \delta t)$. Thus, given the corresponding workload assignment $u_m(t_{k-1})$ and degradation coefficient β_m, the conditional distribution of $\delta S_m(t_k)$ still follows a normal distribution: $\delta S_m(t_k) | u_m(t_{k-1}), \beta_m \sim N(\beta_m u_m(t_{k-1}) \delta t, \sigma_m^2 \delta t)$. By the property of independent increments of the Brownian motion, it is clear that $\delta S_m(t_1), \ldots, \delta S_m(t_k)$ are statistically independent. Therefore, the probability density function of the signal increments can be expressed as follows:

$$p(\delta \mathbf{S}_m(t_k) | \mathbf{u}_m(t_{k-1}), \beta_m) = \prod_{i=1}^{k} p(\delta S_m(t_i) | u_m(t_{i-1}), \beta_m),$$

where $\delta \mathbf{S}_m(t_k) = [\delta S_m(t_1), \ldots, \delta S_m(t_k)]'$ and $\mathbf{u}_m(t_{k-1}) = [u_m(t_0), \ldots, u_m(t_{k-1})]'$.

Using Bayes theorem, the posterior distribution of β_m given $\delta \mathbf{S}_m(t_k)$ and $\mathbf{u}_m(t_{k-1})$ can be computed by using Proposition 5.1.

Proposition 5.1. *$\beta_m | \delta \mathbf{S}_m(t_k), \mathbf{u}_m(t_{k-1})$ follows a normal distribution with mean $\kappa_m(t_k)$ and variance $\tau_m^2(t_k)$ satisfying:*

$$\kappa_m(t_k) = \frac{\tau_m^2 \sum_{i=1}^{k} \delta S_m(t_i) u_m(t_{i-1}) + \kappa_m \sigma_m^2}{\tau_m^2 \sum_{i=1}^{k} [u_m(t_{i-1})]^2 \delta t + \sigma_m^2},$$

$$\tau_m^2(t_k) = \frac{\sigma_m^2 \tau_m^2}{\tau_m^2 \sum_{i=1}^{k} [u_m(t_{i-1})]^2 \delta t + \sigma_m^2}.$$

The detailed proof is in the appendix.

5.2 Residual Life Distribution

The residual life of a component is defined as the first time that its degradation level reaches a pre-defined failure threshold. Here, we denote the failure threshold of component m as H_m. Let T_m be the residual life of component m. The RLD given the degradation coefficient β_m follows an inverse Gaussian (IG) distribution [18]:

$$P(T_m \leq t | S_m(t_k), u_m(t_k), \beta_m) \sim IG(t; \mu_m(t_k), \lambda_m(t_k)), \tag{35}$$

where $IG(t; \cdot, \cdot)$ represents the cumulative distribution function of an IG distribution, $\mu_m(t_k) = \frac{H_m - S_m(t_k)}{\beta_m u_m(t_k)}$ is the mean parameter of the IG distribution, and

$\lambda_m(t_k) = \frac{[H_m - S_m(t_k)]^2}{\sigma_m^2}$ is the shape parameter of the IG distribution. Here, recall that H_m is the failure threshold and $u_m(t_k)$ is the most recent setting of the production rate.

Although the conditional RLD follows Eq. 35, there is no explicit expression of the unconditional RLD, which can be estimated using simulation-based techniques [18]. Since these techniques are computationally expensive, we propose to focus on the conditional RLD and utilize $\kappa_m(t_k)$, (i.e. the posterior mean of β_m) as the point estimator of β_m. As a result, the mean parameter of the IG distribution, $\mu_m(t_k)$ in Eq. 35, is approximated by $\mu_m(t_k) = \frac{H_m - S_m(t_k)}{\kappa_m(t_k) u_m(t_k)}$.

In this work, $\mu_m(t_k)$ is used as an estimate of the predicted residual life. This approach was also used by [37] and was shown to provide a conservative lower bound of the mean of the unconditional RLD. For notational convenience, we define $q_m(t_k) = \frac{H_m - S_m(t_k)}{\kappa_m(t_k)}$ and thus, we have:

$$\mu_m(t_k) = \frac{q_m(t_k)}{u_m(t_k)}. \tag{36}$$

From Eq. 36, we see that given the workload assignment $u_m(t_k)$, a smaller value of $q_m(t_k)$ indicates a shorter residual life and thus a worse health status. At the extreme case, $q_m(t_k) = 0$ implies that a failure has occurred. In addition, given a non-zero$q_m(t_k)$, the predicted residual life is proportional to the reciprocal of the actual workload.

Based on the above results, we discuss a strategy to dynamically control the residual life by adjusting the production rates in the following section.

5.3 Dynamic Workload Adjustment

The goal of dynamically adjusting the workload is to control the residual life/failure time of each component to achieve some type of optimality. Particularly, when a component fails, it will require a certain period of time (hereafter defined as the repair time) for repair and maintenance. In this work, the repair time for component

m is considered to be constant, an integer multiple of the sampling interval, i.e., $P_m \delta t$, where P_m is an integer value.

As we mentioned before, although the parallel configuration provides a certain level of robustness for production, such system will fail to meet the objective when the number of components under repair at the same time exceeds a certain limit. As a result, our key idea here is to prevent the overlap of component failures. To achieve this goal, we propose a strategy that assigns higher workloads to components with worse health status. The underlying premise of this strategy is that a higher workload accelerates the degradation process and thus potentially separates the failure time of this component from the others. To do this, at decision epoch t_k, we rank the individual components according to their health status, which is indicated by $q_m(t_k)$. Recall that $q_m(t_k) = 0$ indicates that the corresponding component has failed. Next, we select components with non-zero $q_m(t_k)$(i.e., functional components) and rank them in the ascending order, such that $q_{(1)}(t_k) \leq q_{(2)}(t_k) \leq \cdots \leq q_{(\tilde{M}(t_k))}(t_k)$, where $\tilde{M}(t_k)$ is referred to the number of functional components at time t_k. In this way, we assign higher workloads to components with worse health status, i.e., $u_{(\tilde{M}(t_k))}(t_k) \leq \cdots \leq u_{(1)}(t_k)$.

This proposed strategy is motivated by the fact that degradation is an inevitable course for components as long as they are in operation. In practice, it is quite common that the repair of a component may take a long time and the system may have only limited maintenance resources to restore failed components at any time. In other words, some failed components have to wait for the release of maintenance resources before finishing the current repair job. Even assuming there are unlimited maintenance resources that could be used for immediate repair once the component failure occurs, the remaining functional components may still not be able to satisfy the production requirement due to the limited capacity of each component for perfuming

operations. As a result, simultaneous component failures will deteriorate the robustness of the system provided by the parallel configuration and thus may potentially lead to loss of production. Consequently, we propose to actively control the failure time of components so as to prevent the overlap of component failures, instead of simply waiting for spontaneous component failure as most of the existing literature assumes. In this way, we better take the advantage of the natural redundancy in a system, which may potentially lead to a better utilization of the maintenance resources as well as a consistently ensured production throughput. In what follows, we will specifically show how we can numerically determine the workloads for individual components at each decision epoch.

Given the posterior means of β_m for the operating components, $\kappa_{(1)}(t_k)$, ... , $\kappa_{\left(\tilde{M}(t_k)\right)}(t_k)$, and the respective degradation levels $S_{(1)}(t_k)$, ..., $S_{\left(\tilde{M}(t_k)\right)}(t_k)$, we propose to minimize the average degradation level of all components at the next decision epoch via adjusting the workloads $u_{(1)}(t_k), \ldots, u_{(\tilde{M}(t_k)}(t_k)$ assigned to components:

$$\min \frac{1}{\tilde{M}(t_k)} \sum_{m=1}^{\tilde{M}(t_k)} \left[\kappa_m(t_k)\, u_{(m)}(t_k)\, \delta t + S_{(m)}(t_k)\right]. \tag{37}$$

Subject to the following constraints:

$$\sum_{m=1}^{\tilde{M}(t_k)} u_{(m)}(t_k) = \min\Big(\sum_{m=1}^{\tilde{M}(t_k)} U_{(m)}, D\Big), \tag{38}$$

$$u_{(\tilde{M}(t_k))}(t_k) \leq \cdots \leq u_{(1)}(t_k), \tag{39}$$

$$0 \leq u_m(t_k) \leq U_m, \text{ for } m = 1, \ldots, M \tag{40}$$

$$\frac{q_{(m)}(t_k)}{u_{(m)}(t_k)} + P_{(m)}\delta t \leq \frac{q_{(m+1)}(t_k)}{u_{(m+1)}(t_k)}, \text{ for } m = 1, \ldots, \tilde{M}(t_k) - 1. \tag{41}$$

The objective function in Eq. 37 is to ensure on average all components fail in a slowest pace, and its objective value somehow provides a new insight on the systems reliability in real time. Constraint Eq. 38 ensures that when the systems capacity is greater than the demand, the throughput is equal to the demand. Conversely,

when the systems capacity is less than the demand, the throughput is set at the systems capacity. Constraint Eq. 39 means that we assign higher production rates to components with more severe degradation status. Constraint Eq. 41 prevents the overlap of component failures; that is, the predicted residual lives of any two components that will fail consecutively should have a difference greater than the repair time $P_{(m)}\delta t$.

Since all decision variables are non-negative, Eq. 41 can be rewritten as:

$$P_{(m)}\delta t u_{(m)}(t_k)u_{(m+1)}(t_k) \leq q_{(m+1)}(t_k)u_{(n)}\left(t_k\right) - q_{(m)}\left(t_k\right)u_{(m+1)}\left(t_k\right) \tag{42}$$

for $m = 1, \ldots, \tilde{M}\left(t_k\right) - 1$. This results in $\left(\tilde{M}\left(t_k\right) - 1\right)$ number of non-convex quadratic constraints. Theoretical studies have shown that this is an NP-hard problem, thus finding feasible solutions can be challenging [67]. The existing literature in quadratically constrained optimization problems often focuses on searching for a convex space that covers the original non-convex space then solving the convex problem [1, 4, 9]. The drawback of this approach is that the optimal solution to the convex problem may not be feasible to the original problem (since the solution space of the convex problem is larger).

In this work, finding a feasible solution is necessary to prevent the overlap of component failures. In other words, using the existing methodology to solve our quadratically constrained optimization problem may provide miss-leading results, since even the optimization problem can be solved, the overlap between component failures may still not be prevented, which is the major objective of this work. Therefore, unlike the existing literature, we focus on a convex subspace of the original non-convex space. In this way, we can guarantee that as long as the optimization problem has a solution, the solution is capable of preventing the overlap of component failures. To do this, we utilize the Arithmetic Mean-Geometric Mean (AM-GM) inequality, which states that $u_{(m)}(t_k)u_{(m+1)}(t_k)$ is no greater than $\frac{1}{4}\left[u_{(m)}\left(t_k\right) + u_{(m+1)}\left(t_k\right)\right]^2$. Thus, inequalities in

Eq. (42) can be modified to the following convex form:

$$\frac{P_{(m)}\delta t}{4}\left[u_{(m)}\left(t_k\right)+u_{(m+1)}\left(t_k\right)\right]^2 \leq q_{(m+1)}\left(t_k\right)\ u_{(m)}\left(t_k\right)-q_{(m)}\left(t_k\right)\ u_{(m+1)}\left(t_k\right) \quad (43)$$

for $m=1,\ldots,\tilde{M}\left(t_k\right)-1$.

In some circumstances (e.g., when the overlap among component failures cannot be avoided), the original constraints in Eq. 42 may not lead to any solution. In such case, the modified constraints in Eq. 43 will also be infeasible. When this occurs, we relax the group of constraints in Eq. 43 by removing the inequality regarding to the component with the least degradation severity:

$$\begin{aligned}&\frac{P_{(\tilde{M}(t_k)-1)}\delta t}{4}\left[u_{(\tilde{M}(t_k)-1)}(t_k)+u_{(\tilde{M}(t_k))}(t_k)\right]^2\\&\leq q_{(\tilde{M}(t_k))}\left(t_k\right)u_{(\tilde{M}(t_k)-1)}\left(t_k\right)-q_{(\tilde{M}(t_k)-1)}\left(t_k\right)u_{(\tilde{M}(t_k))}\left(t_k\right).\end{aligned}$$

In other words, if the solution to the original optimization problem is infeasible, we will allow the overlap of predicted failures between the two components with the least degradation severity (i.e., the two healthiest components). If this relaxation still yields infeasibility, we will continue to remove subsequent inequalities until a feasible solution is obtained.

We define the workload adjustment of a multi-component system at epoch t_k as *controllable* if the optimization problem is feasible when at least one constraint in Eq. 42 remains. If, however, we are forced to remove all $\tilde{M}(t_k)-1$ constraints in Eq. 43 to achieve feasibility, then the problem is referred to as *uncontrollable*. Whether the problem is controllable or not depends on the instantaneous degradation status of the components, which are time-varying due to the dynamic characteristics of degradation processes and their interactions with adjustable workloads. Thus, the level of control of the system may vary at different epochs depending on the degradation status of each component. Since we evaluate the level of control at individual epochs separately, when a component is uncontrollable at a decision epoch, we will derive the solutions

by removing all $\tilde{M}(t_k) - 1$ constraints in Eq. 43 for decision making and then re-evaluate the level of control at the next decision epoch. The flow chart in Fig. 22 summarizes the detailed procedure of the proposed methodology.

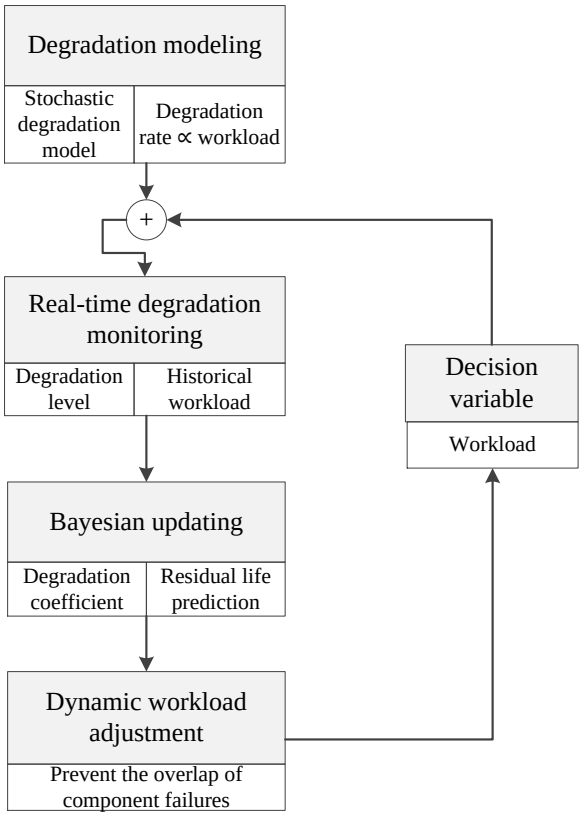

Figure 22: The detailed flow chart of the proposed dynamic control methodology

5.4 Numerical Case Study

5.4.1 Study Set-up and Parameter Settings

In this section, we investigate the performance of our proposed methodology through a numerical case study. We consider a hypothetical stamping system with 5 identical stamping machines working in parallel to fabricate parts. This example is inspired by the single-stage stamping process investigated in [30], which provided both the system description and the degradation-related parameters obtained through real experiments. In this study, parameters utilized to generate degradation signals are obtained through [30]:

1. The unit of workload is the number of parts fabricated in a unit time.

2. The prior mean of degradation coefficient of each machine, i.e., κ_1,,κ_5, is equal to 5.97×10^{-8} inch per part.

3. The diffusion parameter of the Brownian motion error of each machine, i.e, σ_1,,σ_5, is 2.03×10^{-5} inch per unit time. In addition, we assume that the failure threshold of each machine is 0.004 inch to reflect the real manufacturing settings.

4. The maximum workload for each machine is set to be 1500 parts per day and the demand is set to be 6000 parts per day. The decision epoch (unit time) in this study is one day. Once the machine is failed, it will immediately go through the repair process, which is assumed to takes a constant amount of time with at least one decision epoch. Additional repair time may be required in terms of multiple of a day. Under this configuration, if no more than one machine fails simultaneously, the demand can still be satisfied by the remaining four machines. However, if more than one machine fails, the demand can no longer be satisfied.

5. The length of the simulation period is set to be 300 days.

5.4.2 Simulation Procedure and Evaluation Results

We compared the performance of our proposed dynamic workload adjustment methodology with two benchmark strategies. The first benchmark assumes that workloads are equally assigned to all functional components (hereafter referred to as Benchmark 1). The second benchmark assigns production rates randomly (hereafter referred to as Benchmark 2). To be specific, at each epoch, Benchmark 2 identifies all possible solutions of workload assignments and randomly draws one solution from the entire

solution sets. We use two key performance indices (KPIs) for performance comparison: 1) the percentage of time that more than one machine is failed and under repair and 2) The percentage loss of production. Recall that given the study set-up, when there is more than one machine is under repair, the demand can no longer be satisfied, and thus may result in the loss of production.

We evaluated the effects of two factors:

1. The first was the repair time. We evaluated the performance when the repair time is equal to 1, 3, and 5 days.

2. The second factor was the coefficient of variation (CV) of the prior distribution of the degradation coefficient. The CV is defined as the ratio of standard deviation to the mean. In other words, for each component m, its CV of β_m is equal to τ_m/κ_m . Thus, CV captures the variation of the degradation coefficients among components. Note that as the CV decreases, the unit-to-unit variability also decreases. Recall that all machines in this study have the same $\kappa_m = 5.97 \times 10^{-8}$ inch per part. Consequently a smaller CV indicates that the actual β of different machines are more similar to each other, and thus they tend to fail at the same time if they are assigned with similar workloads. Testing was performed under four different levels of CVs: 1/3, 1/6, 1/9, and 1/12.

For each of the $3 \times 4 = 12$ conditions, we ran 30 experiments. The boxplots of the two KPIs in all 12 conditions are shown in Fig. 23 and Fig. 24, respectively. In each figure, the x-axis of all subplots has label I for Benchmark 1, label II for Benchmark 2 and label III for the proposed methodology.

From the results shown in Fig. 23 and Fig. 24, we can make the following conclusions:

1. For a small repair time (1 day in this example), both KPIs were insignificant for all three strategies. This phenomenon is a likely outcome since the probability

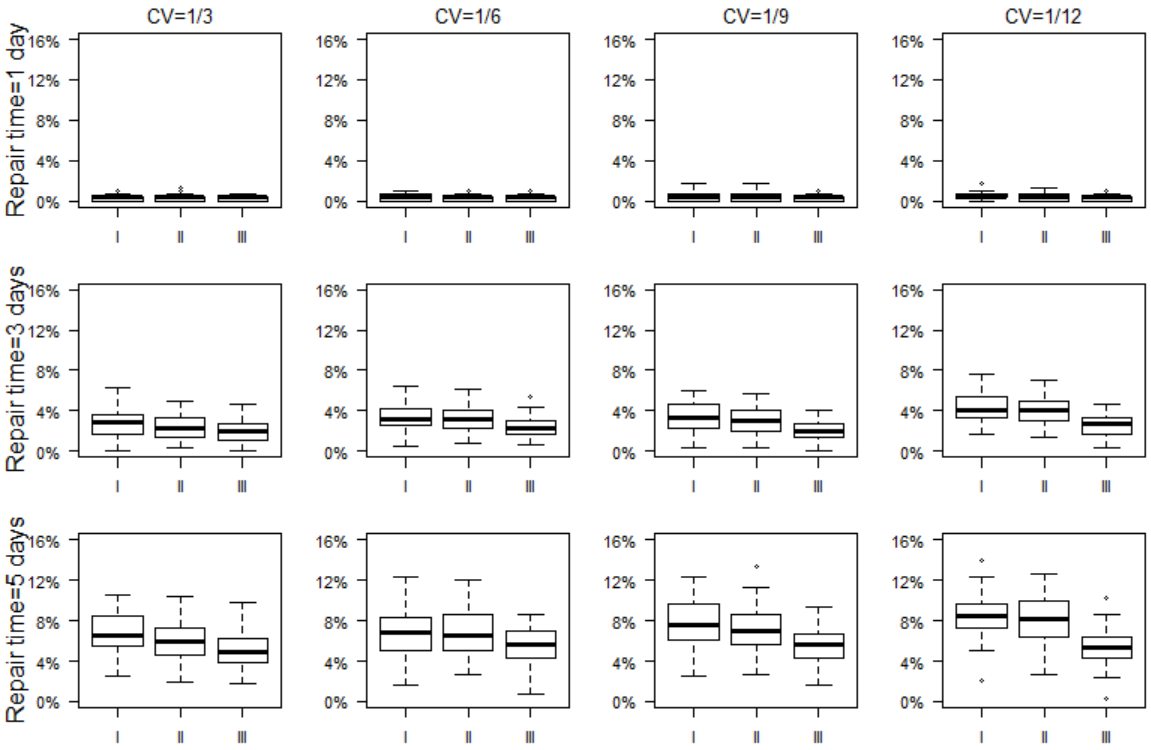

Figure 23: The percentage of time when more than one machine is under repair
X-axis: I - Benchmark 1; II - Benchmark 2; III - Proposed methodology.

of having machines failed at the same time is small when the repair time is short. A longer repair time increases the likelihood of failure overlaps, thus resulting in an apparent increase in both KPIs (in all three policies).

2. The performance of Benchmark 1 was the worst among three strategies. One possibility is that the Benchmark 1 results in very close failure times among individual machines and thus significant amount of overlap among machine failures. The performance of Benchmark 2 was slightly better than Benchmark 1 but was still significantly worse than our proposed methodology. This is because although Benchmark 2 reduces the possibility of having multiple machines that fail closely due to the random distributed workload, it still does not actively control the degradation process of each machine from the overall system point of view.

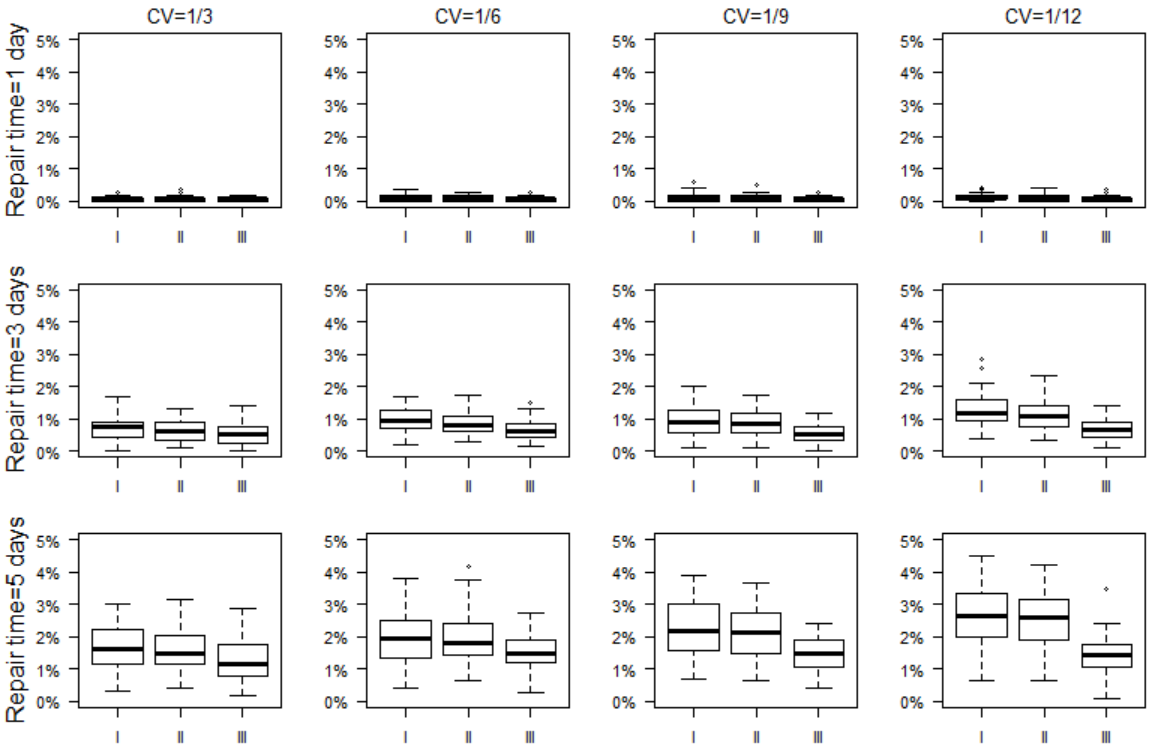

Figure 24: The percentage loss of production
X-axis: I - Benchmark 1; II - Benchmark 2; III - Proposed methodology.

3. Our proposed methodology appeared to be relatively robust to unit-to-unit variability, while the performance of the other two benchmarks decreased significantly as the unit-to-unit variability decreased. This is because when the unit-to-unit variability is small and machines are assigned with equal or random workloads (i.e., without dynamic workload adjustment), they tend to exhibit similar degradation processes and thus several machines are more likely to fail at the same time.

CHAPTER VI

CONCLUSION

6.1 Summary of Original Contributions

In summary, this thesis investigates three major research topics in the area of prognostics of multi-component systems. In Chapter 3, we consider the case when component degradation is crucial but their degradation signals cannot be obtained directly from condition monitoring data. The applicable situation is the vibration monitoring of engineering systems. In Chapter 4, we consider the case when system-level degradation is crucial but the degradation between individual components are interactive. The applicable situation is in the MMPs. In Chapter 5, we consider the case when the degradation process of individual components can be controlled to achieve certain system-level objective. The applicable situation lies in parallel multi-component systems. The original contributions are summarized below.

The original contribution of Chapter 3 is to propose a methodology to separate the degradation signals of identical components that generate an identical frequency from mixed sensor information when the mixing process is unknown. This chapter addresses the research problem that vibration sensors installed on a multi-component system may only capture an unknown mixture of component vibration signals and component vibration signals may share an identical frequency. This problem is very challenging, since 1) the mixing process is unknown and needs to be solely estimated from sensor vibration signals, 2) traditional spectrum analysis is only capable of identifying vibration signals that have distinct frequencies. To solve this problem, in this chapter, we propose a simultaneous signal separation and prognostics framework, which applies ICA on pre-processed sensor signals to identify component degradation

signals in order to predict the RLDs of individual components. This methodology has great potential impacts in the diagnostics and prognostics of many engineering systems, where the condition monitoring and defect detection of an individual component is crucial but challenging to achieve due to the limitation of sensor installation and similar defective frequencies from identical components.

The original contribution of Chapter 4 is to propose an innovative model that captures the relationship between the process of tool wear and the production quality in MMPs for the purpose of accurately predicting the system-level RLD. This chapter addresses the research problem about predicting the system-level failure due to non-conforming products when the tool wear in one stage affects the product quality at current stage, which, on the other hand, may affect the rate of tool wear at subsequent stages. This problem is challenging because of the interactive relationship between tool wear and product quality as well as the stochastic characteristics of tool wear. Existing literature is only limited to modeling the impact of product quality on the tooling catastrophic failure and computing offline lifetime distribution. In this chapter, we utilize a high-dimensional stochastic differential equation model to capture the interaction relationship between the process of tool wear and product quality. We then leverage real-time quality measurements to on-line predict the residual life of the MMP as a system. This methodology has great potential impacts in the maintenance scheduling and inventory planning of MMPs, since it provides accurate real-time residual life prediction.

The major contribution of Chapter 5 is to open a new research direction that focuses on dynamically adjusting the workloads assigned to individual components to actively control their degradation processes and failure times to ensure satisfactory system performance. This chapter addresses the research problem that the overlap of component failures in a parallel system needs to be avoided to reduce the loss of production. This research problem has not been explicitly studied before. The

existing literature in prognostics assumes that the degradation process is self-evolving, and thus only focuses on modeling the degradation process and predicting the residual life, rather than actively controlling the failure time. This chapter assumes that the degradation rate of a component is directly related to the workload assigned to that component and then dynamically adjusts the workloads at every decision epoch to prevent the overlap of component failures. This methodology has great potential impacts in various engineering systems where the failure times of individual components need to be separated for better utilization of maintenance resources and more consistent productivity.

6.2 Future Work

Potential future extension of the work in Chapter 3 is to change the model of the mixing process from a simple linear model to a convolutive model. In fact, the convolutive model that captures time delay in the transmission of vibration from components to sensors may have better modeling accuracy than the simple linear model when analyzing vibration signals, as discussed in [45, 45]. The major limitation of using the convolutive model is the model complexity. Besides changing the model assumption, the proposed prognostics framework needs to be validated using real-world vibration data in the future, besides using simulated study. This may bring new research challenges since real data may have more uncertainty to be addressed.

Potential extension of the work in Chapter 4 is to consider more complex models such as non-linear models to capture the sophisticated relationship between tool wear and product quality degradation. The major limitation of using non-linear model is that higher-order SDE is very complicated to get an explicit solution. Therefore, numerical solutions may need to be investigated. Furthermore, future work may also incorporate catastrophic failure into the model.

Future work of Chapter 5 may include several important topics: (1) In this chapter, we focus on a special case that the instantaneous degradation rate is proportional to the production rate. Such relationship assumption may not be true in different processes. Additional efforts are needed to study the performance of the workload adjustment strategy when the instantaneous degradation rate and the workload exhibit different relationship functions. (2) In addition, future work will focus on the extension of our methodology to the serial-parallel multistage manufacturing processes to prevent the overlap of machine failures and maintain system throughput. (3) Moreover, further studies can be done to develop different strategies of workload adjustment to account for various requirements in reality. For example, in this work, we assume that the repair time of individual components remains constant. However, in practice, the maintenance resource is limited. Thus, some of the failed components may not be repaired in time, which may complicate the problem.

APPENDIX A

SUPPLEMENTARY MATERIALS OF CHAPTER 4

A.1 Choosing the parameter values for different numbers of stages M

1. The elements of matrices $\mathbf{A}$, $\mathbf{B}$, are determined according to Eq. 28.

2. The elements of matrix $\mathbf{C}$ are determined as follows:

$$c_{i,j} \begin{cases} 0.004, & \text{if } \ j = 2i-1 \text{ or } 2i \\ 0.02, & \text{if } \ j = 2i-3 \\ 0.012, & \text{if } \ j = 2i-2 \\ 0, & \text{Otherwise} \end{cases}$$

3. At every stage, the prior mean of the natural rate of tool wear and the variance of the Brownian motion noise in the tool wear model are equal to the values provided by [30] multiply with 1000 (operations per sampling interval).

4. The prior variance of the natural rate of tool wear is determined as follows: $\mathbf{\Sigma_R} = diag\left(\sigma^2_{\mathbf{R},1}, \ldots, \sigma^2_{\mathbf{R},M}\right)$, where $\sigma_{\mathbf{R},i} = \mu_{\mathbf{R},i}/3$.

5. The failure threshold for each stage m= $1, \ldots, M$ is equal to 0.5.

APPENDIX B

SUPPLEMENTARY MATERIALS OF CHAPTER 5

B.1 Proof of Proposition 5.1

$$
\begin{aligned}
p\left(\beta_m|\delta\mathbf{S}_m(t_k),\mathbf{u}_m(t_{k-1})\right) &\propto p\left(\delta\mathbf{S}_m(t_k)|\mathbf{u}_m(t_{k-1}),\beta_m\right)p\left(\beta_m\right)\\
&\propto \prod_{i=1}^{k} p\left(\delta S_m(t_k)|u_m(t_{k-1}),\beta_m\right)p\left(\beta_m\right)\\
&\propto \exp\left\{-\sum_{i=1}^{k}\frac{\left[\delta S_m\left(t_i\right)\beta_m u_m\left(t_{i-1}\right)\delta t\right]^2}{2\sigma_m^2\delta t}-\frac{\left[\beta_m-\kappa_m\right]^2}{2\tau_m^2}\right\}\\
&\propto \exp\left\{-\frac{1}{2}\left[\frac{\sum_{i=1}^{k}\left[u_m\left(t_{i-1}\right)\right]^2\delta t}{\sigma_m^2}+\frac{1}{\tau_m^2}\right]\beta_{m,n}^2\right\}\\
&\times \exp\left\{\left[\frac{\sum_{i=1}^{k}\delta S_{m,n}\left(t_i\right)u_m\left(t_{i-1}\right)}{\sigma_m^2}+\frac{\kappa_m}{\tau_m^2\beta_m}\right]\beta_m\right\}\\
&\propto \exp\left\{-\frac{\left[S_m-\frac{\tau_m^2\sum_{i=1}^{k}\delta S_m(t_i)u_m(t_{i-1})+\kappa_m\sigma_m^2}{\tau_m^2\sum_{i=1}^{k}\left[u_m(t_{i-1})\right]^2\delta t+\sigma_m^2}\right]^2}{\frac{2\sigma_m^2\tau_m^2}{\tau_m^2\sum_{i=1}^{k}\left[u_m(t_{i-1})\right]^2\delta t+\sigma_m^2}}\right\}\\
&\propto N\left(\kappa_m\left(t_k\right),\tau_m^2\left(t_k\right)\right),
\end{aligned}
$$

where $\kappa_m\left(t_k\right)=\frac{\tau_m^2\sum_{i=1}^{k}\delta S_m(t_i)u_m(t_{i-1})+\kappa_m\sigma_m^2}{\tau_m^2\sum_{i=1}^{k}\left[u_m(t_{i-1})\right]^2\delta t+\sigma_m^2}$ and $\tau_m^2\left(t_k\right)=\frac{\sigma_m^2 t_m^2}{\tau_m^2\sum_{i=1}^{k}\left[u_m(t_{i-1})\right]^2\delta t+\sigma_m^2}$.

REFERENCES

[1] Al-Khayyal, F. A., Larsen, C., and Van Voorhis, T., "A relaxation method for nonconvex quadratically constrained quadratic programs," *Journal of Global Optimization*, vol. 6, no. 3, pp. 215–230, 1995.

[2] Ambani, S., Li, L., and Ni, J., "Condition-based maintenance decision-making for multiple machine systems," *Journal of Manufacturing Science and Engineering*, vol. 131, no. 3, p. 31009, 2009.

[3] Amirat, Y., Benbouzid, M., Al-Ahmar, E., Bensaker, B., and Turri, S., "A brief status on condition monitoring and fault diagnosis in wind energy conversion systems," *Renewable and Sustainable Energy Reviews*, vol. 13, no. 9, pp. 2629–2636, 2009.

[4] Anstreicher, K. M., "Semidefinite programming versus the reformulation-linearization technique for nonconvex quadratically constrained quadratic programming," *Journal of Global Optimization*, vol. 43, no. 2-3, pp. 471–484, 2009.

[5] Apley, D. W. and Lee, H. Y., "Identifying spatial variation patterns in multivariate manufacturing processes: a blind separation approach," *Technometrics*, vol. 45, no. 3, pp. 220–234, 2003.

[6] Apley, D. W. and Shi, J., "Diagnosis of multiple fixture faults in panel assembly," *Journal of Manufacturing Science and Engineering*, vol. 120, no. 4, pp. 793–801, 1998.

[7] Astakhov, V. P. and Davim, J. P., "Tools (geometry and material) and tool wear," in *Machining*, pp. 29–57, Springer, 2008.

[8] Åström, K., *Introduction to stochastic control theory*, vol. 70. Elsevier Science, 1970.

[9] Audet, C., Hansen, P., Jaumard, B., and Savard, G., "A branch and cut algorithm for nonconvex quadratically constrained quadratic programming," *Mathematical Programming*, vol. 87, no. 1, pp. 131–152, 2000.

[10] Balageas, D., Fritzen, C., and Güemes, A., *Structural health monitoring*, vol. 493. Wiley Online Library, 2006.

[11] Bartelmus, W. and Zimroz, R., "Vibration condition monitoring of planetary gearbox under varying external load," *Mechanical Systems and Signal Processing*, vol. 23, no. 1, pp. 246–257, 2009.

[12] Baruah, P. and Chinnam, R. B., "HMMs for diagnostics and prognostics in machining processes," *International Journal of Production Research*, vol. 43, no. 6, pp. 1275–1293, 2005.

[13] Basir, O. and Yuan, X., "Engine fault diagnosis based on multi-sensor information fusion using Dempster–Shafer evidence theory," *Information Fusion*, vol. 8, no. 4, pp. 379 – 386, 2007.

[14] Basseville, M. and Nikiforov, I., *Detection of abrupt changes: theory and application*, vol. 15. Prentice Hall Englewood Cliffs, 1993.

[15] Beebe, R., "Condition monitoring of steam turbines by performance analysis," *Journal of Quality in Maintenance Engineering*, vol. 9, no. 2, pp. 102 – 112, 2003.

[16] Belouchrani, A., Abed-Meraim, K., Cardoso, J. F., and Moulines, E., "A blind source separation technique using second-order statistics," *IEEE Transaction on Signal Processing*, vol. 45, no. 2, pp. 434–444, 1997.

[17] Bengtsson, C., "Status and trends in transformer monitoring," *Power Delivery, IEEE Transactions on*, vol. 11, no. 3, pp. 1379–1384, 1996.

[18] Bian, L. and Gebraeel, N., "Computing and updating the first-passage time distribution for randomly evolving degradation signals," *IIE Transactions*, vol. 44, no. 11, pp. 974–987, 2012.

[19] Bian, L. and Gebraeel, N., "Stochastic modeling and real-time prognostics for multi-component systems with degradation rate interactions," *IIE Transactions*, vol. 46, no. 5, pp. 470–482, 2014.

[20] Bishop, C. M., *Pattern recognition and machine learning*. Springer New York, 2006.

[21] Booth, C. and McDonald, J., "The use of artificial neural networks for condition monitoring of electrical power transformers," *Neurocomputing*, vol. 23, no. 1-3, pp. 97 – 109, 1998.

[22] Byrne, G., Dornfeld, D., Inasaki, I., Ketteler, G., König, W., and Teti, R., "Tool condition monitoring (tcm)—the status of research and industrial application," *CIRP Annals-Manufacturing Technology*, vol. 44, no. 2, pp. 541–567, 1995.

[23] Cardoso, J. F., "Blind signal separation: Statistical principles," *Proceedings of the IEEE*, vol. 86, no. 10, pp. 2009–2025, 1998.

[24] Cardoso, J. F. and Souloumiac, A., "Blind beamforming for non-Gaussian signals," *IEE Proceedings F: Radar and Signal Processing*, vol. 140, no. 6, pp. 362–370, 1993.

[25] Caselitz, P. and Giebhardt, J., "Advanced maintenance and repair for offshore wind farms using fault prediction techniques," in *Proceedings of WWEC'02*, 2002.

[26] Caselitz, P., Giebhardt, J., and Mevenkamp, M., "Development of a fault detection system for wind energy converters," in *Proceedings of the EUWEC*, vol. 96, pp. 1004–1007, 1996.

[27] Celen, M. and Djurdjanovic, D., "Operation-dependent maintenance scheduling in flexible manufacturing systems," *CIRP Journal of Manufacturing Science and Technology*, vol. 5, no. 4, pp. 296–308, 2012.

[28] Chao, M. T., Fu, J. C., and Koutras, M. V., "Survey of reliability studies of consecutive-k-out-of-n: F and related systems," *IEEE Transactions on reliability*, vol. 44, no. 1, pp. 120–127, 1995.

[29] Chen, Y. and Jin, J., "Quality-reliability chain modeling for system-reliability analysis of complex manufacturing processes," *IEEE Transactions on Reliability*, vol. 54, no. 3, pp. 475 – 488, 2005.

[30] Chen, Y. and Jin, J., "Quality-oriented-maintenance for multiple interactive tooling components in discrete manufacturing processes," *IEEE Transactions on Reliability*, vol. 55, no. 1, pp. 123–134, 2006.

[31] Chen, Y., Jin, J., and Shi, J., "Integration of dimensional quality and locator reliability in design and evaluation of multi-station body-in-white assembly processes," *IIE Transactions*, vol. 36, no. 9, pp. 827–839, 2004.

[32] Colledani, M. and Tolio, T., "Integrated quality, production logistics and maintenance analysis of multi-stage asynchronous manufacturing systems with degrading machines," *CIRP Annals-Manufacturing Technology*, vol. 61, no. 1, pp. 455–458, 2012.

[33] Dimla, D. E., "Sensor signals for tool-wear monitoring in metal cutting operations—a review of methods," *International Journal of Machine Tools and Manufacture*, vol. 40, no. 8, pp. 1073–1098, 2000.

[34] Ding, Y., Ceglarek, D., and Shi, J., "Fault diagnosis of multistage manufacturing processes by using state space approach," *Journal of manufacturing science and engineering*, vol. 124, no. 2, pp. 313–322, 2002.

[35] Ding, Y., Shi, J., and Ceglarek, D., "Diagnosability analysis of multi-station manufacturing processes," *Journal of Dynamic Systems, Measurement, and Control*, vol. 124, no. 1, pp. 1–13, 2002.

[36] Doksum, K. A. and Hóyland, A., "Models for variable-stress accelerated life testing experiments based on Wiener processes and the inverse Gaussian distribution," *Technometrics*, vol. 34, no. 1, pp. 74–82, 1992.

[37] Elwany, A. and Gebraeel, N., "Real-time estimation of mean remaining life using sensor-based degradation models," *Journal of Manufacturing Science and Engineering*, vol. 131, no. 5, p. 51005, 2009.

[38] Fan, W. and Qiao, P., "Vibration-based damage identification methods: a review and comparative study," *Structural Health Monitoring*, vol. 10, no. 1, pp. 83– 111, 2011.

[39] Farrar, C. and Worden, K., "An introduction to structural health monitoring," *Philosophical Transactions of the Royal Society A: Mathematical, Physical and Engineering Sciences*, vol. 365, no. 1851, pp. 303–315, 2007.

[40] Freiheit, T., Shpitalni, M., and Hu, S. J., "Productivity of paced parallel-serial manufacturing lines with and without crossover," *Journal of Manufacturing Science and Engineering*, vol. 126, pp. 361–367, 2004.

[41] Gebraeel, N., "Sensory-updated residual life distributions for components with exponential degradation patterns," *Automation Science and Engineering, IEEE Transactions on*, vol. 3, no. 4, pp. 382–393, 2006.

[42] Gebraeel, N., Lawley, M., Li, R., and Ryan, J., "Residual life distributions from component degradation signals: A Bayesian approach," *IIE Transactions*, vol. 37, no. 6, pp. 542–557, 2005.

[43] Gebraeel, N., Lawley, M., Liu, R., and Parmeshwaran, V., "Residual life predictions from vibration-based degradation signals: a neural network approach," *IEEE Transactions on Industrial Electronics*, vol. 51, no. 3, pp. 694–700, 2004.

[44] Gelle, G. and Colas, M., "Blind source separation: a tool for rotating machine monitoring by vibrations analysis," *Journal of Sound and vibration*, vol. 248, no. 5, pp. 865–885, 2001.

[45] Gelle, G., Colas, M., and Delaunay, G., "Blind sources separation applied to rotating machines monitoring by acoustical and vibrations analysis," *Mechanical Systems and Signal Processing*, vol. 14, no. 3, pp. 427–442, 2000.

[46] Hameed, Z., Hong, Y., Cho, Y., Ahn, S., and Song, C., "Condition monitoring and fault detection of wind turbines and related algorithms: A review," *Renewable and Sustainable energy reviews*, vol. 13, no. 1, pp. 1–39, 2009.

[47] Hao, L., Gebraeel, N., and Shi, J., "Simultaneous signal separation and prognostics of multi-component systems: The case of identical components," *IIE Transactions*, vol. In Press, 2014.

[48] Hayter, A. J. and Tsui, K.-L., "'identification and quantification in multivariate quality-control problems," *Journal of Quality Technology*, vol. 26, no. 3, pp. 197–208, 1994.

[49] He, Q., Kong, F., and Yan, R., "Subspace-based gearbox condition monitoring by kernel principal component analysis," *Mechanical Systems and Signal Processing*, vol. 21, no. 4, pp. 1755–1772, 2007.

[50] Huang, J., Zuo, M. J., and Wu, Y., "Generalized multi-state k-out-of-n: G systems," *IEEE Transactions on Reliability*, vol. 49, no. 1, pp. 105–111, 2000.

[51] Huang, Q. and Shi, J., "Variation transmission analysis and diagnosis of multi-operational machining processes," *IIE Transactions*, vol. 36, no. 9, pp. 807–815, 2004.

[52] Huang, Q., Shi, J., and Yuan, J., "Part dimensional error and its propagation modeling in multi-operational machining processes," *Journal of manufacturing science and engineering*, vol. 125, pp. 255–262, 2003.

[53] Huang, R., Xi, L., Li, X., Liu, C. R., Qiu, H., and Lee, J., "Residual life predictions for ball bearings based on self-organizing map and back propagation neural network methods," *Mechanical Systems and Signal Processing*, vol. 21, no. 1, pp. 193 – 207, 2007.

[54] Huang, Y.-C. and Huang, C.-M., "Evolving wavelet networks for power transformer condition monitoring," *Power Delivery, IEEE Transactions on*, vol. 17, pp. 412 –416, apr 2002.

[55] Hwang, F. K., "Fast solutions for consecutive-k-out-of-n: F system," *IEEE Transactions on reliability*, vol. 31, no. 5, pp. 447–448, 1982.

[56] Hyvärinen, A., "Blind source separation by nonstationarity of variance: A Cumulant-based approach," *IEEE Transactions on Neural Networks*, vol. 12, no. 6, pp. 1471–1474, 2001.

[57] Hyvärinen, A., Karhunen, J., and Oja, E., *Independent Component Analysis*. New York, NY: John Wiley & Sons, Inc., 2001.

[58] Hyvärinen, A. and Oja, E., "A fast fixed-point algorithm for Independent Component Analysis," *Neural Computation*, vol. 9, no. 7, pp. 1483–1492, 1997.

[59] Jantunen, E., "A summary of methods applied to tool condition monitoring in drilling," *International Journal of Machine Tools and Manufacture*, vol. 42, no. 9, pp. 997–1010, 2002.

[60] Jin, J., "Individual station monitoring using press tonnage sensors for multiple operation stamping processes," *Journal of Manufacturing Science and Engineering*, vol. 126, no. 1, pp. 83–90, 2004.

[61] Jin, J. and Shi, J., "State space modeling of sheet metal assembly for dimensional control," *Journal of Manufacturing Science and Engineering*, vol. 121, no. 4, pp. 756–762, 1999.

[62] Jin, J. and Shi, J., "Diagnostic feature extraction from stamping tonnage signals based on design of experiments," *Journal of manufacturing science and engineering*, vol. 122, no. 2, pp. 360–369, 2000.

[63] Kermit, M. and Tomic, O., "Independent component analysis applied on gas sensor array measurement data," *IEEE Sensors Journal*, vol. 3, no. 2, pp. 218–228, 2003.

[64] Ko, J. and Ni, Y., "Technology developments in structural health monitoring of large-scale bridges," *Engineering structures*, vol. 27, no. 12, pp. 1715–1725, 2005.

[65] Kumar, M., Mukherjee, P. S., and Misra, N. M., "Advancement and current status of wear debris analysis for machine condition monitoring: a review," *Industrial Lubrication and Tribology*, vol. 65, no. 1, pp. 3–11, 2013.

[66] Kurada, S. and Bradley, C., "A review of machine vision sensors for tool condition monitoring," *Computers in Industry*, vol. 34, no. 1, pp. 55–72, 1997.

[67] Lasserre, J. B., "Global optimization with polynomials and the problem of moments," *SIAM Journal on Optimization*, vol. 11, no. 3, pp. 796–817, 2001.

[68] Lee, B. and Tarng, Y., "Cutting-parameter selection for maximizing production rate or minimizing production cost in multistage turning operations," *Journal of Materials Processing Technology*, vol. 105, no. 1, pp. 61–66, 2000.

[69] Lee, D., Hwang, I., Valente, C., Oliveira, J., and Dornfeld, D., "Precision manufacturing process monitoring with acoustic emission," *International Journal of Machine Tools and Manufacture*, vol. 46, no. 2, pp. 176 –188, 2006.

[70] Lee, J., "Machine performance monitoring and proactive maintenance in computer-integrated manufacturing: review and perspective," *International Journal of Computer Integrated Manufacturing*, vol. 8, no. 5, pp. 370–380, 1995.

[71] Li, H., Li, D., and Song, G., "Recent applications of fiber optic sensors to health monitoring in civil engineering," *Engineering structures*, vol. 26, no. 11, pp. 1647–1657, 2004.

[72] Li, W., Fu, F., Ball, A. D., Leung, A. Y. T., and Phipps, C. E., "A study of the noise from diesel engines using the independent component analysis," *Mechanical Systems and Signal Processing*, vol. 15, no. 6, pp. 1165–1184, 2001.

[73] Liu, J., Jin, J., and Shi, J., "State space modeling for 3-d variation propagation in rigid-body multistage assembly processes," *Automation Science and Engineering, IEEE Transactions on*, vol. 7, no. 2, pp. 274–290, 2010.

[74] Liu, K., , Gebraeel, N., and Shi, J., "A data-level fusion model for developing composite health indices for degradation modeling and prognostic analysis," *IEEE Transactions on Automation Science and Engineering*, vol. 10, no. 3, pp. 652–664, 2013.

[75] Lu, B., Li, Y., Wu, X., and Yang, Z., "A review of recent advances in wind turbine condition monitoring and fault diagnosis," in *Power Electronics and Machines in Wind Applications, 2009. PEMWA 2009. IEEE*, pp. 1–7, IEEE, 2009.

[76] Lu, C. J. and Meeker, W. Q., "Using degradation measures to estimate a time-to-failure distribution," *Technometrics*, vol. 35, no. 2, pp. 161–174, 1993.

[77] Molinari, A. and Nouari, M., "Modeling of tool wear by diffusion in metal cutting," *Wear*, vol. 252, no. 1, pp. 135–149, 2002.

[78] Montgomery, D. C., *Introduction to Statistical Quality Control*. John Wiley & Sons, 2007.

[79] Nandi, S., Toliyat, H. A., and Li, X., "Condition monitoring and fault diagnosis of electrical motors-a review," *IEEE Transactions on Energy Conversion*, vol. 20, no. 4, pp. 719–729, 2005.

[80] Nelson, W., *Accelerated testing: statistical models, test plans and data analyses*. Wiley Online Library, 1990.

[81] Nikias, C. L. and Petropulu, A. P., *Higher-Order Spectral Analysis-A Nonlinear Signals Processing Framework*. Englewood Cliffs, NJ.: Prentice Hall, 1993.

[82] Pettit, L. I. and Young, K. D. S., "Bayesian analysis for inverse Gaussian lifetime data with measures of degradation," *Journal of Statistical Computation and Simulation*, vol. 63, no. 3, pp. 217–234, 1999.

[83] Rafiee, J., Arvani, F., Harifi, A., and Sadeghi, M., "Intelligent condition monitoring of a gearbox using artificial neural network," *Mechanical Systems and Signal Processing*, vol. 21, no. 4, pp. 1746–1754, 2007.

[84] Rao, B. K. N., *Handbook of Condition Monitoring*. Oxford, UK.: Elsevier, 1996.

[85] Rao, S., Strojwas, A. J., Lehoczky, J. P., and Schervish, M. J., "Monitoring multistage integrated circuit fabrication processes," *IEEE Transactions on Semiconductor Manufacturing*, vol. 9, no. 4, pp. 495–505, 1996.

[86] Rehorn, A. G., Jiang, J., and Orban, P. E., "State-of-the-art methods and results in tool condition monitoring: a review," *The International Journal of Advanced Manufacturing Technology*, vol. 26, no. 7-8, pp. 693–710, 2005.

[87] Roan, M. J., Erling, J. G., and Sibul, L. H., "A new, non-linear, adaptive, blind source separation approach to gear tooth failure detection and analysis," *Mechanical Systems and Signal Processing*, vol. 16, no. 5, pp. 719–740, 2002.

[88] Scheffer, C. and Heyns, P., "Wear monitoring in turning operations using vibration and strain measurements," *Mechanical Systems and Signal Processing*, vol. 15, no. 6, pp. 1185–1202, 2001.

[89] Servière, C. and Fabry, P., "Blind source separation of noisy harmonic signals for rotating machine diagnosis," *Journal of Sound and Vibration*, vol. 272, no. 1-2, pp. 317 – 339, 2004.

[90] Shanthikumar, J. G., "Recursive algorithm to evaluate the reliability of a consecutive-k-out-of-n: F system," *IEEE Transactions on reliability*, vol. 31, no. 5, pp. 442–443, 1982.

[91] Shi, J. and Ceglarek, D., "Diagnosability analysis of multi-station manufacturing processes," *Ann Arbor*, vol. 1001, p. 48109, 2002.

[92] Shu, L., Apley, D. W., and Tsung, F., "Autocorrelated process monitoring using triggered cuscore charts," *Quality and Reliability Engineering International*, vol. 18, no. 5, pp. 411–421, 2002.

[93] Shu, L., Tsung, F., and Tsui, K.-L., "Run-length performance of regression control charts with estimated parameters," *Journal of Quality Technology*, vol. 26, no. 3, pp. 280–292, 2004.

[94] Shu, L., Tsung, F., and Tsui, K. L., "Effects of estimation errors on cause-selecting charts," *IIE Transactions*, vol. 37, no. 6, pp. 559–567, 2005.

[95] Sick, B., "On-line and indirect tool wear monitoring in turning with artificial neural networks: a review of more than a decade of research," *Mechanical Systems and Signal Processing*, vol. 16, no. 4, pp. 487–546, 2002.

[96] Siddhpura, A. and Paurobally, R., "A review of flank wear prediction methods for tool condition monitoring in a turning process," *The International Journal of Advanced Manufacturing Technology*, vol. 65, no. 1-4, pp. 371–393, 2013.

[97] Sloan, T. and Shanthikumar, J., "Combined production and maintenance scheduling for a multiple-product, single-machine production system," *Production and Operations Management*, vol. 9, no. 4, pp. 379–399, 2000.

[98] Sloan, T. and Shanthikumar, J., "Using in-line equipment condition and yield information for maintenance scheduling and dispatching in semiconductor wafer fabs," *IIE transactions*, vol. 34, no. 2, pp. 191–209, 2002.

[99] Smaragdis, P., "Blind separation of convolved mixtures in the frequency domain," *Neurocomputing*, vol. 22, no. 1, pp. 21–34, 1998.

[100] Taylor, F. W., "On the art of cutting metals," *Transactions of ASME*, vol. 28, pp. 31–350, 1907.

[101] Thi, H.-L. N. and Jutten, C., "Blind source separation for convolutive mixtures," *Signal Processing*, vol. 45, no. 2, pp. 209–229, 1995.

[102] Tong, L., Soon, V., Huang, Y. F., and Liu, R., "AMUSE: a new blind identification algorithm," in *Proceedings of ISCAS'90*, vol. 3, pp. 1784–1787, 1990.

[103] Tsung, F., Li, Y., and Jin, M., "Statistical process control for multistage manufacturing and service operations: a review and some extensions," *International Journal of Services Operations and Informatics*, vol. 3, no. 2, pp. 191–204, 2008.

[104] Tumer, I. and Bajwa, A., "A survey of aircraft engine health monitoring systems," *Proceedings of AIAA*, 1999.

[105] Wang, P. and Coit, D. W., "Reliability prediction based on degradation modeling for systems with multiple degradation measures," in *Reliability and Maintainability, 2004 Annual Symposium-RAMS*, pp. 302–307, IEEE, 2004.

[106] Wang, X., "Wiener processes with random effects for degradation data," *Journal of Multivariate Analysis*, vol. 101, no. 2, pp. 340–351, 2010.

[107] Wang, Y. and Pham, H., "Modeling the dependent competing risks with multiple degradation processes and random shock using time-varying copulas," *IEEE Transactions on Reliability*, vol. 61, no. 1, pp. 13–22, 2012.

[108] Whitmore, G. A. and Schenkelberg, F., "Modeling accelerated degradation using Wiener diffusion with a time scale transformation," *Lifetime Data Analysis*, vol. 3, no. 1, pp. 27–45, 1997.

[109] Wu, C. F. and Hamada, M. S., *Experiments: Planning, Analysis, and Optimization, 2nd Edition*. Wiley, 2009.

[110] Xiang, L. and Tsung, F., "Statistical monitoring of multi-stage processes based on engineering models," *IIE Transactions*, vol. 40, no. 10, pp. 957–970, 2008.

[111] Yang, D. and Penman, J., "Intelligent detection of induction motor bearing faults using current and vibration monitoring," in *COMADEM 2000: 13 th International Congress on Condition Monitoring and Diagnostic Engineering Management*, pp. 461–470, 2000.

[112] Ypma, A., Leshem, A., and PW Duin, R., "Blind separation of rotating machine sources: bilinear forms and convolutive mixtures," *Neurocomputing*, vol. 49, no. 1, pp. 349–368, 2002.

[113] Zhang, B., Khawaja, T., Patrick, R., Vachtsevanos, G., Orchard, M. E., and Saxena, A., "Application of blind deconvolution denoising in failure prognosis," *IEEE transactions on instrumentation and measurement*, vol. 58, no. 2, pp. 303–310, 2009.

[114] Zhou, J., Djurdjanovic, D., Ivy, J., and Ni, J., "Integrated reconfiguration and age-based preventive maintenance decision making," *IIE Transactions*, vol. 39, no. 12, pp. 1085–1102, 2007.

[115] Zhou, R., Serban, N., and Gebraeel, N., "Degradation modeling applied to residual lifetime prediction using functional data analysis," *The Annals of Applied Statistics*, vol. 5, no. 2B, pp. 1586–1610, 2011.

[116] Zhou, S., Huang, Q., and Shi, J., "State space modeling of dimensional variation propagation in multistage machining process using differential motion vectors," *Robotics and Automation, IEEE Transactions on*, vol. 19, no. 2, pp. 296–309, 2003.

[117] Zhu, K., Wong, Y., and Hong, G., "Wavelet analysis of sensor signals for tool condition monitoring: a review and some new results," *International Journal of Machine Tools and Manufacture*, vol. 49, no. 7, pp. 537–553, 2009.

[118] Zuo, M. J. and Tian, Z. T., "Performance evaluation of generalized multi-state k-out-of-n systems," *IEEE Transactions on reliability*, vol. 55, no. 2, pp. 319–327, 2006.

VITA

Li Hao grew up in Jilin City, Jilin Province, China. She received the B.S. Degree in Automotive Engineering from Tsinghua University in 2009 and the M.S. degree in Statistics from the Georgia Institute of Technology in 2012.